Macromolecular Rapid Communications
www.mrc-journal.de

Developing Anisotropy in Self-Assembled Block Copolymers: Methods, Properties, and Applications

Mark Robertson, Qingya Zhou, Changhuai Ye, and Zhe Qiang**

Block copolymers (BCPs) self-assembly has continually attracted interest as a means to provide bottom-up control over nanostructures. While various methods have been demonstrated for efficiently ordering BCP nanodomains, most of them do not generically afford control of nanostructural orientation. For many applications of BCPs, such as energy storage, microelectronics, and separation membranes, alignment of nanodomains is a key requirement for enabling their practical use or enhancing materials performance. This review focuses on summarizing research progress on the development of anisotropy in BCP systems, covering a variety of topics from established aligning techniques, resultant material properties, and the associated applications. Specifically, the significance of aligning nanostructures and the anisotropic properties of BCPs is discussed and highlighted by demonstrating a few promising applications. Finally, the challenges and outlook are presented to further implement aligned BCPs into practical nanotechnological applications, where exciting opportunities exist.

1. Introduction

The ability to generate periodic nanostructures with exact control over morphology, size, and functionality is key to various nanotechnology applications,[1–8] which has attracted numerous research efforts in both industry and academia over the past few decades. The most common approaches to attain ordered nanoscale features involve "top-down" and "bottom-up" methods. In the first case, lithographic techniques are commonly used to selectively remove base materials by exposure to photons, electrons, ions, or chemical reactions in order to produce desired nanostructures.[9,10] These methods, including e-beam lithography,[11–13] dip-pen lithography,[14–16] nanoimprinting,[17,18] photolithography,[19,20] and ion-beam etching,[21,22] are able to produce precisely defined nanopatterns at a high resolution. However, they may require high costs and strict operation conditions, and could often be limited to relatively low throughput production.[23] Alternatively, the "bottom-up" approach provides facile access to construct nanostructures over a large area, by self-organization of building blocks with typical characteristic pattern size ranging from few hundreds of nanometers down to the size of a molecule.[24–28] Additionally, approaches such as photolithography can also be applied in "bottom-up" assembly to grow polymer chains from the substrate.[29] While the resulting morphology assembled from self-assembly based method is typically "polycrystalline," containing multiple defects and grain boundaries over large ensembles, the "bottom-up" strategy offers unique advantages of low-cost processing conditions and high potential of scalability, which is particularly attractive for applications where cheap and quick manufacturing is desired and a small density of defects and/or pattern size variation could be acceptable.

The block copolymer (BCP) is a canonical system for "bottom-up" assembly,[29–33] consisting of two or more chemically dissimilar segments that are covalently linked. The immiscibility between different blocks can drive the spontaneous microphase separation process on a length scale that directly corresponds with the size of the polymer chains.[34–36] The expected morphologies for a classical diblock copolymer system as a function of constituent volume fraction are depicted in **Figure 1**, including lamellae (L), gyroids (G), cylinders (C), and spheres (S), where the majority constituent forms a matrix around the minority domains of the BCP system. For triblock copolymers, they can exhibit similar morphologies as the conventional diblock copolymer, while complex morphologies, such as gyroids, become more accessible.[37] Early studies also found that the introduction of a third chemically distinct block to the conventional diblock copolymer system results in an even richer phase diagram with additional accessible morphologies, including coaxial cylinders, cylinder-ring phases, and concentric spherical domains in a body-centered cubic structure.[38] The additional morphologies and manipulation of the phase diagram present in triblock copolymer systems make them potentially more appealing for various applications than their diblock counterparts.

M. Robertson, Dr. Z. Qiang
School of Polymer Science and Engineering
University of Southern Mississippi
Hattiesburg, MS 39406, USA
E-mail: zhe.qiang@usm.edu
Q. Zhou, Dr. C. Ye
State Key Laboratory for Modification of Chemical Fibers and Polymer Materials
College of Materials Science and Engineering
Donghua University
Shanghai 201620, China
E-mail: cye@dhu.edu.cn

The ORCID identification number(s) for the author(s) of this article can be found under https://doi.org/10.1002/marc.202100300

DOI: 10.1002/marc.202100300

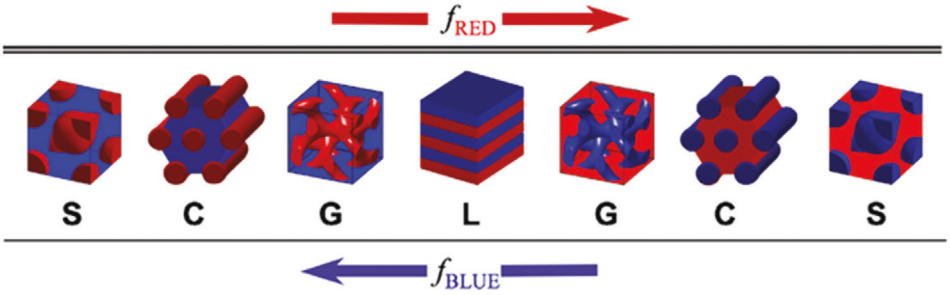

Figure 1. Illustrations of the typical morphologies that can be obtained from a diblock copolymer system. When both blocks are present in equal volume fractions, lamellae (L) are present. Upon increasing the volume fraction of one of the blocks, the system can transition to gyroids (G), cylinders (C), and spheres (S) with the continuous phase consisting of the block with the larger volume fraction. Reproduced with permission.[36] Copyright 2008, Elsevier.

When a block copolymer is at equilibrium, its minimum free energy conformation is determined by enthalpic and entropic contributions from local mixing. The thermodynamically favorable structure of a BCP at a given temperature is determined by the minimum Gibbs free energy, which consists of enthalpic contributions which are negative based upon incompatibility, and temperature-dependent entropic contributions that represent conformational freedom of the molecules in the system. The enthalpic contributions to Gibbs' free energy scale with the Flory-Huggins parameter, χ, and inversely with the degree of polymerization, N, respectively.[37–39] The product of these two parameters (χN), often referred to as BCP segregation force, needs to be at least larger than 10.495 for a symmetric diblock copolymer to produce ordered nanodomains.[39] Another critical parameter for determining BCP morphology is the chemical composition, represented by the volume fraction of the constituent blocks (f).[40–42] A linear diblock copolymer with segments of comparable volume fractions typically exhibits a lamellar morphology, while increasing asymmetry of chemical composition can lead to phase transitions to other morphologies such as gyroids, cylinders, and spheres.[43,44] The accessible size of these features is directly related with the χ of BCP systems, in which a higher χ leads to a lower number of repeat units that are required to achieve sufficient segregation force to induce spontaneous phase separation in the system. Through engineering and system design of high-χ block copolymers, feature sizes smaller than 3 nm have been achieved.[45] Moreover, χN also determines the order-to-disorder transition temperature (T_{ODT}) of a BCP system. As χ is inversely proportional to temperature, segregation force decreases as temperature increases. As a result, BCP systems with higher χN could exhibit higher T_{ODT} and require higher amounts of energy to effectively screen unfavorable interactions between the blocks and induce disorder.

Moreover, many studies indicate that polydispersity plays an important role in the determination of final BCP morphologies. Generally, polydispersity in BCP systems can increase the sizes of the assembled microdomains and may result in morphologies different from BCPs of equivalent molecular weights and compositions.[46–48] Bicontinuous morphologies have been exhibited by these polydisperse systems, highlighting that the interplay between polymer chains of differing lengths can result in phase behaviors that may be distinct from conventional monodisperse systems.[49] A broader polydispersity may also lead to the shift from the expected phase diagram of triblock copolymers, while also enhancing the thermal stability of the ordered domains.[50]

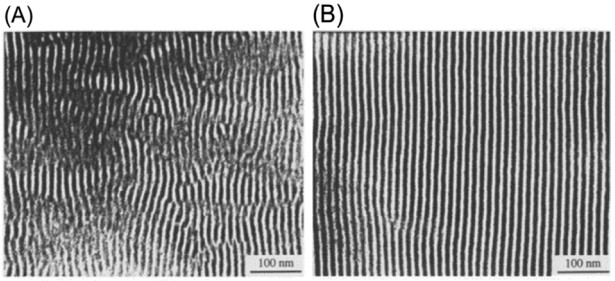

Figure 2. TEM images of a roll-cast polystyrene-block-polybutadiene-block-polystyrene (PS-*b*-PI-*b*-PS) BCP A) before and B) after thermally annealing above the glass transition temperatures of all constituents. Reproduced with permission.[72] Copyright 1997, Elsevier.

Initial theoretical and experimental investigations have been largely focused on linear diblock and triblock copolymers,[51–58] the most established systems of BCP self-assembly. The advances in polymer chemistry now enable higher complexity in chemical composition (e.g., multiblock copolymers) and chain architecture (e.g., cyclic copolymers and bottlebrush copolymers) to provide additional opportunities to access many complex BCP morphologies such as A15 phase, Frank-Kasper phase, σ phase, and other quasicrystal phases, or obtain hierarchical nanostructure at multiple length scales.[59–68] These discoveries bring a host of new and exciting opportunities for potential BCP applications led by broadening the landscape of their attainable structures.

While final equilibrium structure can be predicted by thermodynamics theory, the actual BCP morphology is often processing pathway-dependent because self-assembly is a stochastic process and can be highly nonergodic.[40,69–71] Even for neat diblock copolymers, a relatively simple system, the attainable nanostructure is determined by rich competition between thermodynamic and kinetic factors. A highly nonequilibrium state of a BCP can often be kinetically trapped during processing and an additional annealing step is generally required. The improvement of long-range ordering and annihilation of defects is important for mitigating adverse effects on material performance associated with poorly ordered nanostructures.[72–77] As shown in **Figure 2**, thermal annealing is a common approach for ordering BCP nanostructures by heating the BCP above their glass transition

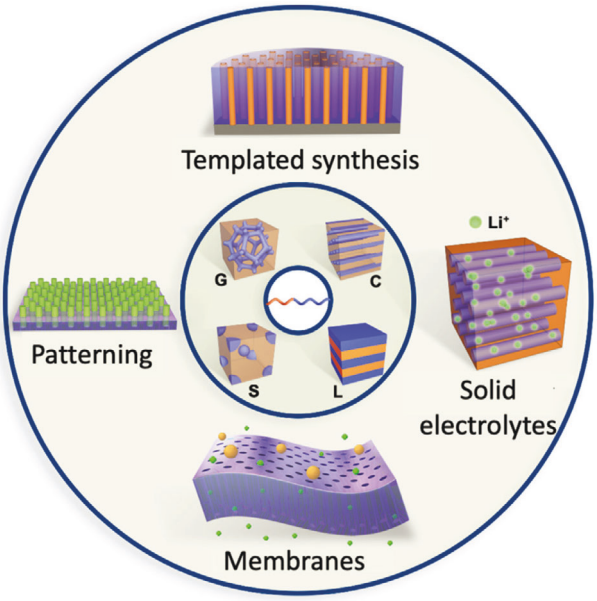

Figure 3. The use of block copolymer assembled structures can provide various opportunities for the development of nanotechnologies that range from filtration membranes to optical materials.

temperature (T_g) of all components in order to provide sufficient chain mobility to achieve equilibrated morphologies.[72] The initial film in Figure 2 consists of many structural defects, which can be annihilated after a thermal annealing step.

While effective, thermal annealing sometimes could require long annealing times (hours or days) for the BCP to reach modest ordering and can be constrained by a narrow window of applicable processing temperatures due to polymer thermal stability or its intrinsic slow/hindered ordering dynamics.[78,79] To address these challenges, a diversity of annealing approaches has been demonstrated to enhance the ordering kinetics of BCPs in order to accelerate the self-assembly process.[80,81] Solvent vapor annealing (SVA) in particular is one of the most widely utilized methods as an effective alternate for improving long-range ordering of BCP films within hours or minutes, in which sorption of solvent imparts chain mobility through swelling of the BCP domains, and screens unfavorable interactions between distinct segments.[82–88] This methodology also enables manipulation of nanostructural orientation by varying processing parameters such as solvent selection and vapor removal rate,[89–92] which will be discussed in detail in the next section. Readers who are interested in other emerging methods for rapid ordering of block copolymers, such as thermal-assisted solvent vapor annealing,[93–95] direct solvent immersion annealing,[96–98] microwave annealing,[94,99–101] and laser annealing,[102,103] can be directed to an excellent review by Majewski and Yager for relevant fundamentals of BCP ordering kinetics with different annealing approaches.[80]

The advantages of bottom-up control over order, including low manufacturing costs and widely tunable morphologies, render BCPs to be critical structure-directing agents for a wide array of nanotechnology applications (**Figure 3**).[3,104–107] For example, selective removal of a minority domain from a BCP matrix by ultraviolet oxidation, plasma etching, or acid/solvent wash, can produce porous membranes for gas or liquid separation[108–115]; controlled transportation of species (e.g., ion, electron and small molecules) in one of the nanodomains in BCPs can be achieved when strongly preferred interactions exist due to distinct material chemistry from different blocks which is useful for water remediation, and energy generation/storage applications[116–126]; incorporation of dopants, such as nanoparticles and drugs, into BCP domains also introduces additional functionality into systems for enabling more diverse applications including, but not limited to, photonics and biomedicine.[127–135] Furthermore, methodologies for converting and/or replicating BCP morphologies to functional inorganic materials with nearly perfect pattern transfer have been established in industrial applications for manufacturing electronic and magnetic devices.[136–139] All of these examples demonstrate the enormous promise of BCPs, but the realization of their full potential still requires many essential steps. One central challenge is associated with the ability to provide macroscopic control of nanoscale orientation, as in many of the aforementioned applications the performance of these nanomaterials is very sensitive to the degree of long-range ordering and/or alignment.[29,140–142] For instance, stringent control of long-range registry in BCP thin films is a necessity for their potential applications in microelectronic devices.[31,143] For other applications associated with transport phenomena, alignment of nanodomains can minimize the tortuosity of pathways in order to facilitate species transporting along the conducting (aligned) direction.[144–147] Furthermore, BCPs with unidirectional nanostructures often exhibit enhanced material properties along the alignment direction compared to their random-oriented analogues.[148,149]

Self-assembly of BCPs from conventional methods does not generically afford such long-range control of nanostructural orientation, and therefore numerous research efforts have been dedicated to this area.[150–156] These efforts include the use of theory and molecular simulation approaches,[157,158] paired with developing advanced processing techniques and in situ characterization techniques to explore assembly dynamics and pathway toward producing highly aligned BCPs. While several excellent contributions have already discussed directed self-assembly (DSA) of polymers within the scope of assembly physics and instrumentation in great detail,[30,105,159–163] our goal here is to describe the physical phenomena and mechanisms of each experimental approach for BCP alignment, and more importantly to highlight the significance of the structure–property relationship in anisotropic block copolymers and their relevant applications. Herein, we first review the established aligning techniques for bulk BCP (or thick films, where thickness is at least 1 μm), which are typically assisted with the application of an external force or field, followed by introducing additional methods that are available for thin film systems (Note: here we define thin film as thickness less than 1 μm), where confinement and interfaces could play vital roles in manipulating BCP phase behaviors. Each method is briefly discussed with the aim of providing readers a sufficient working knowledge for conducting experimental investigations and understanding the corresponding mechanisms of BCP alignment. While programming polymer chain

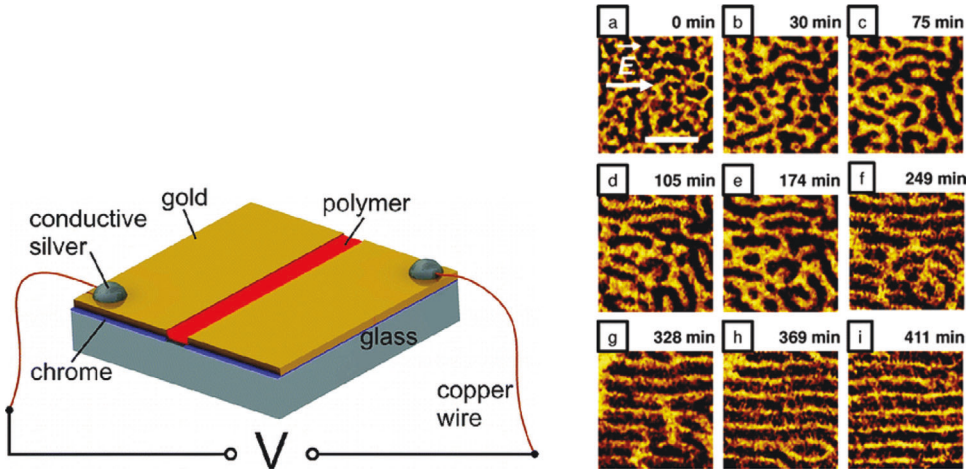

Figure 4. Schematic illustration of a generalized method for applying electric fields to block copolymer systems. Inset a-i) illustrate the effect of annealing time on a PS-*b*-PHEMA-*b*-PMMA BCP in the presence of saturated chloroform vapor and a 15 V μm^{-1} electric field. As the system is annealed, the BCP domains transition from disordered to highly oriented at longer exposure times. Reproduced with permission.[179] Copyright 2009, American Chemical Society.

architecture and chemical composition could also provide a critical mechanism to enable orientation control of BCP nanostructure, especially in thin films,[164–170] the progress in this research and related methodologies are not extensively discussed in this review. We also highlight some examples of BCP systems where the alignment of the nanostructure is of paramount importance for developing anisotropic properties with directional enhancement. The structure–property relationship of these macroscopically aligned BCP systems is then further elaborated by demonstrating their particular applications in nanotechnology such as filtration membranes, solid polymer electrolytes, and templates for inorganic materials. With plentiful research articles available in this field, we apologize in advance if some important contributions are missing due to our inadvertence or space constraints. Finally, we provide a brief perspective on current challenges that need to be addressed for enabling broader practical applications of anisotropic BCP materials and the opportunities to further advance this research area.

2. Established Methods for Aligning BCP in Bulk and Thin Films

In this section, we will discuss the approaches that have been developed for aligning BCP nanostructures. Specifically, Sections 2.1–2.3 describe the use of electric, magnetic, and shear fields, respectively, to produce anisotropic nanopatterns, while Section 2.4 outlines the use of light and optically active moieties in BCPs. Sections 2.5 and 2.6 primarily focus on BCP thin films and cover the ability to direct the self-assembly of BCPs using physically or chemically patterned substrates, as well as through engineering the polymer–substrate and polymer–air interfaces. Section 2.7 focuses on the development of techniques that are based on localized heating or deposition. Section 2.8 summarizes the efforts of using combined methods for aligning BCPs. These sections represent a broad range of effective and promising approaches to efficiently align BCPs to produce unidirectional nanopatterns.

2.1. Electric Field

Electric fields have been used to produce macroscopically aligned BCPs with nanodomains oriented parallel to the field lines in both bulk and thin-film geometries by taking advantage of the differences in dielectric permittivity of chemically distinct segments.[171,172] The dielectric contrast of the block copolymer constituents drives the orientation of the nanodomains parallel to the applied electric field to minimize free energy. The difference in dielectric constant between the blocks facilitates the electric field-induced orientation, indicating that this technique is more efficient for BCP systems with high dielectric contrasts. Generally, the application of an electric field favors phase separation through increasing the immiscibility between the BCP segments. Additionally, electric fields can increase domain spacings, alter the T_{ODT} of the BCP systems, and shift phase diagrams to different concentrations.[171,173–177] This technique can be employed in a variety of systems that include solutions, bulk samples, and thin films. Direct-current (DC) is primarily employed for both in-plane and out-of-plane alignment of BCP nanostructures, while alternating-current (AC) can also be used when field alternation is faster than ion response.[178] **Figure 4** shows the scheme of a typical set-up where a block copolymer thin film is sandwiched between two electrodes. In this study, the alignment of a chloroform vapor-swollen polystyrene-*block*-poly(2-hydroxyethyl methacrylate)-*block*-poly(methyl methacrylate) (PS-*b*-PHEMA-*b*-PMMA) BCP upon the application of an electric field was monitored. The as-cast BCP film exhibited a poorly ordered morphology, which gradually becomes more aligned as the film is swollen and the electric field is applied with increasing annealing time. This work demonstrated that improving the ordering of the BCP films occurred in two distinct stages where at earlier times, the annihilation of ring-like and open-end defects dominated the ordering process. At higher degrees of alignment and longer times of exposure to the applied electric field, the nanostructural alignment is established through the removal of classic topological defects such as disclinations or dislocations. Commonly, these

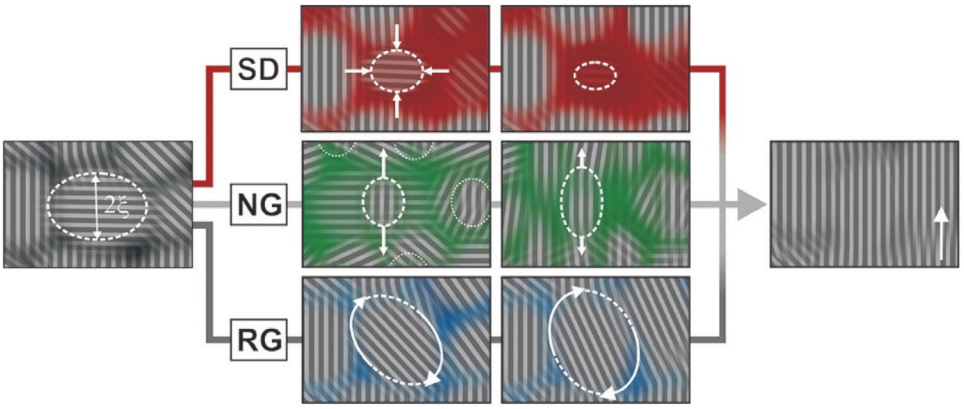

Figure 5. Generalized schematic of different orientation mechanisms in electric field alignment of block copolymer systems. Selective disordering (SD) is accomplished by systems close to their order-to-disorder transition. Poorly aligned lamellae are disintegrated by the electric field and oriented in-plane with the electric field. Nucleation and growth (NG) is a result of layer instabilities nucleating the growth of lamellae, which propagates throughout the system. In systems with highly dissimilar chemical segments, alignment is achieved through a rotation of grains (RG) mechanism. The established grains rotate and align through the annihilation of defects in the ordered structure. Reproduced with permission.[173] Copyright 2013, American Chemical Society.

structures must be quenched or kinetically trapped prior to the removal of the applied field to ensure the maintenance of the developed nanostructure.

The application of an electric field to induce ordering in a BCP can follow multiple different mechanisms depending on the segregation strength between the BCP segments, as well as the operation conditions of the alignment (**Figure 5**). For BCPs near their ODT, the application of electric field orders the BCP domains through a mechanism of "selective disordering" where domains oriented in-line with the electric field are unaffected, and defects are annihilated. When an electric field is applied to BCPs away from their ODT, randomly oriented grains of a BCP are initially nucleated and grown until a critical grain size is reached for triggering the reorientation of grains along the field direction, often associated with sufficient energy penalty and governed by the rule of minimizing the orientation-dependent field energy.[180–184]

For strongly segregated BCPs, rotation of grains dominates the aligning process and with the decrease of segregation force, the "nucleation and growth" mechanism becomes more favored.[185,186] The driving force for this process is from local dielectric anisotropy, which is proportional to $\frac{(\Delta\epsilon^2)}{\langle\epsilon\rangle}E^2$, where $\Delta\epsilon$ is the dielectric constant difference between two blocks, $<\epsilon>$ is the mean dielectric constant, and E is the field strength.[187,188] Therefore, a higher contrast in dielectric permittivity of different BCP segments and a stronger field (need to be careful to avoid dielectric breakdown) are generally desired, especially for overcoming the affinity of BCPs to surfaces in thin-film systems. Moreover, the inclusion of ion-containing dopants into BCP nanodomains could be useful to enhance the degree of alignment and aligning kinetics by improving the dielectric permittivity contrast.[189–191]

Typical field strengths for electric field-induced alignment are on the order of 10^7 V m^{-1} and BCP films need to be either annealed above the glass transition temperatures of all blocks or in a solvent-swollen state in order to obtain sufficient chain mobility for ordering and alignment.[179,182,192–194] Many conventional BCPs have been successfully aligned by electric field, including polystyrene-*block*-polymethyl methacrylate (PS-*b*-PMMA),[195–200] polystyrene-*block*-polyisoprene (PS-*b*-PI),[176,188,201,202] polystyrene-*block*-polylactic acid (PS-*b*-PLA),[203,204] polystyrene-*block*-poly(4-vinyl pyridine) (PS-*b*-P2VP),[199,205,206] as well as other sophisticated systems such as rod-coil BCPs and BCP nanocomposites.[207–210] To highlight some recent work for BCP alignment using E-field, Kim et al. demonstrated the use of patternable graphene electrodes to induce patterned ordering of symmetric PS-*b*-PMMA thin films through the application of DC voltages. The BCP was thermally annealed, accompanied with a 25 V μm^{-1} electric field. This technique, along with blending short-chain polymers to enhance the polymer diffusivity, resulted in rapid ordering and aligning over large areas.[182] More recently, this method was extended to a poly(methyl methacrylate)-*block*-polyacrylonitrile (PMMA-*b*-PAN) thin-film system where graphene electrodes were lithographically patterned on a substrate, and the PMMA-*b*-PAN was assembled within the patterns upon exposure to electric fields.[211] The assembled domains were then employed as carbon nanowire precursors for potential applications as gas sensors. Ryu et al. demonstrated successful ordering of high-χ fluoroacrylic BCP thin films through the application of an electric field.[212] Due to the high mismatch in surface energies of the polystyrene and poly(2,2,2-trifluoroethyl acrylate) blocks, both polymer–substrate and polymer–air interface of the BCP films were engineered to be neutral to the BCP constituents, a concept that will be discussed in further detail in Section 2.6, allowing for domains aligned perpendicular to the substrate. Thermal annealing and a direct current potential of 25 V μm^{-1} allowed for rapid alignment (≈5 min) due to the high dielectric contrast between the two constituents. Overall, the electric field alignment method provides an attractive tool for aligning BCPs due to its high availability and low cost of required instrumentation, namely a low barrier for conducting experiments, but the risk of dielectric breakdown and the requirement of high field strengths may hinder its ability to be widely employed as a highly industrially relevant process.

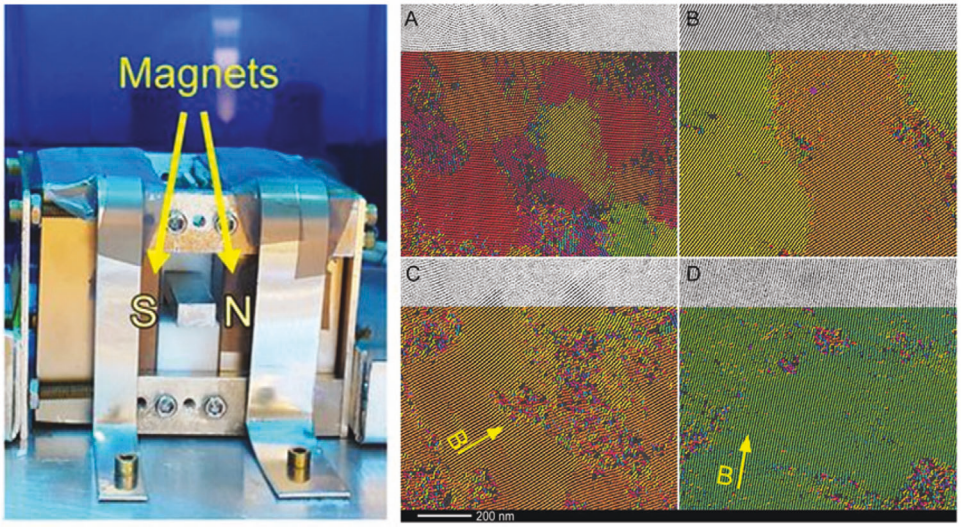

Figure 6. Image of a low-intensity magnetic field apparatus where two permanent magnets are placed on either side of the sample stage which can be cooled to pass the BCP sample through its ODT. A,C) A neat PEO-PMA liquid crystalline block copolymer under high intensity (6 T) before and after alignment, respectively. Similarly, B,D) The poly(ethylene oxide)-*block*-poly(methyl acrylate) (PEO-*b*-PMA) liquid crystal BCP with the inclusion of mesogens to assist the magnetic field alignment before and after alignment in a 1 T field. Reproduced with permission.[214] Copyright 2017, National Academy of Sciences.

2.2. Magnetic Field

Many parallels can be drawn between electric field and magnetic field alignment of BCPs as both approaches require originating energetic bias from the anisotropy between different blocks in order to produce the preferred alignment of nanostructures parallel to the field. The driving force to induce macroscopic alignment in a magnetic field is the angle-dependent magnetostatic energy, resulting from the differences in the magnetic susceptibility of the BCP structures.[213,214] This relationship can be described as:

$$F(\theta, B) = -\frac{\Delta\chi B^2}{3\mu_0}\left\langle \frac{3\cos^2\theta - 1}{2} \right\rangle \quad (1)$$

$$\Delta\chi = \left|\chi_{\parallel} - \chi_{\perp}\right| \quad (2)$$

where B is the strength of magnetic field; $\Delta\chi$ represents differences in magnetic susceptibility along the parallel and perpendicular directions with respect to the field lines; θ is the angle difference between the field and $\chi_{\parallel}$, and μ_0 is the vacuum permeability.[215] This approach is particularly attractive for bulk systems that include liquid crystalline BCPs[216–222] and rod-coil BCPs,[223,224] since these materials intrinsically compose rigid moieties (such as aromatic mesogens) that impart relatively high magnetic anisotropy at the microdomain level. This can lead to nearly two orders of magnitude enhancement in magnetic property contrast compared with conventional coil–coil BCPs (from $\approx 10^{-8}$ to $\approx 10^{-6}$, dimensionless units).[216,225,226] In general, magnetic fields can be applied to samples with arbitrary shape since there is no requirement for direct contact between sample and instrument. A representative example apparatus that applies magnetic fields to bulk BCP samples is shown in **Figure 6**.[214] This apparatus used low-cost, permanent magnets to provide a field strength to align the nanostructures of liquid crystal BCPs that are parallel to the applied magnetic field.

Magnetic field alignment is the most effective when the BCP sample is cooled across the order–disorder transition temperature (T_{ODT}) within the presence of the field, as opposed to the isothermal process at a temperature below T_{ODT}, which is attributed to the enhanced ordering kinetics from higher thermal energy and lower viscosity of the polymer matrix.[149] Pioneering efforts of magnetic field aligning BCP nanodomains in bulk systems usually demand high field strength (at least 2 T, and in most cases it varies from 4 T to 6 T) using superconducting magnets, which potentially constrains its widespread applications in other research labs and industry.[227] As demonstrated in Figure 6, cooperative assembly of BCPs with labile mesogens in the system is able to address this limitation, which only requires a low-intensity magnetic field for producing highly aligned BCP nanostructures due to reduced polymer viscosity and enhanced magnetostatic energy from mesogenic additives.[214] This study employed mesogenic additives into a poly(ethylene oxide)-*block*-poly(methyl acrylate) (PEO-*b*-PMA) BCP in order to enhance the alignment through low-intensity magnetic fields. The BCP samples containing mesogens exhibit similar degrees of ordering in low-intensity fields (Figure 6B,D) compared to the pristine BCP in a 6 T field (Figure 6A,C). This strategy was also demonstrated to be generalizable to other BCP systems,[228–232] which significantly broadens the applicability of magnetic field alignment to a wide variety of functional polymer materials.

In a recent work, Guiver et al. developed electrolyte membranes with proton-conducting channels through the magnetic field-assisted assembly of a bulk polymer containing phosphotungstic acid. The paramagnetic complex was successfully aligned by magnetic field, providing stable proton channels that exhibited higher performance than commercial membranes.[233] Similarly, Matos et al. employed electric and magnetic fields

separately during casting of commercial Nafion membranes to induce structural alignment for enhancing performance. Both methods provided the orientation of ion-containing domains, and the magnetic field-aligned systems exhibited much higher performance and proton conductivity than random-oriented counterparts.[234] Chan et al. aligned metallo-supramolecular poly(3-hexylthiophene)-*block*-poly(ethylene oxide) (P3HT-*b*-PEO) BCP thick films using a 9 T magnetic field.[235] These specialized BCPs bound by zinc complexation formed well-ordered domains upon casting. The PEO domains could be selectively removed to produce functional, ordered P3HT nanofibers. Furthermore, it is worthwhile to point out a recent study successfully produced a nearly single-crystal texture of BCP over a large area (> 1cm$^{[2]}$) by employing two modes of directed self-assembly, involving physical confinement and magnetic field.[236] The perfectly aligned BCP nanodomains from such potentially scalable approaches provide great opportunities for advancing future nanotechnology.

2.3. Shear Field

Shear aligning was first incepted in the 1970s by Willmouth et al.,[237] which has now been applied in various BCP melts and concentrated solutions with different morphologies including lamellae,[69,238–244] cylinders,[245–251] and spheres.[252–256] Shear alignment has also been employed to align complex BCP architectures, such as bottlebrushes, through the application of large amplitude shear.[257] The primary underlying mechanism for shear alignment can be attributed to the desire of different segments, containing distinct mechanical and/or viscoelastic properties, to collectively avoid domain mixing and minimize viscous dissipation and entropy loss during chain stretching and deformation. The response of a BCP to shear force, such as the timescale of aligning process and degree of alignment, can be dependent on several parameters including polymer chain architecture, molecular weight, processing temperature, shear rate or frequency, and the amplitude of deformation.[69,251,256,258–261]

Shear force can be imposed on a BCP using a relatively simple set-up without involving specialized equipment and high cost. Many commercial instruments such as rheometers and extruders are often used by confining BCP melt within two parallel surfaces and then displacing one surface relative to the other for imposing shear with controlled strain amplitude, shear stress, and deformation timescale.[262,263] A similar method that uses roll-casting is developed to align highly concentrated BCP solutions upon solvent evaporation.[264] In general, BCP nanodomains are commonly aligned parallel to the velocity direction of the shear (or normal to the shear direction for lamellae), however when very high strain rates are imposed, the transverse arrangements of nanostructure can be formed due to the extensive polymer chain elongation in the shear direction.[265–267] For shear aligning BCP thin films, required stress is often applied by flowing a highly viscous silicone oil or using a crosslinked elastomeric PDMS cap in contact with the film surface.[243,257,268,269] (**Figure 7**).

A generalized set-up for shear aligning uses mechanical rubbing of a PDMS pad across a BCP thin film surface. This simple and cost-effective technique enables nanostructural orientation

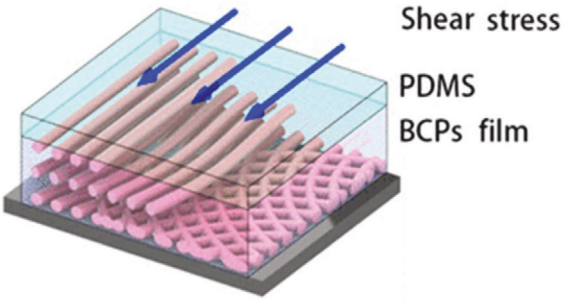

Figure 7. Generalized schematic of employing shear stress provided by a PDMS pad (mechanical rubbing, or expansion and contraction induced by heating or solvent vapor) on the surface of a BCP film to induce alignment. Reproduced with permission.[269] Copyright 2018, American Chemical Society.

along the shear direction. Alternatively, local thermal or solvent expansion of a PDMS cap by a spatial sharp temperature gradient or gradient contraction of the PDMS cap from a solvent swollen state can also effectively transduce shear force on BCP thin films in order to produce highly aligned nanodomains.[270–275] As shown in **Figure 8**, alignment of BCP domains can be locally controlled through adhering a PDMS pad to a BCP film surface, and subsequently swelling the system with solvent vapor. This work found that the contraction of a PDMS pad upon solvent removal resulted in a shear force that was responsible for inducing alignment in the BCP domains. While this technique is simple and efficient for achieving alignment over large areas, it can be limited to ultrathin BCP films (i.e., monolayer) as the influence of the shear force dissipates in regions of the film closer to the substrate,[269] leading to limited orientation in structures near the polymer–substrate interface. More recently, the concept of shear-aligning was paired with laser zone annealing to provide ordering over large areas (>2 cm^2). PDMS pads were adhered to BCP films prior to laser annealing which, upon exposure to thermal gradients from the laser annealing process, produced shear forces responsible for aligning the BCP domains.[103]

Notably, the case studies discussed here do not often quantify the applied shear stress and its effect on the orientation of the BCP domains. Register et al. systematically studied the effect of varying shear stress and polymer characteristics on the progression of alignment in cylinder forming PS-*b*-PHMA thin films.[250] It was determined that the requisite shear stress to induce alignment increases linearly with molecular weight of the BCP constituents and decreases with film thickness until the films were roughly five domains thick.

Key advantages of the shear alignment process include its versatility and simplicity to macroscopically align BCP domains without any particular requirement for polymer chemistry, sample geometry, and instrument set-up, which makes it attractive and valuable for scale-up. As examples of the versatility of shear alignment, more complex systems than the conventional diblock and triblock copolymers, such as bottlebrush block copolymers, have been aligned through the application of a shear force. Rzayev et al. demonstrated the fabrication of nanoporous materials derived from a cylinder forming PS-*b*-PLA BCP. After the application of macroscopic shear by passing the bulk polymer through

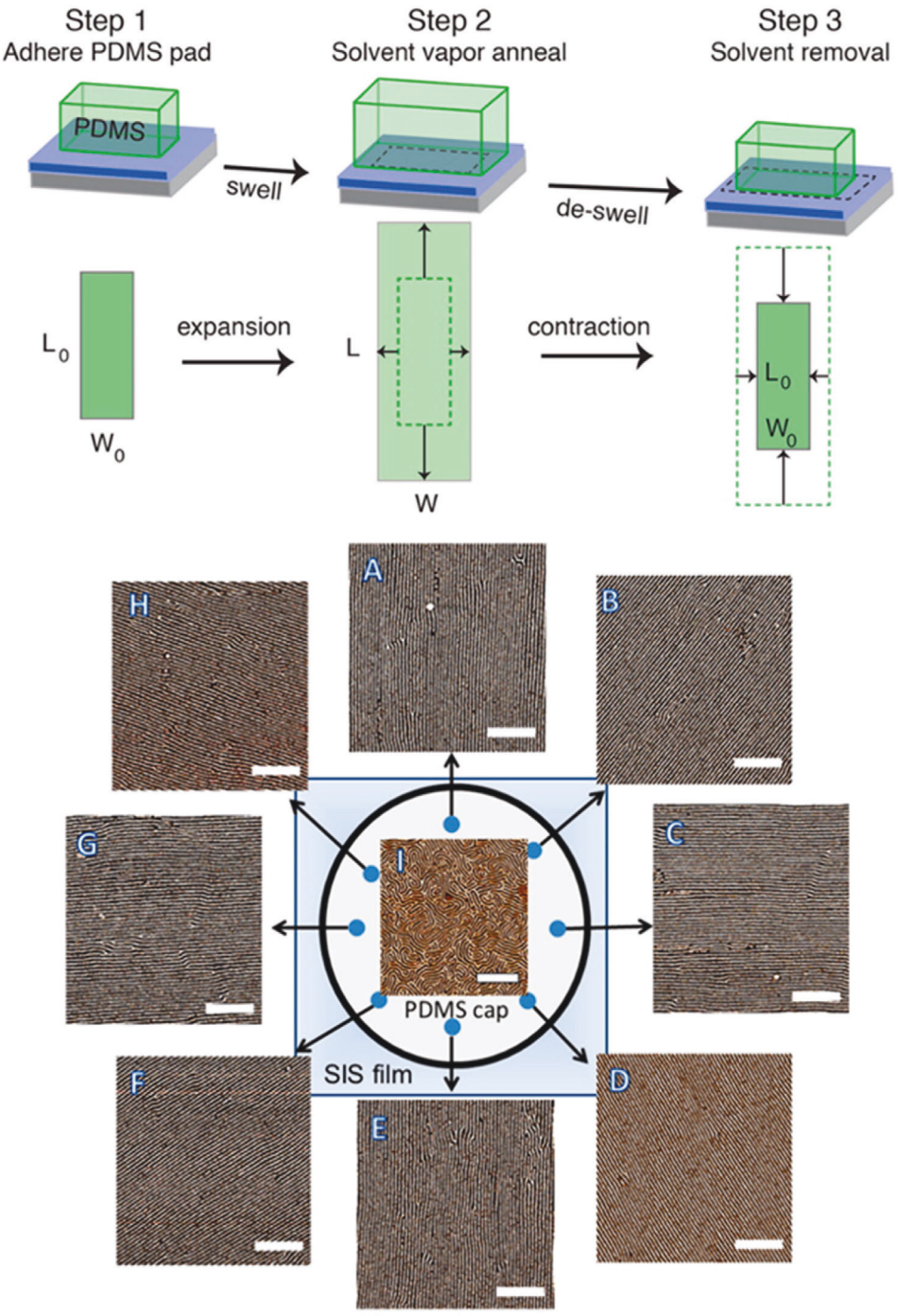

Figure 8. Illustration of soft shear alignment of a model block copolymer induced through the solvent swelling and contraction of a PDMS pad. The PDMS pad is placed on top of the BCP film, swollen during solvent vapor annealing, then contracts upon removal of solvent. This contraction induces a shearing force, aligning the BCP domains. Reproduced with permission.[273] Copyright 2014, American Chemical Society.

a channel die, the BCP melt exhibits a highly ordered structure which can be further processed towards a functional material.[276] Similarly, Watkins et al. utilized controlled oscillatory shear to provide highly ordered lamellar PS-*b*-PEO BCPs. This technique was demonstrated to order the BCP nanostructure over large sample volumes on the order of mm^3 in bulk samples.[257] Additionally, recent work has demonstrated that shear rolling can be used to produce uniform, perpendicular nanostructures over large areas (4 in diameter) at time scales as short as 1 min. This indicates the commercial viability of this simple, powerful technique.[277] However, it is generally hard to achieve ideal, defect-free patterns from shear alignment due to the presence of their characteristic undulations within BCP morphology. Furthermore, the shear alignment method has not demonstrated

its ability to consistently produce vertically aligned nanodomains throughout the entire film thickness.

2.4. Optical Alignment

Photoalignment of BCP thin films, triggered by directional excitation of molecules from linear polarized light, has become a rising interest in the past decade due to its unique ability to noninvasively manipulate nanopatterns by simply controlling the optical pathway (i.e., exposing selective regions to the light).[278] Since alignment originates from the change in polarity of nanodomains induced by *trans*-to-*cis* isomerization upon illumination, this approach requires the incorporation of photoresponsive units such as azobenzene groups into polymers for triggering the anisotropic photoexcitation.[279–282] Advances in material chemistry/synthetic approaches for enabling the photoalignment of BCPs are essential but will not be explicitly discussed in this article. Interested readers can find several excellent reviews by Seki et al. for fundamentals of the synthetic aspect of this technique.[283,284] While the mechanism of how BCP nanostructure is macroscopically aligned through controlling local molecular motions is still not completely understood, an in situ study revealed a possible three-stage process from an induction period for forming subdomains to multiscale aligning events, in which each stage is proposed as a result of different degrees of irradiation. At low amounts of irradiation, azobenzene mesogens isomerize to the less energetically favored cis-state until this transformation plateaus. In the second stage, the *cis*-isomerized azobenzene moieties undergo a highly cooperative alignment process with the BCPs where ordered domains can realigned through a nucleation and growth mechanism. Stage three involves the fusion of domains to grow the aligned grains.[285] This hypothesis was supported by the observation of a rapid BCP domain spacing shrinkage upon illumination due to the softening of the azobenzene matrix.

Orientation direction of BCP nanodomains after photoalignment is usually perpendicular to the plane wave's electric field vector, *E*, of linearly polarized light, while in some cases it could also be sensitive to the film thickness. Early work demonstrated a critical film thickness for controlling the alignment direction of a BCP consisting of polyethylene oxide and polymethacrylate with azobenzene units decorated side chains.[286] When the BCP film thickness is above 70 nm, out-of-plane orientation is achieved for cylindrical domains and decreasing film thickness below a threshold thickness of several tens of nanometers leads to a change in alignment to the in-plane direction. Yu et al. performed a series of systematic investigations to understand the impact of many processing parameters such as light intensity, film thickness, and polymer molecular weight of a model diblock copolymer on the alignment direction.[287] It was found that increasing light intensity greatly reduced the required amount of illumination time to produce a phase/orientation transition in BCP films. However, photothermal degradation could occur at elevated intensities (>100 mW cm^{-2}). This work also observed that at film thicknesses less than 80 nm, phase transitions occurred in less than 2 s throughout the film, but at shorter exposure times or for thicker films, the induced ordering began to attenuate closer to the film-substrate interface. Additionally, BCP with higher molecular weight could result in higher viscosities and inhibiting the photoinduced alignment of their nanodomains. Recent work demonstrated photoalignment through the development of liquid crystal BCPs bound by halogen bonding. This supramolecular liquid crystal BCP is able to produce highly ordered nanostructures that were susceptible to photo-alignment/photo-reorientation.[288] In another seminal work, azobenzene and siloxane copolymers were used to induce assembly through exposure to linearly and circularly polarized light. The difference in polarization resulted in distinct morphological characteristics and could be performed at room temperature without necessitating plasticization or additives.[289] Since this method mainly requires light and specialized photoresponsive groups on polymer chains, we believe there are many opportunities to combine this method with other aligning techniques to achieve highly ordered structures over large areas, or possibly selectively pattern/orient BCP morphologies at different regions. For example, applying a photomask to a BCP film during annealing could allow for long-range order to be established in the film, while illuminating exposed regions could result in altered orientations of the BCP domains for simple methods of developing patterned morphologies. In addition, the light regulation of nanostructures shows its capability to easily pattern, align, and rewrite BCP nanostructures over a local area,[288,290] which is very important for many BCP applications such as for templating synthesis of nanoparticles and producing hierarchical patterns of functional materials.

2.5. Directed Self-Assembly

Directed self-assembly (DSA) integrates "top-down" and "bottom-up" approaches for producing highly aligned nanopatterns by utilizing prepatterned substrates to guide microdomain formation of BCP thin films as shown in (**Figure 9**).[291–296] As this is one of the most well-developed fields in BCP nanostructure alignment, a number of excellent reviews already have comprehensive discussion focusing on this area.[105,160,163] Here, we will only succinctly discuss the physical (graphoepitaxy) and chemical (chemoepitaxy) patterning of substrates to induce nanostructural alignment in BCP systems.

Two main DSA techniques are graphoepitaxy and chemoepitaxy, which involve topographical and chemical patterning of a substrate surface to direct the orientation of BCP self-assembled nanostructures, respectively.[105] Rectangular trenches are most commonly used in graphoepitaxy, in which preferential wetting of a BCP component with side walls enforces BCP nanodomains to align along the trenches, leading to effective density multiplication of original patterns when there is commensurability between the BCP domain size and trench width.[297,298] Many studies also utilized more geometrically complex patterns on substrates, such as 2D postarrays, for controlling both in-plane and out-of-plane orientation of BCP nanopatterns through manipulating the distance between the periodic posts.[299,300] Russell et al. employed faceted surfaces of commercially available sapphire for generating hexagonally packed cylindrical domains (3 nm in diameter) that are normal to the film surface with perfect orientational order over large areas.[301] The effectiveness of graphoepitaxy is generally dependent on many important parameters including

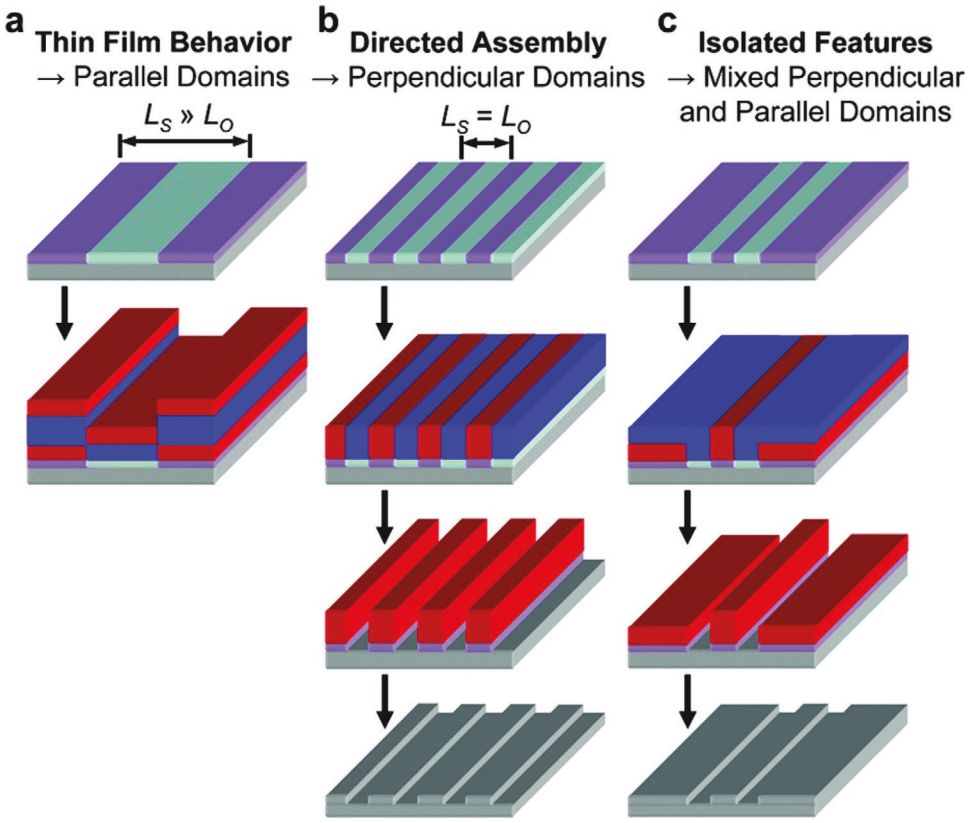

Figure 9. Scheme depicting the use of chemically patterned substrates to direct the self-assembly of BCPs. The top row represents patterned substrates where the different colored regions depict chemical patterns that are preferred by one of the blocks of a BCP. The second row of images demonstrates the effect of the chemical patterns, showing the BCP domains preferentially assembling on their respective regions of the chemical pattern. The third and fourth rows show how portions of the BCP domains can be selectively removed in order to provide materials for further applications. Reproduced with permission.[296] Copyright 2007, American Chemical Society.

the commensurability of BCP domain size and substrate pattern lateral dimensions, the interfacial interactions of the BCP segments with the substrate, substrate surface roughness, and film thickness.[302–305] Furthermore, modifying patterned substrate surfaces with random copolymers can establish neutral layers for encouraging vertically aligned BCP domains through the film thickness direction.[306] As opposed to graphoepitaxy, which uses physical confinement to induce alignment, the chemoepitaxy method takes the advantage of surface energy contrast from chemical heterogeneity of the substrate to register directional BCP nanodomains.[307,308] By lithographically patterning grafted polymer chains or monolayers on the surface, one particular BCP component can be thermodynamically favored to assemble on top of the chemically modified regions.[309,310]

Pioneering work in this area demonstrates the ability to control BCP domain alignment using heterogenous inorganic surfaces.[311] Nealey et al. have successfully employed advanced lithographic processes to produce well-defined chemical patterns for aligning cylindrical and lamella-forming BCPs.[309,312] The resulting BCP morphology from DSA methods is sensitive to the substrate pattern size relative to its BCP domain periodicity. For example, perpendicularly oriented BCP lamellae are formed when these two values are very close.[309,311,313–316] Similar to graphoepitaxy, preferential chemical stripes can also be placed at varying distances equal to integer multiples of the natural size of the domains, thus allowing the domains to align in between the trenches on the substrate.[156,296,317,318]

Compared with other aligning techniques, DSA provides extraordinary ability to induce exquisite control of BCP nanostructure orientation in thin films for achieving nearly single-crystal texture, but it also requires expensive instruments and a sophisticated fabrication process. The development of this field has been highly relevant with the microelectronic industry as a device-oriented manufacturing process due to its advantages of density multiplications for reducing electron beam lithography write time and pattern rectification for improving line edge roughness of resulting patterns.[160,319,320] There are also several other important aspects for implementing BCP DSA techniques for the nanopatterning industry such as pattern transfer, BCP etching contrast, and servo formation that are not covered in this review but interested readers can refer to excellent reviews from other research groups.[159,321,322]

It is important to note that while most alignment techniques are focused on planar geometries, work has been done to investigate alignment techniques of BCP samples of arbitrary shape. Kim et al. presented a technique centered around chemically modified graphene to direct the self-assembly of PS-*b*-PMMA thin films.[323,324] Through casting graphene oxide monolayers,

followed by subsequent thermal reduction to graphene, a neutral surface is provided and the BCP is directed to assemble into perpendicular domains. BCPs of both lamellar and cylindrical morphologies were demonstrated to be applicable to this technique, providing ordered structures, which could be further useful in BCP nanolithography.

2.6. Interfacial Engineering

Engineering interfacial energies of polymer thin films, at both the air–polymer interface and polymer–substrate interface, enables the production of highly oriented BCP nanodomains in the direction perpendicular to the substrate.[325] Similar to directed self-assembly, both physical confinement and chemical interactions determine the final morphology of the ordered BCP domains. When a neutral layer is established on the polymer-substrate interface, no preferential wetting behaviors from distinct BCP segments exist, and thus, in most cases, leads to out-of-plane oriented domains since all blocks want to be present at the interface.[325–329] The modification of substrate surface energy to create such neutral layer can be achieved by using random copolymer brushes that are either crosslinked,[330–333] covalently grafted,[334,335] or physically adsorbed on the substrate.[336] Additionally, the composition of the neutral layer does not need to strictly match with the BCP chemistry, as homopolymer,[336,337] random copolymer,[338–340] graphene,[324,341] teflon,[342] and polydopamine all demonstrate the ability to produce a neutral layer for yielding vertically aligned BCP thin films.[343,344] Utilizing a self-assembled BCP monolayer that is chemically or physically attached to the substrate surface is also an effective strategy to provide a neutral wetting layer.[338] While controlling the polymer-substrate interfacial energy produces aligned domains, this influence usually only dominates at the bottom few layers of the BCP film and can dissipate away from the substrate, resulting in a loss of alignment near the air-polymer interface.[333] Therefore, producing a neutral air–polymer interface is essential to generate highly aligned vertical domains through the entire film thickness. Thermal annealing of PS-*b*-PMMA thin films within a specific temperature window has been extensively studied for achieving this neutrality since the surface energy difference between PS and PMMA domains vanishes at high temperatures.[100,331,345,346] Alternatively, solvent vapor annealing of BCP thin films at optimized processing conditions, such as selected vapor pressures, can produce a neutral free surface.[88,90,91,326,347,348] Since the neutral surface is only present during processing in the aforementioned methods, many methods often require a sequential step of rapid cooling or fast solvent removal to kinetically trap oriented BCP domains.[90,92,100,167,349–351] Furthermore, the effectiveness of these methods is largely dependent on polymer chemistry and can be challenged when a BCP consists of segments with large differences in surface energy.

Introduction of a top-coating layer to manipulate the air–polymer interface is another generalizable approach, which typically uses a polymer film that is neutral, or very weakly preferential, to the blocks of the BCP film. As demonstrated in **Figure 10**, the nonpreferential interactions of the blocks at the air–polymer interface allow for the perpendicular domains to propagate throughout the thickness of the film.[352–357] However, the

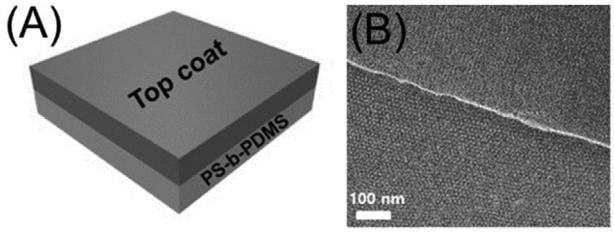

Figure 10. Schematic demonstration of the effect A) a top-coat layer on B) a BCP film nanostructure. The AFM image of a BCP film depicts perpendicularly aligned cylinders in portions of the film covered with the top-coat, and parallel alignment in regions that were exposed during solvent annealing. Reproduced with permission.[357] Copyright 2015, Wiley-VCH GmbH.

top-coating layer must be sufficiently thin, or be able to be removed from the surface of the thin film without causing damage in order to preserve intended material functionality. These topcoats are often spin-coated directly on the surface of the thin film but can also be deposited from the vapor phase.[325–328,354,357] Nealey et al. demonstrated using initiated chemical vapor deposition (iCVD) to graft a topcoat onto the BCP-free surface through film exposure to monomer vapor and initiator in a vacuum chamber with thermally initiated free-radical polymerization.[358] The resulting topcoat layer on the BCP film was neutral to both blocks and allows for through-film thickness orientation of the BCP domains upon thermal annealing. Furthermore, this top-coating strategy can be achieved by the inclusion of polymeric additives into a BCP thin film, in which the additives can segregate to the top of BCP film and balance the surface tensions after annealing for generating highly oriented out-of-plane nanodomains.[359,360] The interfacial engineering method can often be combined with other methods such as DSA for producing large-area vertically oriented domains with single-crystal texture.

2.7. Zone Casting/Deposition/Annealing

Zone casting, originally developed to align small molecule crystallites in thin films,[361,362] can be performed by supplying a solution of BCP molecules through a nozzle onto a moving substrate in a continuous manner. As the solvent evaporates, ordered BCP domains are able to orient perpendicularly to the substrate and/or the direction of motion. Kowalewski et al. investigated the development of long-range ordered block copolymer films through zone-casting. Using a model lamellae-forming diblock copolymer poly(butyl acrylate)-*block*-polyacrylonitrile (PBA-*b*-PAN), films were cast through a nozzle onto the substrate that was moving at a constant rate (**Figure 11**). The nanostructures of deposited films exhibited a high degree of orientation (perpendicular to the substrate) across the entire sample, and the mechanism of forming perpendicular domains with respect to the flow direction is due to BCPs being driven to align along the solvent evaporation front.[363] Further experiments demonstrated the potential for implementation of zone-casting to commercially viable processes. The aligned PAN domains of the BCP films were stabilized at elevated temperatures and carbonized, resulting in mesoporous carbon films through converting aligned PAN domains to carbonaceous materials and complete removal of PBA domains via thermal decomposition. Subsequent work extends

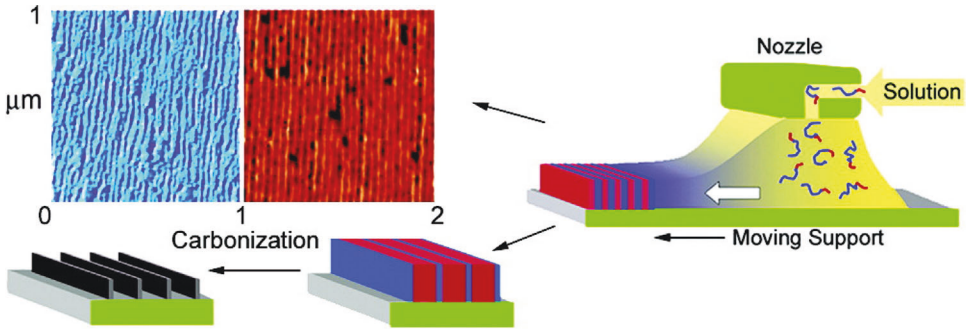

Figure 11. Schematic representation of zone casting where polymer solution is fed into a nozzle and cast onto a substrate. Lamellar domains are oriented perpendicularly to the substrate. In this work, the well-ordered nanostructures of a PAN-*b*-PBA BCP before and after carbonization of the PAN block are depicted in the AFM images. Reproduced with permission.[363] Copyright 2005, American Chemical Society.

this method to cylinder forming BCPs, showing the zone casted films contain vertically aligned domains and the grain size increases with decreasing substrate velocity.[364]

Zone annealing is another method that requires localized heating for providing alignment of BCP domains that was first established in the field of metallurgy for crystal-forming materials.[365] Briefly, the BCP domain alignment from zone annealing is accomplished by applying a moving thermal gradient across a BCP film where alignment occurs along the planar front of the cooling thermal gradient.[157,366–368] Traditional zone annealing is carried out above the T_{ODT} of the BCP system, but cold zone annealing, CZA, is performed in the temperature range between the T_g of all segments and T_{ODT} of BCPs. Karim et al. demonstrated the successful use of CZA to enable cylinders to be perpendicularly aligned to the substrate in PS-*b*-PMMA films.[369] The CZA technique provided control over the perpendicular orientation of the cylindrical domains and the aligned films exhibited grain sizes of up to 1 μm. Importantly, this work employed a "sharp" temperature gradient with a 45 K difference between the heating and cold sections on the substrate, which is largely responsible for the control over domain order. In later works, CZA was used to align the systems composed of BCPs/surfactants and oligomeric resol matrices.[370,371] Using poly(ethylene oxide)-*block*-poly(propylene oxide)-*block*-poly(ethylene oxide) (PEO-*b*-PPO-*b*-PEO) triblock copolymers, the characteristics of the BCP nanostructure was tuned by manipulating the moving velocity of the thermal gradient. It was determined that at low velocities, the cylinder forming BCPs were aligned perpendicular to the direction of the moving thermal gradient. Upon increasing the velocity, the orientation of the BCP cylinders abruptly changed to parallel to the movement direction, which was attributed to the development of shear forces from the flow caused by motion of thermal gradients. This work also elucidated the effect of BCP chemistry and composition on the degree of alignment induced through CZA. Specifically, increasing the molecular weight of BCPs, and consequently their viscosity, leads to more hinderance to perfectly align nanostructures.

Electrospray deposition is an important continuous processing method for locally producing aligned BCP thin films on a substrate.[372–374] A dilute BCP solution is subjected to high voltages in a capillary and upon exiting the capillary, the shear stress produced by the electric field causes the solution to elongate and form a jet, which subsequently breaks down into droplets and are deposited onto the substrate and heated to allow polymers to equilibrate.[373,375] Optimizing different processing parameters for the electrospray deposition of BCP films is important to achieve high degree of orientation, including solvent choice, substrate temperature, BCP–substrate interactions, and the induced flow rate of the solution.[372,373] Specifically, previous work demonstrated this technique can be used to kinetically trap vertically aligned BCP cylinders before allowing them to equilibrate to their preferred state, parallel to the substrate, which removes the requirement for substrate neutralization treatments prior to deposition.[376] Out-of-plane aligned cylinders were achieved by manipulating solvent conditions, as well as the collection distance of the substrate from the nozzle. Generally, solutions containing more volatile solvents can exhibit a higher dependence on the collection distances for producing highly aligned cylinders along the out-of-plane direction. This is due to the requirement of a small amount of residual solvent in the deposited films to provide chain mobility for orienting the BCP domains. Zone casting/deposition represents a promising strategy for addressing pressing needs for directly achieving aligned BCP nanostructures via rational design of a film deposition process and could be potentially applied to different BCP chemistry/compositions. This continuous fabrication method is also highly beneficial from an industrial production perspective. Future work to rationalize these approaches to a broader selection of BCP systems would allow further exploration of on-demand alignment control over nanostructured thin films with tailorable composition and structures.

2.8. Combined Techniques for BCP Alignment

As previously discussed, a wide variety of techniques have been developed for aligning BCP domains across many systems. In order to fully leverage the power of these techniques, work has been done to combine multiple of these approaches to further enhance alignment in BCP systems. Most often, these approaches involve directed self-assembly of BCP systems through physical confinement, while using various other techniques to further facilitate alignment of the assembled domains. For instance, Nealey et al. aligned PS-*b*-PMMA thin films using chemically altered, topographically patterned substrates. By coating grooved substrates with a surface-neutralizing random copolymer brush,

highly ordered, perpendicular lamellar domains were achieved which could be applied to further lithographic applications.[377] Russell et al. demonstrated a simple and versatile approach which incorporated graphoepitaxy and solvent vapor annealing in order to align PS-*b*-P2VP thin films.[378] Patterns were generated into various substrates by simply dragging a poly(tetrafluoroethylene) (PTFE) block across the surface of the substrate above the PTFE melting temperature. A highly ordered pattern of PTFE was then transferred to the substrate through friction to provide topographic confinement and induce alignment in the cast BCP films. After casting, the BCP films were swelled with solvent vapor, and ordering was enhanced, compared to samples cast on substrates without the PTFE pattern. This work provides a simple, cost-effective method to develop anisotropic BCP films on various substrates.

More complex approaches, such as electric field alignment, have also been demonstrated as compatible with graphoepitaxy. PS-*b*-PI BCP thin films were aligned within a fabricated mesh of interconnected nanoconfined channels, facilitated through the application of an electric field.[379] Electric field-aligned samples exhibited single-orientation domains of the cylinder forming BCP. When quadrupolar electrodes were used to apply the electric field, the orientation of the sample could be readily switched between the possible structures. Ross et al. demonstrated a similar technique to align PS-*b*-PDMS BCPs which were confined within topographical trenches, swelled with solvent vapor, and subsequently aligned through the application of an electric field.[380] By manipulating the size of the confining trenches, and the direction of the applied electric field, the ordered cylindrical domains could be controllably oriented in various directions parallel to the substrate. An important note found by this work regarding the combination of these two techniques is that at narrow trench widths and short annealing times, mass transport of the polymer from the trench wall competes with the electric field, resulting in reduced degrees of alignment.

Various unique thermal techniques have also been used to further facilitate BCP alignment under physical confinement. Berggren et al. found that a thermally induced shear stress created through differences in thermal expansion of a BCP film, the substrate, and a rigid inorganic topcoat, could successfully orient domains of the BCP.[381] This was accomplished by controllably cracking an SiO_2 topcoat on the surface of a PS-*b*-PDMS film which resulted in rapid ordering of the cylindrical structures in less than a minute of processing time. Importantly, these combinations of techniques could provide highly valuable insight into the development of practices to fabricate highly aligned BCP structures.

3. Anisotropic Properties from Alignment

The alignment of BCPs that are composed of blocks with distinct physical characteristics can lead to directional dependencies in many material properties, such as chain diffusivity, rheological and mechanical properties, and ionic/electrical conductivity. This section will highlight the development of anisotropic material properties from BCP nanostructural alignment. Understanding structure-property relations of these aligned BCPs is important for their implementation in many practical applications that will be discussed in Section 4.

3.1. Anisotropic Diffusion

The diffusivity of an individual BCP chain along the microdomains (D_{par}) and across the microdomains interface (D_{perp}) can be substantially different when the nanostructure is aligned. For the self-diffusion behaviors of a diblock copolymer (i.e., AB-type), the A segments need to overcome a thermodynamic barrier that is exponentially dependent on χN for diffusing through the B-rich microdomains. Therefore, the diffusivity across the microdomain interface in a BCP follows a hindered diffusion mechanism.[382] For unentangled BCPs, polymer chains can diffuse along the microdomain interface without the occurrence of significant mixing between A and B blocks, however for entangled BCPs, these chains have to follow a reptation process to diffuse along the interface, forcing the mixing of A and B blocks at the interface. As a result, the degree of entanglement plays a critical role on determining the anisotropic self-diffusion of polymer chains in aligned BCP systems.[383]

In general, the anisotropy in the diffusion coefficient of polymer chains along and across the microdomain interface decreases when polymer chains are more entangled. This is because the polymer chain entanglement makes it more difficult for molecules to "reptate" through the matrix without mixing different blocks, which often leads to low (or even undetectable) anisotropy of diffusivity in aligned BCPs.[384–386] For example, Lodge et al. measured the anisotropic diffusivity of both entangled and unentangled BCPs thick films (0.6 mm), aligned through the application of an oscillatory shear field parallel to the surface of the film, that contains the same chemical composition and macroscopically aligned lamellar domains by forced Rayleigh scattering.[384,387] The anisotropy in diffusivity (D_{para}/D_{perp}) of a highly entangled and lamellar-forming poly(ethylene propylene)-*block*-poly(ethylene) (PEP-*b*-PE) is < 3 at temperatures below the T_{ODT}.[384] Compared to entangled polymers, diffusion perpendicular to the microdomain interface is much more retarded as opposed to diffusion along the alignment direction for unentangled polymers, which increases as a function of χ. The anisotropy in diffusivity for an unentangled PS-*b*-PI is approximately 40 °C at 90 °C, which is significantly larger than that of the entangled BCP counterparts. The anisotropy of diffusivity decreases to approximately 4 at an elevated temperature of 110 °C, due to a substantially decreased segmental friction factor of PS when the temperature is above its T_g. In seminal works, the anisotropic diffusion of unentangled poly(ethylene-*co*-propylene-*block*-dimethyl siloxane) (PEP-*b*-PDMS) was investigated.[388,389] The PEP-*b*-PDMS BCPs bulk samples were aligned by thermal annealing to produce oriented polycrystalline structures and diffusion coefficients were extracted through the nonexponentiality of signal decay during pulsed field gradient NMR experiments. As a result, the evolution of anisotropic diffusion in the BCP systems was investigated as a function of temperature, and consequently the degree of the alignment of the BCP domains. For a cylinder forming BCP, a decrease in D_{para}/D_{perp} was observed monotonously with increasing temperature (**Figure 12**), indicating a loss of anisotropy of the system as the aligned domains become disordered.[389] The diffusivity along the cylinder interface is approximately 60 times higher than cross the microdomain interface at 60 °C, below the T_{ODT} of the BCP. When temperatures are above the T_{ODT} of the system, D_{para}/D_{perp} decreases to approximately 5.

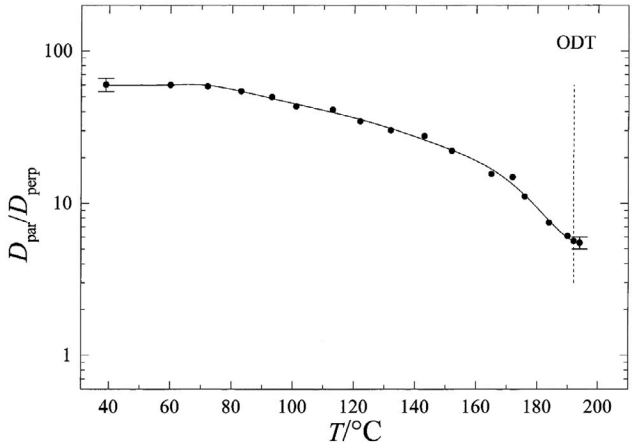

Figure 12. A demonstration of the evolution of anisotropic diffusion in a cylinder forming PEP-*b*-PDMS BCP as the sample becomes more ordered below its T_{ODT}. With decreasing temperature, the BCP domains become more aligned, resulting in increased anisotropy of diffusion. Reproduced with permission.[389] Copyright 1999, American Chemical Society.

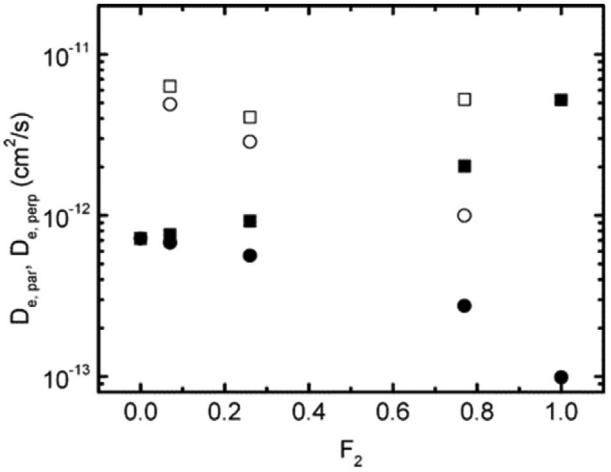

Figure 13. The effect of the degree of alignment (F_2) on the theoretical (open markers) and experimental (closed markers) diffusivity values for diffusion parallel (squares) and perpendicular (circles) to the BCP domain interface. F_2 is calculated as a function of the SAXS intensity profiles of the PEP-b-PDMS BCP. Reproduced with permission.[382] Copyright 2004, American Chemical Society.

The use of pulsed field gradient NMR to quantify self-diffusion behaviors of BCPs was also extended to both lamellae and sphere-forming PEP-*b*-PDMS BCPs.[388] Additionally, a large anisotropic diffusivity factor of 83 is found in unentangled poly(ethylene oxide)-*block*-polyethylethylene (PEO-*b*-PEE) with aligned cylindrical morphology,[390] corresponding to the high enthalpic penalty of removing PEO segments from ordered cylinders to insert into another.

The degree of alignment in BCPs is a critical factor for determining the diffusivity of polymer chains in different directions and their associated anisotropic factor. Cavicchi and Lodge measured the diffusion coefficient of an entangled PEP-*b*-PDMS along (D_{par}) and across (D_{perp}) the cylindrical domains with varying degrees of macroscopic alignment of minority PDMS phase (second-order orientation factor F_2 changes from 0.07 to 0.72).[382] **Figure 13** depicts the effect of alignment on theoretical and experimental diffusivity values in the PEP-*b*-PDMS. In all cases, D_{par}/D_{perp} is larger than 1. The D_{perp} decreases significantly as the degree of alignment improves, while D_{par} is almost independent on the degree of alignment. Therefore, the apparent anisotropic diffusivity increases as the degree of alignment in BPCs improves.

Moreover, the diffusivity of aligned BCPs also varies in different directions relative to the orientation direction. The angular dependent diffusion coefficients in an aligned BCP can be estimated by Equation 3, confirmed by the experiment results[391]

$$D\ (\phi) = D_{perp}\ \sin^2(\phi) + D_{par}\cos^2(\phi) \tag{3}$$

This equation depicts the angular dependence of overall polymer diffusion properties as a function of the diffusion coefficients across the microdomain interface, along the microdomain interface, and the orientation angle. As the angle difference increases, the anisotropy of the system decreases, resulting in a lower effective diffusion coefficient of the system.

3.2. Rheological and Mechanical Properties

Mechanical and rheological properties are key parameters that must be considered to implement BCPs into applications such as tissue engineering,[392–394] fuel cells,[395–397] and water filtration membranes.[398–400] Previous results have demonstrated that aligned BCPs can exhibit anisotropic viscoelastic behaviors.[401] For example, Luo and Yang investigated the rheological properties of a symmetric diblock copolymer with aligned lamellar layers under a simple shear flow using the time-dependent Ginzburg-Landau method.[402] In their model, the parallel alignment of lamellae is defined as when the lamellar normal is parallel to the velocity gradient direction, and perpendicular alignment is defined as when the lamellar normal is parallel to the vortex direction (transverse). After lamellar domains are oriented by the shear force, they found maximum shear stress becomes larger for the aligned samples, which increases with the increase of χN of BCP systems. In general, both degree of alignment and orientation direction can determine the rheological properties of BCP matrix. Such anisotropic rheological properties in aligned BCPs were also confirmed by many experimental investigations. For an unentangled shear-aligned PS-*b*-PI,[403] distinct differences have been demonstrated in the rheological behaviors between the disordered and aligned lamellar states. Generally, the introduction of aligned domains can induce reductions in both viscosity and compliance when compared to disordered or poorly ordered systems. The storage and loss moduli, as well as the compliance of the highly aligned BCP sample, were in agreement with calculations from the Rouse model. This result demonstrates that under these conditions, molecular relaxation is the slowest mode of relaxation in the aligned samples, indicating very limited contribution from large concentration fluctuations due to polymer chains continuously attempting to equilibrate that has been observed in disordered samples. Moreover, Noda et al. studied the shear-rate dependence of N_1 (first normal

stress difference) of PS-*b*-PI in a concentrated solution, where the alignment is in situ formed during the measurement (shear-induced alignment). When the alignment is weak, N_1 was proportional to shear rate $\dot{\gamma}$ at low shear rate region, and increasing the degree of alignment at higher shear rate leads to N_1 being proportional to $\dot{\gamma}^2$.[404,405] These results demonstrate the impact of microdomain alignment on the shear rate dependence of normal stress differences in BCP systems. Wilhelm et al. employed a combination of in-situ rheology and small-angle X-ray scattering to investigate polymer rheological and structural responses to various strain amplitudes of oscillatory shear using PS-*b*-PI as a model system.[406] Azimuthally averaged SAXS patterns and G" measurements throughout the course of the experiments demonstrated that, for low strain amplitudes, the standard deviation of the first-order scattered reflections and loss moduli of the samples decayed exponentially upon aligning, indicating the development of shear aligned domains. However, the alignment was much less stable when larger strain amplitudes were applied, evidenced by an initial decrease in loss moduli at short time scales, but a disrupted exponential decay as the aligned domains deteriorated.

The mechanical properties of BCPs are also dependent on the degree of ordering and alignment of nanodomains. In some cases, BCPs with slightly improved ordering may result in a significant difference in their derived mechanical properties.[407–409] For instance, at least 50% increase of elastic modulus, 30% increase in fracture strength, and a decrease of onset fracture strain were observed in cylinder-forming poly(butylnorbornene)-*block*-poly(hydroxyhexafluoroisopropyl norbornene) thin films, with domain spacings of 47.2 nm, when their long-range ordering of nanostructures are developed by SVA.[410] Furthermore, when BCPs nanodomains are globally aligned, highly anisotropic mechanical properties can be developed, such as modulus and small strain responses. Early work on understanding the anisotropy in mechanical properties of highly aligned BCP have been primarily focused on thermoplastic elastomers.[411–413] Most of these systems are commercially available, containing a hard glassy domain (PS, minority phase) and a soft rubbery matrix (majority phase). The minority domains of these BCPs can be aligned by several conventional processing methods, such as using shear force from extrusion and injection molding,[414,415] often resulting in pronounced differences in mechanical properties in the directions parallel and perpendicular to the axis of induced shear.

In the early 1970s, Arridge and Folkes investigated the angular-dependent Young's modulus of a unidirectionally aligned PS-*b*-PB-*b*-PS triblock copolymer containing hexagonally packed polystyrene cylinders as a minority phase.[416] The Young's modulus along the orientation direction is significantly higher than that of perpendicular to the orientation direction of the nanodomains, which decreases rapidly as the angular difference (opposed to the alignment direction) increases from 0° to 45° and then remains nearly constant. Similar anisotropic mechanical properties were demonstrated for glassy BCPs that have rubbery domains as a minority phase. For example, PS-*b*-PDMS thin films with the aligned cylindrical structure were aligned by using cold zone annealing-soft shear method,[417] and their angular dependent mechanical properties are characterized by wrinkling methods.[418–421] As shown in **Figure 14**, the modulus of the PS-*b*-PDMS is directly dependent upon the angle of the applied strain.

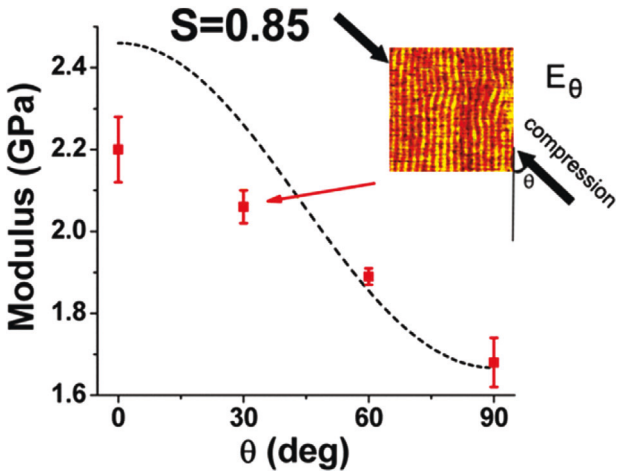

Figure 14. The effect of the angle of applied strain with respect to the oriented domains of a cylinder-forming PS-b-PDMS BCP on the BCP film modulus demonstrating increased modulus along the orientation direction of the cylinders. The moduli of the films were determined using established surface wrinkling methods. Reproduced with permission.[417] Copyright 2013, American Chemical Society.

When the strain is along the aligned cylinders, the modulus exhibits a maximum at approximately 2.2 GPa which decreases significantly as the strain direction is altered to be perpendicular to the aligned cylinders. The dashed line in Figure 14 is a theoretical prediction for the modulus of the film at varying angles, when the systems are perfectly aligned. At high angles, the data is in good agreement with the model, but deviates at low angles, which this discrepancy is as a result of the film not being perfectly aligned (orientation factor = 0.85).

Additionally, this work indicated that the mechanical properties of the BCP film were directly determined by the degree of global order of the BCP domains. The modulus in the direction parallel to the oriented cylindrical domains increases as the degree of orientation improves, while the modulus in the direction perpendicular to the cylinder orientation direction is much less dependent with the degree of microdomains orientation. Moreover, the angular dependent modulus for the best aligned PS-*b*-PDMS thin film can be successfully described by the classical composite theory for aligned systems, such as fiber-reinforced systems and drawn semi-crystalline polymers,[417,422,423] using the following equations,

$$1/E_\theta = \frac{1}{E_{90}}\sin^4\theta + \left(2S_{13} + S_{44}\right)\sin^2\theta\cos^2\theta + \frac{1}{E_0}\cos^4\theta \quad (4)$$

$$S_{44} \approx \left(1 + f_{\mathrm{PDMS}}\right) / \left[\left(1 - f_{\mathrm{PDMS}}\right) G_{\mathrm{PS}}\right] \quad (5)$$

$$-S_{13} = \upsilon_{13}/E_{90} \quad (6)$$

where G_{PS} is the shear modulus of PS phase and υ_{13} is Poisson's ratio. The classical composite theory for the aligned system can also be generalized to other BCPs with other morphologies, such as lamellae-forming PS-*b*-PB-*b*-PS triblock copolymers.[424–426] The mechanical properties of BCPs with aligned double gyroid phase can also exhibit large anisotropy, as evidenced by the modulus along the oriented [111] direction of gyroid structure

in PS-*b*-PI-*b*-PS being approximately five times higher than that of transverse to this direction.[412] In this work, the authors attributed the higher yield stresses along this axis to the nanostructure, rather than the volume fraction of the glassy block in the BCP. Alterations in the SAXS patterns upon the onset of necking suggest that the three-dimensionally interconnected domains deform synergistically along multiple planes to provide improved mechanical properties. Furthermore, stretching parallel to the [111] direction can result in the formation and propagation of a distinct neck in BCP films while stretching in the transverse direction to [111] only leads to diffused yielding without the formation of a distinct neck.

It has been shown that blending BCPs composed of aligned domains with homopolymers can impart improved mechanical properties of the BCP into the behavior of the entire composite. Through multilayer coextrusion and alignment of poly(methyl methacrylate-*b*-butyl acrylate-*b*-methyl methacrylate) (PMA-*b*-PBA-*b*-PMA) and PMMA, alternating layers with distinct components were fabricated.[427] These systems demonstrated approximately 20 times higher fracture toughness than pristine PMMA films, and roughly five times greater toughness than conventionally extruded BCP/homopolymer blends where the alignment of nanodomains is absent, demonstrating the toughening effect from domain orientation. The effect of the alignment of BCP domains on mechanical properties has also been investigated in other BCP systems. For example, Picken et al. demonstrated this concept through spinning fibers of poly(p-phenylene terephthalamide)-*block*-poly(amide 6,6) BCPs.[408] The increase of draw ratio results in enhanced the moduli of fibers due to the alignment of polyamide segments within the BCPs through the production of the fibers.

3.3. Anisotropic Ionic/Electrical Conductivity

A key application for nanostructured BCPs is their use for ion-conducting membranes in many energy applications such as batteries and fuel cells.[428–432] Briefly, these BCPs are often composed of microchannels for desired ion transport and glassy domains for the enhancement of mechanical integrity. The effect of different BCP domain morphologies of fabricated ion-conducting membranes has been demonstrated to affect the transport properties of the systems. For example, Balsara et al. investigated the effect of different morphologies on the transport of bis(trifluoromethane)sulfonimide lithium (LiTFSI) salt ions in polystyrene-*block*-poly(ethylene oxide) (PS-*b*-PEO) BCPs, where the PS segments acted as glassy mechanical supports and PEO domains facilitated ion transport.[433] This work demonstrated that morphologies containing 3D ion-conducting pathways (gyroids, cylinders, and spheres with PEO as the majority domain) greatly outperformed lamellar and other morphologies where the PEO domains are not interconnected, which was also confirmed by simulation studies from Hall et al.[147] Notably, this work also determined the effects of tortuosity in different morphologies on the ion conduction. When ion conduction pathways are established as the majority phase in a gyroid morphology, the lowest tortuosity and highest performance of the 3D phases are achieved. In general, improving the degree of alignment and ordering in BCPs can significantly enhance the transport behaviors

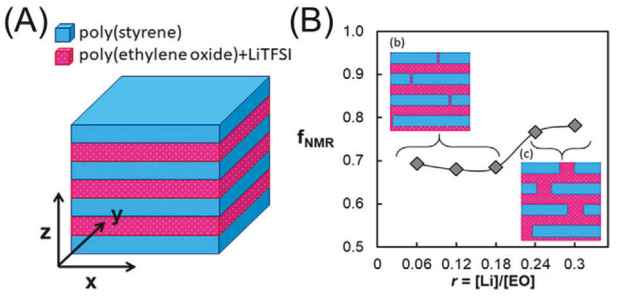

Figure 15. A) Schematic of ordered PS-*b*-PEO lamellae with LiTFSI included in the PEO domains. The provided axes can be used to demonstrate the orientation of diffusion vectors where *x* and *y* represent diffusion through the lamellae, and the *z* axis represents diffusion across the lamellar domains. B) Depiction of the effect of defect size on the morphology factor (f_{NMR}) as calculated through NMR. Reproduced with permission.[431] Copyright 2018, American Chemical Society.

of different species within the nanochannels, thus controlling their macroscopic properties.[434–438] In addition to the nanostructure ordering, the alignment of microdomains in BCP membranes often triggers anisotropic ion/proton diffusion behaviors, and optimizing the alignment degree could further enhance the conductivity of these BCP membranes by minimizing the presence of defects and/or structural tortuosity.

The anisotropic ion diffusion in PS-*b*-PEO containing LiTFSI with macroscopic aligned lamellar structure was investigated by pulsed-field gradient NMR as shown in **Figure 15**.[431] A morphology factor (f_{NMR}) is used to estimate the anisotropic ion transport, which is defined as

$$f_{NMR} = \frac{D_{xx} + D_{yy} + D_{zz}}{3D_{xx}} \quad (7)$$

where D_{xx} and D_{yy} are the diffusion coefficients parallel to the lamellae plane, and D_{zz} is the diffusion coefficient normal to the lamellae plane. f_{NMR} equals to 2/3 for a perfectly aligned lamellar structure in a BCP membrane assuming ions could not diffuse through the PS phase while f_{NMR} equal to 1 represents a completely isotropic BCP matrix. The experimental results show the diffusion coefficient parallel to the lamellae (D_{para}) is an order of magnitude larger than that perpendicular to the lamellae direction (D_{perp}) at low salt concentrations. The difference between D_{para} and D_{perp} becomes less pronounced as the salt concentration increases. Correspondently, f_{NMR} is approximately 2/3 for PS-*b*-PEO/LiTFSI at low salt concentration and increases to approximately 0.8 at high salt concentration due to more defects formed in lamellar domains induced by high salt content, leading to possible ion transportation across neighboring domains. Similarly, the anisotropic proton conductivity of poly(styrenesulfonate)-*block*-polymethylbutylene films with aligned lamellar structure was studied using a variety of different established techniques.[122] The flow and electric field aligned lamellar domains resulted in the highest proton conductivities normal to the plane of the film which is important for many practical applications.

Anisotropic ionic conductivity can also be developed in BCP membranes with aligned cylindrical domains. Iyoda et al. fabricated PEO-*b*-PMA/lithium trifluoromethanesulfonate

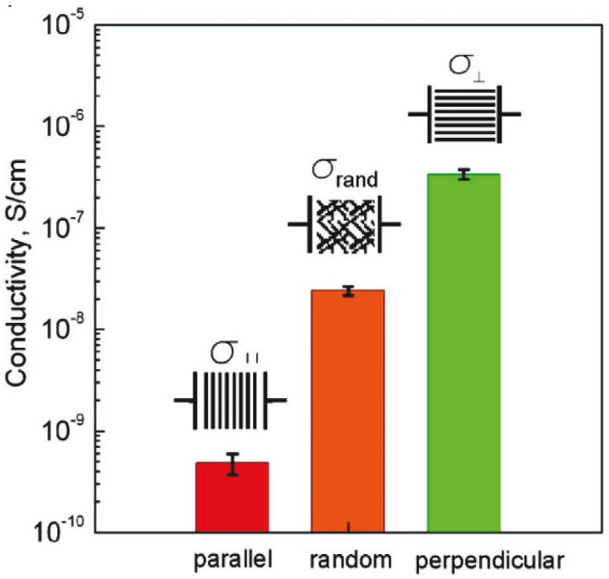

Figure 16. The electrical conductivity of 120:1 molar ratio PEO:Li+ BCP aligned in 5 T magnetic field parallel and perpendicular to the plane of orientation, as well as randomly oriented BCP domains. The conductivity perpendicular to the alignment direction exhibits hindered mobility across the domain interfaces, while the conductivity parallel to the orientation of the BCP domains is facilitated by transport of the ions through the conducting channels. Reproduced with permission.[149] Copyright 2010, American Chemical Society.

($LiCF_3SO_3$) membranes with vertically aligned cylinders by a thermal annealing method, where the oriented PEO cylinder domains serve as channels for ion transport.[439] In this study, the ionic conductivity along the oriented cylinder axes is observed to be much higher than that across the cylinder orientation direction at different Li^+ contents in PEO domains. A high anisotropy in ionic conductivity of 450 was found for the aligned BCP electrolytes with a PEO:Li^+ molar ratio of 20:1. The anisotropy in ionic conductivity decreases significantly to 40 as this ratio decreases to 4:1 due to disturbing the ordering and alignment in BCP nanostructures from high salt concentration. Moreover, Osuji et al. macroscopically aligned, lithium perchlorate ($LiClO_4$) doped, cylinder-forming poly(ethylene oxide)-*block*-poly(6-(4-cyanobiphenyl-4-yloxy)hexyl methacrylate) (PEO-*b*-PMA/CB) by magnetic field and investigated the effect of alignment on the ionic conductivity of these polymeric membranes.[149] The conductivity along the cylinder alignment direction exhibits an almost 10 fold increase compared to that of unaligned BCPs, while the conductivity across the aligned cylinder axis direction is approximately one magnitude lower than that of unaligned samples at room temperature, as shown in **Figure 16**. These results suggest that the high degree of alignment enhances the ability to direct the transport of ions along the aligned channels. Additionally, model systems of lamellar and cylinder forming oligo(ethylene glycol) alkyl ether surfactants were studied in order to systematically assess the anisotropy in transport properties of these mesophases. The mesophases were aligned through the application of a magnetic field, and the conductivity was investigated parallel and perpendicular to the plane of alignment. Interestingly, the results were different from commonly accepted models for uniaxial systems with conductivity enhancements that were significantly higher than the predicted values for cylindrical and lamellar systems, suggesting that theoretical predictions may not consider some practical variables such as disruptions of connectivity and domains that are not infinitely long that can significantly contribute to ionic conductivity.

Study also investigated a BCP system derived from inherently electrically conductive polymers.[440] The polymer system used a conjugated constituent, poly(3-hexylthiophene) (P3HT), to conduct electric charge in tandem with commonly used PEO to conduct ionic charge when mixed with LiTFSI salt. The thick film samples assembled into lamellar domains which became disordered at elevated temperatures and exhibited lower conductivities compared to the ordered counterparts. While the P3HT-PEO system exhibited lower ionic conductivities compared to PEO/LiTFSI mixtures due to the presence of the non-ionically conductive P3HT constituent, the BCP is able to conduct electronic and ionic charges simultaneously. Furthermore, polyelectrolyte systems are generally difficult to align. However, Nealey et al. have employed a method to convert P2VP constituents of a block copolymer film to anionic 2-vinyl n-methylpyridinium groups in situ to provide perpendicularly oriented lamellae that yielded excellent ionic conductivity.[125] Similarly, block copolymer lithography has been used to synthesize anionic and cationic polymer brushes which take on the ordered nanostructure of the BCP template. This method provided polyelectrolyte brushes with desired orientations which exhibited enhanced ionic conductivities.[441]

4. Applications of Aligned BCPs

The ability of BCPs to produce nanostructures with defined orientation enables them to be useful for many nanotechnological applications. As previously discussed, the alignment of microdomains gives rise to various enhanced physical properties that can directly benefit different applications, including but not limited to, nanolithography, patterning, the development of functional porous structures, and filtration membranes. It is worth noting the ion-conduction membranes also represent a large application space for BCPs but will not be included in this section considering they have been discussed at length in the previous section.

4.1. Nanolithography for Microelectronics Fabrication

As discussed earlier, DSA of BCP thin films into ordered and periodic nanodomains provide a great opportunity as patterning templates for large-scale and low-cost nanolithography for microelectronics fabrication.[442] In the 1990s, Thomas et al. suggested the possibility of using monolayer BCPs with 2D ordered spherical structure or perpendicularly aligned cylinder structure for lithographic-based patternings.[443] Since then, numerous research works about BCP lithography have been reported over the past decades with the aim to provide alternative and promising patterning technologies to complement conventional optical lithography, highlighted by several excellent

reviews.[28,291–295,444–448] In a typical nanolithography process using BCPs as templates, a BCP thin film is first aligned to obtain patterned nanofeatures using various annealing strategies as described in the previous section. Subsequently, these nanopatterns can be replicated on a solid substrate by a variety of pattern transfer methods, including dry etching, wet etching, and ion beam etching. To facilitate the transfer of nanopatterns, one of the blocks of the BCP should be selectively etched while the remaining portion can act as an etching mask to replicate the pattern on a solid substrate.[322] Several BCPs, such as PS-*b*-PB, PS-*b*-PI, PS-*b*-PMMA, PS-*b*-P4VP, and PS-*b*-PDMS, with highly ordered structures, have been demonstrated as effective patterning templates for BCP-based lithography technologies.[443,449–455] Additionally, sequential infiltration synthesis (SIS) has been demonstrated as a versatile method for the production of large-area ordered inorganic nanopatterns from polymer templates.[456,457] This technique involves the selective infiltration of inorganic precursors into a domain of the BCP system, followed by subsequent synthesis of the inorganic material. The polymer template can be removed to result in patterned inorganic materials with desired properties for use in various microelectronic applications.

BCP lithography enables the construction of densely packed inorganic nanolines or nanodots for integrated circuits and functional nanodevice applications. Early work from Adamson et al. demonstrated the fabrication of hexagonally packed spherical nanoholes and nanodots on silicon nitride substrates using PS-*b*-PB as the template.[442] Using a similar strategy/concept, various inorganic nanodots or nanowires can be fabricated on semiconducting substrates to construct different functional devices, such as metal oxide semiconductor capacitors,[458] flash memory transistors,[459,460] field effect transistors,[461,462] biosensors, and gas sensors.[3,162,450,463] For example, Gösele et al. fabricated ordered Si nanorods with a highly uniform diameter of 15 nm through BCP lithography method, as shown in **Figure 17**.[464] Specifically in this work, a cylinder-forming PS-*b*-PMMA thin film (thickness: 35 nm) was first aligned perpendicular to the substrate driven by establishing a neutral air-polymer interface. Subsequently, the PMMA matrix was selectively removed by UV exposure to produce a PS nanodots mask. The nanopattern of ruthenium tetroxide-stained PS nanodots was transferred to the underlying silicon nitride (Si_3N_4) by reactive ion etching (RIE) method. Finally, ordered Si nanorods were obtained by removing Si_3N_4 nanorods through the additional RIE step using hydrobromic acid (HBr). Moreover, Ross et al. demonstrated the fabrication of a wide variety of different metallic nanowire arrays, such as Ti, W, Co, Ta, Ni, and Pt, using aligned PS-*b*-PDMS as the templating agent.[465]

High density sub-10 nm nanopatterns for BCP lithography were developed to manufacture ultrahigh density electronic devices in microelectronics industry,[466] typically using low molecular weight and high χ block copolymers since the domain size of a BCP is proportional to $\chi^{1/6}N^{2/3}$ when it is strongly segregated ($\chi N >> 10$).[45,467,468]55–57 Ross et al. fabricated field-effect transistors based on sub-10 nm graphene nanoribbon arrays using PS-*b*-PDMS ($\chi = 0.11$)[466] as the lithography mask.[469] Nealey et al. fabricated sub-10 nm alumina patterns using directed self-assembled P2VP-*b*-PS-*b*-P2VP ($\chi = 0.40$) triblock copolymer pattern as lithography mask.[358] Overall, these examples show the promise of aligned BCP as a facile template to develop high-density nanopatterns of various inorganic materials, which is important for their further use in microelectronics applications.

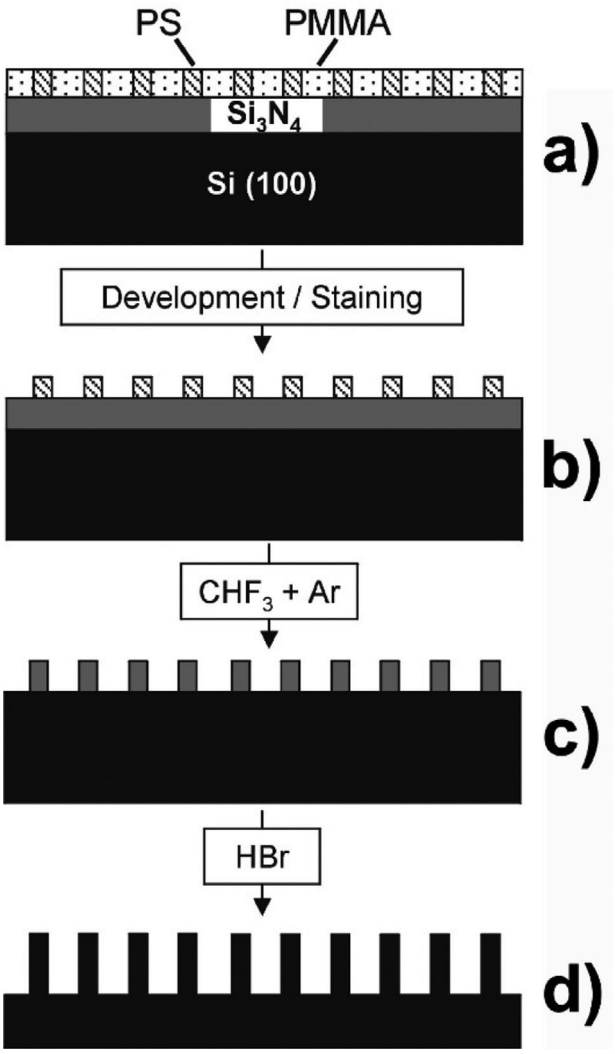

Figure 17. Illustration of processing steps for developing Si nanorods through BCP lithography. Panel A) depicts a Si_3N_4 coated silicon substrate with a thin PS-*b*-PMMA film. B) The cylindrical PS domains are ordered perpendicular to the substrate, forming nanodots upon removal of the PMMA matrix. C) The patterned nanodots are transferred to the Si_3N_4 layer through RIE which act as a mask during. D) Si nanowire fabrication. Reproduced with permission.[464] Copyright 2007, American Chemical Society.

4.2. Nanotemplates for Constructing 3D Nanopatterns

In recent years, aligned BCP nanopatterns have been utilized to effectively construct multilayer or 3D structures of well-aligned inorganic arrays for a variety of applications such as resistors, biosensors, and electrocatalysts,[107,449,470–473] further extending their use in patterning-based nanotechnology. Yager et al. fabricated large-area nanomesh wire arrays with controllable size, symmetry, and compositions using aligned PS-*b*-P2VP patterns

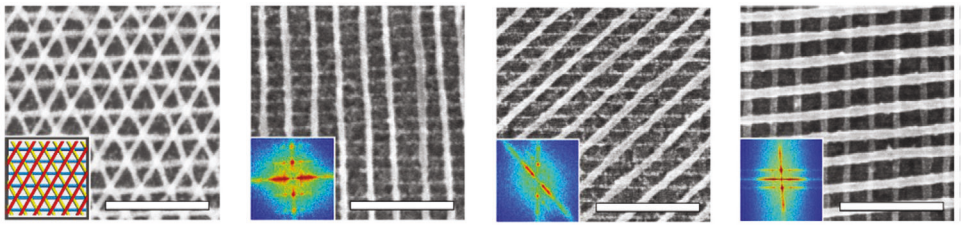

Figure 18. SEM micrographs of inorganic nanomeshes fabricated using unidirectionally aligned PS-*b*-P2VP BCP templates. The BCPs were aligned through a combination of soft shear and laser zone annealing and subsequently converted to inorganic patterns which enabled additional depositions of BCP films to form nanomeshes with varying orientations and compositions. Reproduced with permission.[474] Copyright 2015, Springer Nature.

as templates.[474] Specifically, a PS-*b*-P2VP monolayer with cylinder structure was first aligned by laser zone annealing with soft shear. Subsequently, the aligned P2VP microdomains were converted into metal nanowires using metal salt complexation followed by the removal of polymer components using oxygen plasma etching. Nanomesh structures of metal nanowires were obtained by converting the aligned PS-*b*-P2VP thin films into nanowires through the sequential layer by layer stacking method (**Figure 18**). Similarly, Vogt et al. fabricated a 3D silica nanomesh by stacking two different layers of unidirectionally aligned cylinder forming PS-*b*-PDMS nanotemplates and followed by ultraviolet-zone exposure and calcination in air at high temperature to remove organic components.[475] Very recently, Deng et al. developed a general strategy to construct 3D multilayer-crossed metal oxide nanowire arrays, such as Si-doped metastable ϵ-phase WO_3, through co-assembly of PEO-*b*-PS and polyoxometallates followed by the calcination induced structure transformation. The 3D multilayer-structured metal oxide semiconducting material exhibits not only ultrahigh sensitivity and fast response-recovery dynamics, but also excellent selectivity, rendering it to be an excellent candidate as acetone sensors.[476]

In addition to homogeneous 3D nanostructures, structural complexity and chemical diversity of nanostructures can be derived through BCP nanopatterning approaches, which are promising for advanced electronics, electrocatalysts, and photonics applications.[477–479] Kim et al. demonstrated the fabrication of highly aligned and chemically heterogeneous nanowire arrays with controlled metallic components at desired locations using aligned PS-*b*-P2VP as template.[480] Reversible metal ion loading resulted in metal ion complexation within the BCP nanodomains. The spatial control of these domains was achieved through the application of patterned masks to provide areas of selective chemical segmentation. The alignment of BCP domains provides an important foundation to construct complex 3D structures by providing facile access via bottom-up assembly.

4.3. Deriving Functional Inorganic Porous Materials

Porous carbon materials have attracted much attention due to their excellent properties for various applications, such as energy storage electrodes,[481–484] supercapacitors,[485–487] and separations.[488–490] The properties of porous carbon materials are significantly affected by pore structures, such as pore size, pore connectivity, and ordering of pores.[484,491–493] It is important to note that while most BCP patterning applications involve films with thicknesses that correspond to 1–2 layers of BCP domains, the development of porous materials is often accomplished in films 100 nm to micrometer thicknesses. Aligned mesoporous carbon materials can be fabricated by using BCPs as soft templates.[494–496] In this process, carbon precursors, such as phenolic resins, are typically selectively swelling in the continuous phase of BCPs and a wide variety of BCP systems have been used as structural directing agents.[497–501] After BCP assembly, the precursor matrix can be crosslinked, and then exposed to elevated temperatures (>350 °C) to remove the organic template.[502] PS-*b*-P4VP has been used as a structural directing agent through casting BCP/resorcinol-formaldehyde resin precursor composites. The system was annealed using solvent annealing, and the resin precursor infiltrated the majority P4VP phase of the BCP system. This alignment technique allowed for resin to be crosslinked around the cylinders formed by the PS domains, resulting in pores that are perpendicularly aligned to the substrate upon carbonization.[503] The alignment of BCP templated carbon precursors can be further enhanced by various annealing process.[370,371] For instance, Sakurai et al. demonstrated the use of compressional flow in a cylindrical BCP system to achieve superior orientations of nanostructures.[504] Additionally, Pluronic surfactants and resol carbon precursors have been aligned by simply applying air flow to the surface of the system.[505] Manipulating variables like the airflow velocity and precursor concentration resulted in high degrees of orientation, highlighting the potential of this technique to be applied to large-scale production processes. Using solvent vapor annealing with shear method, mesoporous carbon films with aligned cylindrical structures can be prepared. These samples exhibit anisotropic electrical conductivity with approximately 40% enhancement of conductivity in parallel direction compared to that of perpendicular direction.[274] Moreover, Kim et al. fabricated highly aligned N-doped carbon nanowire arrays by thermal carbonization of aligned PAN domains using PMMA-*b*-PAN.[211] The aligned carbon nanowire array exhibits a much superior NO_2 sensitivity compared to that of a randomly aligned carbon array.

In addition to the production of porous carbons, soft-templating using BCPs as structural directing agents can be employed in the development of other highly ordered mesoporous inorganics, such as metal oxides. Early work in this technique involved assembling Pluronic surfactants with various metal salts with subsequent calcination steps to remove the block copolymer template, resulting in a porous metal oxide matrix.[506] This technique is highly generalizable to a variety of metal oxides,[506–510] but the precursors, namely metal

chlorides, could react violently with alcohols used in processing solutions. Similarly, other approaches have been demonstrated to produce mesoporous metal oxides under more mild reaction conditions.[511–515] However, most examples in the literature associated with the topic are focused on improving the degree of ordering in the developed nanostructures and control over alignment has been rarely demonstrated. Controlling the alignment of these systems could present a large amount of potential in the development of functional inorganics with complex patterns and geometries for various applications.

4.4. Filtration Membranes

Self-assembled BCP thin films have been extensively reported as separation membranes due to wide tunability in morphology, chemistry/chemical composition, functionality, and potential for large-scale manufacturing.[516–520] Well-defined, monodisperse nanopores can be derived by selectively etching or swelling the vertically aligned domains in BCPs, enabling porous membranes with excellent capability for the size-selective separation. Common methods to create these pores include phase inversion,[521,522] selective swelling,[521,523] chemical etching,[398,524] and ultraviolet ozone exposure.[525] The narrow pore size distribution of these BCP-derived membranes provides advantages of high selectivity and high pore densities for enabling a high flux.[526] Therefore, nearly one order of magnitude increase in water permeability can be achieved by using isoporous BCP membranes for ultrafiltration applications compared to commercial membranes with similar pore sizes.[527] For these filtration relevant applications, development of perpendicularly aligned domains throughout the entire film thickness is essential. Leveraging the approaches that are discussed in Section 2, a variety of reports have demonstrated the capability of fabricating filtration membranes from aligned BCP systems. For example, Kim et al. fabricated PS-*b*-MMA thin film with vertically aligned nanopores for efficient filtration of viruses with ultrahigh selectivity and flux.[108,528] The developed membranes have exhibited cylindrical pores with diameters of roughly 15 nm. The size and structure of these pores allowed for high sensitivity to human rhinovirus, responsible for the common cold, rejecting all virion based on size exclusion principles which was evidenced by plaque assays. Russell et al. demonstrated the excellent size selectivity of membranes with high rejection of Au nanoparticles can be achieved from using aligned nanoporous PS-*b*-PMMA thin films as ultrafiltration membranes.[523] The membrane with a pore diameter of 17.5 nm, rejected roughly 87% of 20 nm gold nanoparticles. Upon swelling with acetic acid, the membrane was able to reject 100% of the gold nanoparticles in the process stream which was determined through UV–vis experiments. Cussler et al. fabricated nanoporous PS-*b*-PLA BCP thin films with an approximately 24 nm monodisperse pores for efficient ultrafiltration.[398] While the fabricated membranes exhibited a sharper rejection behavior than many other membranes developed using similar techniques, it suffered from low flux, possibly attributed to the presence of mixed cylindrical morphologies hindering the flow.

Furthermore, many BCPs contain efficient reactive handles for post-modification so that the selectivity and flux of membranes can be readily tuned.[529–531] For example, Abetz et al. demonstrated the tunability of size selectivity of isoporous membranes derived from polystyrene-*block*-poly(2-hydroxyethyl methacrylate) through a chemical post-modification by urethane-based chemistry followed by a thermal annealing process.[530] The resultant membranes show a significant improvement in retention of various investigated proteins. Further work involved the fabrication of PS-*b*-P4VP based membranes with tunable water flux by functionalizing membranes with temperature and pH-responsive polymers, such as poly(*N*-isopropylacrylamide) (pNIPAM) or pNIPAM-NH_2.[532] In this study, the researchers developed membranes with tunable fluxes across a pH range from 3.2-4.7. Additionally, the double stimuli-responsive membranes demonstrated easily tunable flux upon exposure to temperatures varying from 0–50 °C, making them potentially applicable to biomolecule separations. In addition to these ultrafiltration applications, aligned BCP thin films can be also used as pervaporation membranes and membranes for water remediation.[410,525,533,534] In an effort to separate organic molecules with 1–2 nm lateral dimensions, a customized triblock copolymer membrane was developed that underwent post-functionalization to provide unparalleled separation selectivity based on charge of the pore interfaces.[535] The BCP membrane was prepared through phase inversion and then postfunctionalized with gas-surface interface interactions to provide both negatively and positively charged pores. The charged pores were demonstrated to selectively reject charged dyes in mixtures of positive, negative, and neutral species, all less than 1.5 nm in diameter. Similarly, BCP membranes fabricated through phase inversion method were used to investigate the effect of hydrophobicity of solketal methacrylate units on the membrane performance.[536] The results of this work confirmed that inducing hydrophilicity in the fabricated membranes leads to the decreased fouling, evidenced by lower retention of proteins during adsorption experiments. As evidenced by many instances in literature, BCPs provide a platform for functional porous membranes with tunable characteristics that show promise in many applications.

5. Challenges and Outlook

Macroscopic alignment of BCP nanostructure apparently offers massive potential for designing nanomaterials with anisotropic properties for the advancement of nanotechnology, but these optimized BCP systems to date still have been limited in practice. The gap between academic research and industrial relevant applications suggests several critical challenges still remain unresolved despite the varying degrees of success obtained from the rich development of BCP self-assembly. Here, we provide some of our perspectives by identifying three key directions for compelling new and interdisciplinary researchers into this arena in order to further expand the role of macroscopically aligned BCPs in practical applications.

5.1. Scalability

As with many other nanotechnologies, translation of bench-top experiments to scalable production is always a key difficulty. Many reported methods exhibit a high sensitivity to processing

conditions including temperature, humidity, and sample thickness. Therefore, scaling-up existing BCP aligning approaches needs to be carefully designed in order to warrant high repeatability and minimize batch-to-batch variation of material quality. In this regard, continuous fabrication/processing methods are usually preferred, such as roll-to-roll (R2R) manufacturing, which has potential to meet the industrial production volume. Several methodologies introduced in the previous content can be performed on an industrial-scale R2R processing line such as zone annealing and direct immersion annealing.[96,97,369,537,538] Other methods such as raster annealing also show some promises as an inexpensive approach with potentially compatible production rate.[276,539] However, these methods could sometimes suffer from a long processing time for aligning BCP nanostructures (at least hours) since typical workflow of many applications could require multiple processing steps to be finished within minutes.

In this vein, photothermal-assisted BCP ordering methods have much to offer, especially when combined with shear force or epitaxy methods.[474,540–542] Extreme processing conditions with high temperature, high heating rate, and sharp temperature gradient induced by application of illumination or laser energy lead to very rapid ordering and aligning of BCP films over large areas. These robust approaches hold great promise for rapid and scalable production, but most of these reports are so far still focused on in-plane orientation of thin films and the ability of out-of-plane alignment from bulk BCP samples (c.a. >200 μm) remains unclear. While most current photothermal methods require a light-absorbing layer placed underneath the BCP film, a very recent study shows the capability to produce macroscopic alignment of BCPs on silicon substrates using laser-based annealing methods.[103] The expansion of processing windows, as well as substrate selection, would be useful to further enhance the value of these techniques. Additionally, reducing the defect density of BCP films is of paramount importance for their practical implantation into microelectronic applications, which has been explicitly discussed in many research articles.[543–545] Nevertheless, these emerging techniques provide exciting new opportunities to hasten the leap from research lab to large-scale manufacturing.

5.2. Precise Spatial Control

While numerous efforts have been pursued to achieve a perfect "single-crystal" morphology over the entire substrate, many applications actually require complex nanopatterns, meaning fabricating regions that contain different features on one substrate with each region being locally aligned.[296,546–550] Kinetic trapping of a nonequilibrium morphology in a local area with assistance from lithographic patterning provides some degree of flexibility to alter local structure orientation and/or degree of order, but such methods may not be able to produce a highly diverse nanopattern. Alternatively, selective deposition of different BCPs on different regions can lead to a hierarchical nanopattern, but it becomes more challenging when the complexity of final patterning increases since each BCP corresponds to only one fixed size and morphology.[477,551–557] Recently, an in-film polymerization approach is demonstrated to enable local production of homopolymers within a BCP film matrix in order to alter nanostructures (both size and morphology) with simultaneous improvement of the degree of ordering from monomer vapors, leading to distinct morphologies on one substrate when a photomask is applied.[549,550] While this in-film polymerization is still limited with a batch process, this approach opens a new avenue for on-demand nanopattern manipulation over a defined area. Moving forward, it is likely that combining in-film polymerization with other previously established aligning techniques would enable exact registration of local nanostructures over different regions. However, challenges still remain associated with improving nanopattern resolution in the interfacial region between exposed and unexposed areas since it can contain coexistence of two distinct morphologies.

5.3. Advanced Characterization

Concurrent with all of these research efforts, another key component is the development of advanced characterization techniques for high-throughput and real-time study of BCP nanostructural evolution, which is particularly important for revealing fundamental mechanisms associated with aligning dynamics in order to inform improved engineering process design. In situ X-ray scattering measurements have made strides in studying polymer assembly kinetics due to its advantage of high temporal resolution and progress has also been made by using microbeam grazing-incidence small-angle X-ray scattering (μGISAXS) to probe local BCP thin film morphology (50–500 μm beam diameter) and resonant soft X-ray scattering (RSOXS) for resolving structural information over a very large area (≈1 mm^2).[84,348,406,558–565] Recent reports further demonstrate the capability of X-ray-based techniques for studying nanostructural heterogeneity and BCP interfacial roughness.[566–568] Similarly, neutron scattering has also been employed for numerous block copolymer systems.[569–574] These techniques have been successfully implemented for understanding BCP aligning dynamics by providing real-time nanostructure information, but only in reciprocal space and microscopic details such as defect annihilation kinetics and grain growth could be missing.

In order to rationally design processing pathways, it is necessary to directly visualize BCP self-assembly phenomena in real space and real time. Tremendous progress has been made in expanding imaging capability for BCPs including using in situ electron microscopy and atomic force microscopy (AFM) for revealing assembly dynamics at nanometer resolution in order to quantitatively understand important parameters such as activation energy required for defect annihilation in BCP thin films.[575–583] High-resolution transmission electron microscopy has also been employed to image polymer samples with resolutions as low as 3.6 Å.[584–586] Super-resolution optical microscopy has also been introduced to visualize morphological evolution of polymer systems upon solvent swelling, which offers advantages of large imaging volume, non-invasive imaging condition and customizable contrast by fluorophore labeling.[587–596] Finally, theoretical and computational approaches are still at the forefront for providing significant insights about BCP aligning kinetics and recent studies have enabled understanding of processing-dependent polymer properties using dynamics self-consistent field theory (SCFT) and nonequilibrium molecular dynamics.[597–605] It is

apparent that synergizing efforts from computational and experimental approaches is the most effective way to further advance the development of BCPs for future nanotechnology.

Acknowledgements

This work was partially supported by the National Science Foundation Office of Integrative Activities #1757220. M.R. acknowledges traineeship support provided through NSF-NRT "Interface" program (DGE-1449999) through the University of Southern Mississippi.

Conflict of Interest

The authors declare no conflict of interest.

Keywords

alignment, anisotropic copolymers, nanostructures, nanotechnology, patterning

Received: May 10, 2021
Revised: June 23, 2021
Published online:

[1] G. Liu, J. Cui, R. Luo, Y. Liu, X. Huang, N. Wu, X. Jin, H. Chen, S. Tang, J. K. Kim, X. Liu, *Appl. Surf. Sci.* **2019**, *469*, 854.
[2] C. Cummins, G. Pino, D. Mantione, G. Fleury, *Mol. Syst. Des. Eng.* **2020**, *5*, 1642.
[3] H. C. Kim, S. M. Park, W. D. Hinsberg, I. R. Division, *Chem. Rev.* **2010**, *110*, 146.
[4] J. Jeevanandam, A. Barhoum, Y. S. Chan, A. Dufresne, M. K. Danquah, *Beilstein J. Nanotechnol.* **2018**, *9*, 1050.
[5] E. Pomerantseva, F. Bonaccorso, X. Feng, Y. Cui, Y. Gogotsi, *Science* **2019**, *366*, eaan8285.
[6] G. Wei, P. X. Ma, *Adv. Funct. Mater.* **2008**, *18*, 3568.
[7] S. Y. Ding, J. Yi, J. F. Li, B. Ren, D. Y. Wu, R. Panneerselvam, Z. Q. Tian, *Nat. Rev. Mater.* **2016**, *1*, 16021.
[8] Z. Ren, Y. Guo, C. H. Liu, P. X. Gao, *Front. Chem.* **2013**, *1*, 18.
[9] M. Fromel, M. Li, C. W. Pester, *Macromol. Rapid Commun.* **2020**, *41*, 2000177.
[10] S. W. Chung, D. S. Ginger, M. W. Morales, Z. Zhang, V. Chandrasekhar, M. A. Ratner, C. A. Mirkin, *Small* **2005**, *1*, 64.
[11] M. Tu, B. Xia, D. E. Kravchenko, M. L. Tietze, A. J. Cruz, I. Stassen, T. Hauffman, J. Teyssandier, S. De Feyter, Z. Wang, R. A. Fischer, B. Marmiroli, H. Amenitsch, A. Torvisco, M. Velásquez-Hernández, J. de, P. Falcaro, R. Ameloot, *Nat. Mater.* **2021**, *20*, 93.
[12] P. M. Mendes, S. Jacke, K. Critchley, J. Plaza, Y. Chen, K. Nikitin, R. E. Palmer, J. A. Preece, S. D. Evans, D. Fitzmaurice, *Langmuir* **2004**, *20*, 3766.
[13] U. Y. Lau, S. S. Saxer, J. Lee, E. Bat, H. D. Maynard, *ACS Nano* **2016**, *10*, 723.
[14] L. Huang, A. B. Braunschweig, W. Shim, L. Qin, J. K. Lim, S. J. Hurst, F. Huo, C. Xue, J. - W. Jang, C. A. Mirkin, *Small* **2009**, *6*, 1077.
[15] K. Salaita, Y. Wang, C. A. Mirkin, *Nat. Nanotechnol.* **2007**, *2*, 145.
[16] R. Kumar, A. Urtizberea, S. Ghosh, U. Bog, Q. Rainer, S. Lenhert, H. Fuchs, M. Hirtz, *Langmuir* **2017**, *33*, 8739.
[17] M. C. Traub, W. Longsine, V. N. Truskett, *Annu. Rev. Chem. Biomol. Eng.* **2016**, *7*, 583.
[18] S. V. Sreenivasan, *Microsyst. Nanoeng.* **2017**, *3*, 17075.
[19] C. Chen, D. Hirdes, A. Folch, *Proc. Natl. Acad. Sci. USA* **2003**, *100*, 1499.
[20] L. Feng, J. Romulus, M. Li, R. Sha, J. Royer, K. T. Wu, Q. Xu, N. C. Seeman, M. Weck, P. Chaikin, *Nat. Mater.* **2013**, *12*, 747.
[21] M. G. Stanford, K. Mahady, B. B. Lewis, J. D. Fowlkes, S. Tan, R. Livengood, G. A. Magel, T. M. Moore, P. D. Rack, *ACS Appl. Mater. Interfaces* **2016**, *8*, 29155.
[22] I. Utke, P. Hoffmann, J. Melngailis, *J. Vac. Sci. Technol. B: Microelectron. Nanometer. Struct.–Process., Meas., Phenom.* **2008**, *26*, 1197.
[23] J. A. Liddle, G. M. Gallatin, *ACS Nano* **2016**, *10*, 2995.
[24] P. Guo, *Nat. Nanotechnol.* **2010**, *5*, 833.
[25] M. Heiss, Y. Fontana, A. Gustafsson, G. Wüst, C. Magen, D. D. O'Regan, J. W. Luo, B. Ketterer, S. Conesa-Boj, A. V. Kuhlmann, J. Houel, E. Russo-Averchi, J. R. Morante, M. Cantoni, N. Marzari, J. Arbiol, A. Zunger, R. J. Warburton, A. Fontcuberta I Morral, *Nat. Mater.* **2013**, *12*, 439.
[26] K. S. Makarenko, Z. Liu, M. P. de Jong, F. A. Zwanenburg, J. Huskens, W. G. van der Wiel, *Adv. Mater.* **2017**, *29*, 1702920.
[27] J. Cai, P. Ruffieux, R. Jaafar, M. Bieri, T. Braun, S. Blankenburg, M. Muoth, A. P. Seitsonen, M. Saleh, X. Feng, K. Müllen, R. Fasel, *Nature* **2010**, *466*, 470.
[28] M. Li, R. B. Bhiladvala, T. J. Morrow, J. A. Sioss, K. K. Lew, J. M. Redwing, C. D. Keating, T. S. Mayer, *Nat. Nanotechnol.* **2008**, *3*, 88.
[29] M. Li, M. Fromel, D. Ranaweera, S. Rocha, C. Boyer, C. W. Pester, *ACS Macro Lett.* **2019**, *8*, 374.
[30] C. Cummins, R. Lundy, J. J. Walsh, V. Ponsinet, G. Fleury, M. A. Morris, *Nano Today* **2020**, *35*, 100936.
[31] R. A. Segalman, *Mater. Sci. Eng., R* **2005**, *48*, 191.
[32] C. M. Bates, F. S. Bates, *Macromolecules* **2017**, *50*, 3.
[33] F. S. Bates, M. A. Hillmyer, T. P. Lodge, C. M. Bates, K. T. Delaney, G. H. Fredrickson, *Science* **2012**, *336*, 434.
[34] M. W. Matsen, F. S. Bates, *Macromolecules* **1996**, *29*, 1091.
[35] K. Almdal, J. H. Rosedale, F. S. Bates, G. D. Wignall, G. H. Fredrickson, *Phys. Rev. Lett.* **1990**, *65*, 1112.
[36] N. A. Lynd, A. J. Meuler, M. A. Hillmyer, *Prog. Polym. Sci.* **2008**, *33*, 875.
[37] M. W. Matsen, F. S. Bates, *Macromolecules* **1996**, *29*, 7641.
[38] F. Bates, *Annu. Rev. Phys. Chem.* **1990**, *41*, 535.
[39] L. Leibler, *Macromolecules* **1980**, *13*, 1602.
[40] G. H. Fredrickson, F. S. Bates, *Annu. Rev. Mater. Sci.* **1996**, *26*, 501.
[41] A. N. Semenov, *Macromolecules* **1993**, *26*, 2273.
[42] C. Dae Han, D. Man Baekf, J. Kon Kim, T. Ogawa, N. Sakamoto, T. Hashimoto, *Macromolecules* **1995**, *28*, 5043.
[43] G. S. Doerk, K. G. Yager, *Mol. Syst. Des. Eng.* **2017**, *2*, 518.
[44] M. J. Park, N. P. Balsara, *Macromolecules* **2008**, *41*, 3678.
[45] J. Kwak, A. K. Mishra, J. Lee, K. S. Lee, C. Choi, S. Maiti, M. Kim, J. K. Kim, *Macromolecules* **2017**, *50*, 6813.
[46] N. A. Lynd, M. A. Hillmyer, *Macromolecules* **2007**, *40*, 8050.
[47] N. A. Lynd, M. A. Hillmyer, *Macromolecules* **2005**, *38*, 8803.
[48] D. T. Gentekos, B. P. Fors, *ACS Macro Lett.* **2018**, *7*, 677.
[49] J. M. Widin, A. K. Schmitt, K. Im, A. L. Schmitt, M. K. Mahanthappa, *Macromolecules* **2010**, *43*, 7913.
[50] J. M. Widin, A. K. Schmitt, A. L. Schmitt, K. Im, M. K. Mahanthappa, *J. Am. Chem. Soc.* **2012**, *134*, 3834.
[51] S. H. Anastasiadis, T. P. Russell, S. K. Satija, C. F. Majkrzak, *Phys. Rev. Lett.* **1989**, *62*, 1852.
[52] A. Menelle, T. P. Russell, S. H. Anastasiadis, S. K. Satija, C. F. Majkrzak, *Phys. Rev. Lett.* **1992**, *68*, 67.
[53] G. Kim, M. Libera, *Macromolecules* **1998**, *31*, 2569.
[54] Y. Mogi, M. Nomura, H. Kotsuji, K. Ohnishi, Y. Matsushita, I. Noda, *Macromolecules* **1994**, *27*, 6755.
[55] Y. Mogi, H. Kotsuji, Y. Kaneko, K. Mori, Y. Matsushita, I. Noda, *Macromolecules* **1992**, *25*, 5408.

[56] O. Glatter, G. Scherf, K. Schillén, W. Brown, *Macromolecules* **1994**, *27*, 6046.
[57] H. Elbs, C. Drummer, V. Abetz, G. Krausch, *Macromolecules* **2002**, *35*, 5570.
[58] K. Fukunaga, T. Hashimoto, H. Elbs, G. Krausch, *Macromolecules* **2002**, *35*, 4406.
[59] K. Yue, M. Huang, R. L. Marson, J. Hec, J. Huang, Z. Zhou, J. Wang, C. Liu, X. Yan, K. Wu, Z. Guo, H. Liu, W. Zhang, P. Ni, C. Wesdemiotis, W. B. Zhang, S. C. Glotzer, S. Z. D. Cheng, *Proc. Natl. Acad. Sci. USA* **2016**, *113*, 14195.
[60] M. Huang, C. H. Hsu, J. Wang, S. Mei, X. Dong, Y. Li, M. Li, H. Liu, W. Zhang, T. Aida, W. B. Zhang, K. Yue, S. Z. D. Cheng, *Science* **2015**, *348*, 424.
[61] S. A. Kim, K. J. Jeong, A. Yethiraj, M. K. Mahanthappa, *Proc. Natl. Acad. Sci. USA* **2017**, *114*, 4072.
[62] K. Hayashida, T. Dotera, A. Takano, Y. Matsushita, *Phys. Rev. Lett.* **2007**, *98*, 195502.
[63] S. Lee, M. J. Bluemle, F. S. Bates, *Science* **2010**, *330*, 349.
[64] S. Chanpuriya, K. Kim, J. Zhang, S. Lee, A. Arora, K. D. Dorfman, K. T. Delaney, G. H. Fredrickson, F. S. Bates, *ACS Nano* **2016**, *10*, 4961.
[65] B. K. Cho, A. Jain, S. M. Gruner, U. Wiesner, *Science* **2004**, *305*, 1598.
[66] M. W. Matsen, *Macromolecules* **2012**, *45*, 2161.
[67] J. E. Poelma, K. Ono, D. Miyajima, T. Aida, K. Satoh, C. J. Hawker, *ACS Nano* **2012**, *6*, 10845.
[68] Y. Zhu, S. P. Gido, H. Iatrou, N. Hadjichristidis, J. W. Mays, *Macromolecules* **2003**, *36*, 148.
[69] V. K. Gupta, R. Krishnamoorti, Z. R. Chen, J. A. Kornfield, S. D. Smith, M. M. Satkowski, J. T. Grothaus, *Macromolecules* **1996**, *29*, 875.
[70] D.-P. Song, G. Jacucci, F. Dundar, A. Naik, H.-F. Fei, S. Vignolini, J. J. Watkins, *Macromolecules* **2021**, *16*, 51.
[71] J. Mijovic, M. Shen, J. W. Sy, I. Mondragon, *Macromolecules* **2000**, *33*, 5235.
[72] R. J. Albalak, E. L. Thomas, M. S. Capel, *Polymer* **1997**, *38*, 3819.
[73] X. Li, J. Peng, Y. Wen, D. H. Kim, W. Knoll, *Polymer* **2007**, *48*, 2434.
[74] J. Peng, Y. Han, W. Knoll, D. H. Kim, *Macromol. Rapid Commun.* **2007**, *28*, 1422.
[75] A. M. Welander, H. Kang, K. O. Stuen, H. H. Solak, M. Müller, J. J. De Pablo, P. F. Nealey, *Macromolecules* **2008**, *41*, 2759.
[76] M. S. She, T. Y. Lo, R. M. Ho, *ACS Nano* **2013**, *7*, 2000.
[77] S. M. Hur, G. S. Khaira, A. Ramírez-Hernández, M. Müller, P. F. Nealey, J. J. De Pablo, *ACS Macro Lett.* **2015**, *4*, 11.
[78] E. Kim, H. Ahn, S. Park, H. Lee, M. Lee, S. Lee, T. Kim, E. A. Kwak, J. H. Lee, X. Lei, J. Huh, J. Bang, B. Lee, D. Y. Ryu, *ACS Nano* **2013**, *7*, 1952.
[79] Z. Qiang, J. Xue, G. E. Stein, K. A. Cavicchi, B. D. Vogt, *Langmuir* **2013**, *29*, 8703.
[80] P. W. Majewski, K. G. Yager, *J. Phys.: Condens. Matter* **2016**, *28*, 403002.
[81] J. N. L. Albert, T. H. Epps, *Mater. Today* **2010**, *13*, 24.
[82] S. Park, J. Y. Wang, B. Kim, W. Chen, T. P. Russell, *Macromolecules* **2007**, *40*, 9059.
[83] S. Park, B. Kim, J. Xu, T. Hofmann, B. M. Ocko, T. P. Russell, *Macromolecules* **2009**, *42*, 1278.
[84] C. Sinturel, M. Vayer, M. Morris, M. A. Hillmyer, *Macromolecules* **2013**, *46*, 5399.
[85] X. Yu, J. Peng, L. Cui, H. Wang, B. Li, Y. Han, *Macromolecules* **2004**, *37*, 7301.
[86] S. Niu, R. F. Saraf, *Macromolecules* **2003**, *36*, 2428.
[87] J. Zhao, S. Jiang, X. Ji, L. An, B. Jiang, *Polymer* **2005**, *46*, 6513.
[88] J. N. L. Albert, T. D. Bogart, R. L. Lewis, K. L. Beers, M. J. Fasolka, J. B. Hutchison, B. D. Vogt, T. H. Epps, *Nano Lett.* **2011**, *11*, 1351.
[89] K. Fukunaga, H. Elbs, R. Magerle, G. Krausch, *Macromolecules* **2000**, *33*, 947.
[90] J. N. L. Albert, W. S. Young, R. L. Lewis, T. D. Bogart, J. R. Smith, T. H. Epps, *ACS Nano* **2012**, *6*, 459.
[91] K. W. Gotrik, A. F. Hannon, J. G. Son, B. Keller, A. Alexander-Katz, C. A. Ross, *ACS Nano* **2012**, *6*, 8052.
[92] M. A. Chavis, D. - M. Smilgies, U. B. Wiesner, C. K. Ober, *Adv. Funct. Mater.* **2015**, *25*, 3057.
[93] K. W. Gotrik, C. A. Ross, *Nano Lett.* **2013**, *13*, 5117.
[94] P. Mokarian-Tabari, C. Cummins, S. Rasappa, C. Simao, C. M. S. Torres, J. D. Holmes, M. A. Morris, *Langmuir* **2014**, *30*, 10728.
[95] S. S. Dinachali, W. Bai, K. H. Tu, H. K. Choi, J. Zhang, M. E. Kreider, L. C. Cheng, C. A. Ross, *ACS Macro Lett.* **2015**, *4*, 500.
[96] M. Longanecker, A. Modi, A. Dobrynin, S. Kim, G. Yuan, R. Jones, S. Satija, J. Bang, A. Karim, *Macromolecules* **2016**, *49*, 8563.
[97] A. Modi, S. M. Bhaway, B. D. Vogt, J. F. Douglas, A. Al-Enizi, A. Elzatahry, A. Sharma, A. Karim, *ACS Appl. Mater. Interfaces* **2015**, *7*, 21639.
[98] W. I. Park, J. M. Kim, J. W. Jeong, Y. S. Jung, *ACS Nano* **2014**, *8*, 10009.
[99] X. Zhang, K. D. Harris, N. L. Y. Wu, J. N. Murphy, J. M. Buriak, *ACS Nano* **2010**, *4*, 7021.
[100] Z. Qiang, C. Ye, K. Lin, M. L. Becker, K. A. Cavicchi, B. D. Vogt, *J. Polym. Sci., Part B: Polym. Phys.* **2016**, *54*, 1499.
[101] C. Jin, J. N. Murphy, K. D. Harris, J. M. Buriak, *ACS Nano* **2014**, *8*, 3979.
[102] J. Jiang, A. G. Jacobs, B. Wenning, C. Liedel, M. O. Thompson, C. K. Ober, *ACS Appl. Mater. Interfaces* **2017**, *9*, 31317.
[103] A. A. Leniart, P. Pula, A. Sitkiewicz, P. W. Majewski, *ACS Nano* **2020**, *14*, 4805.
[104] Y. Mai, A. Eisenberg, *Chem. Soc. Rev.* **2012**, *41*, 5969.
[105] H. Hu, M. Gopinadhan, C. O. Osuji, *Soft Matter* **2014**, *10*, 3867.
[106] C. A. Ross, K. K. Berggren, J. Y. Cheng, Y. S. Jung, J. - B. Chang, *Adv. Mater.* **2014**, *26*, 4386.
[107] M. Stefik, S. Guldin, S. Vignolini, U. Wiesner, U. Steiner, *Chem. Soc. Rev.* **2015**, *44*, 5076.
[108] S. Y. Yang, J. Park, J. Yoon, M. Ree, S. K. Jang, J. K. Kim, *Adv. Funct. Mater.* **2008**, *18*, 1371.
[109] H. Uehara, T. Yoshida, M. Kakiage, T. Yamanobe, T. Komoto, K. Nomura, K. Nakajima, M. Matsuda, *Macromolecules* **2006**, *39*, 3971.
[110] H. Kosonen, S. Valkama, A. Nykänen, M. Toivanen, G. Brinke, J. Ten Ruokolainen, O. Ikkala, *Adv. Mater.* **2006**, *18*, 201.
[111] H. Sai, K. W. Tan, K. Hur, E. Asenath-Smith, R. Hovden, Y. Jiang, M. Riccio, D. A. Muller, V. Elser, L. A. Estroff, S. M. Gruner, U. Wiesner, *Science* **2013**, *341*, 530.
[112] J. S. Lee, A. Hirao, S. Nakahama, *Macromolecules* **1989**, *22*, 2602.
[113] T. Hashimoto, K. Tsutsumi, Y. Funaki, *Langmuir* **1997**, *13*, 6869.
[114] L. Chen, W. A. Phillip, E. L. Cussler, M. A. Hillmyer, *J. Am. Chem. Soc.* **2007**, *129*, 13786.
[115] P. L. Drzal, A. F. Halasa, P. Kofinas, *Polymer* **2000**, *41*, 4671.
[116] M. J. Park, K. H. Downing, A. Jackson, E. D. Gomez, A. M. Minor, D. Cookson, A. Z. Weber, N. P. Balsara, *Nano Lett.* **2007**, *7*, 3547.
[117] M. J. Park, S. Kim, A. M. Minor, A. Hexemer, N. P. Balsara, *Adv. Mater.* **2009**, *21*, 203.
[118] A. K. Jha, L. Chen, R. D. Offeman, N. P. Balsara, *J. Membr. Sci.* **2011**, *373*, 112.
[119] M. G. Buonomenna, G. Golemme, C. M. Tone, M. P. De Santo, F. Ciuchi, E. Perrotta, B. Zappone, F. Galiano, A. Figoli, *J. Membr. Sci.* **2011**, *385–386*, 162.
[120] R. Watanabe, K. Kamata, T. Iyoda, *J. Mater. Chem.* **2008**, *18*, 5482.
[121] M. J. Park, N. P. Balsara, *Macromolecules* **2010**, *43*, 292.
[122] W.-S. Young, W.-F. Kuan, T. H. Epps, *J. Polym. Sci., Part B: Polym. Phys.* **2014**, *52*, 1.
[123] J. Hou, J. Li, L. A. Madsen, *Macromolecules* **2010**, *43*, 347.
[124] C. G. Arges, Y. Kambe, H. S. Suh, L. E. Ocola, P. F. Nealey, *Chem. Mater.* **2016**, *28*, 1377.

[125] D. T. Hallinan, S. A. Mullin, G. M. Stone, N. P. Balsara, *J. Electrochem. Soc.* **2013**, *160*, A464.
[126] X. Feng, Q. Imran, Y. Zhang, L. Sixdenier, X. Lu, G. Kaufman, U. Gabinet, K. Kawabata, M. Elimelech, C. O. Osuji, *Sci. Adv.* **2019**, *5*, eaav9308.
[127] M. R. Bockstaller, Y. Lapetnikov, S. Margel, E. L. Thomas, *J. Am. Chem. Soc.* **2003**, *125*, 5276.
[128] J. J. Chiu, B. J. Kim, E. J. Kramer, D. J. Pine, *J. Am. Chem. Soc.* **2005**, *127*, 5036.
[129] Y. Lin, A. Böker, J. He, K. Sill, H. Xiang, C. Abetz, X. Li, J. Wang, T. Emrick, S. Long, Q. Wang, A. Balazs, T. P. Russell, *Nature* **2005**, *434*, 55.
[130] R. Miyata, M. Ueda, H. Jinno, T. Konno, K. Ishihara, N. Ando, Y. Kitagawa, *Int. J. Cancer* **2009**, *124*, 2460.
[131] G. Gaucher, M. H. Dufresne, V. P. Sant, N. Kang, D. Maysinger, J. C. Leroux, *J. Controlled Release* **2005**, *109*, 169.
[132] Q. Zhang, N. Re Ko, J. Kwon Oh, *Chem. Commun.* **2012**, *48*, 7542.
[133] H. K. Murnen, A. M. Rosales, J. N. Jaworski, R. A. Segalman, R. N. Zuckermann, *J. Am. Chem. Soc.* **2010**, *132*, 16112.
[134] A. M. Rosales, R. A. Segalman, R. N. Zuckermann, *Soft Matter* **2013**, *9*, 8400.
[135] D. P. Song, C. Li, W. Li, J. J. Watkins, *ACS Nano* **2016**, *10*, 1216.
[136] C. Tang, E. M. Lennon, G. H. Fredrickson, E. J. Kramer, C. J. Hawker, *Science* **2008**, *322*, 429.
[137] T. Kubo, J. S. Parker, M. A. Hillmyer, C. Leighton, *Appl. Phys. Lett.* **2007**, *90*, 233113.
[138] K. H. Tu, W. Bai, G. Liontos, K. Ntetsikas, A. Avgeropoulos, C. A. Ross, *Nanotechnology* **2015**, *26*, 375301.
[139] A. P. Lane, X. Yang, M. J. Maher, G. Blachut, Y. Asano, Y. Someya, A. Mallavarapu, S. M. Sirard, C. J. Ellison, C. G. Willson, *ACS Nano* **2017**, *11*, 7656.
[140] M. Luo, T. H. Epps, *Macromolecules* **2013**, *46*, 7567.
[141] S. E. Mastroianni, T. H. Epps, *Langmuir* **2013**, *29*, 3864.
[142] A. P. Marencic, R. A. Register, *Annu. Rev. Chem. Biomol. Eng.* **2010**, *1*, 277.
[143] C. A. Ross, *Ann. Rev. Mater. Res.* **2001**, *31*, 203.
[144] J. Song, B. K. Cho, *Chem. Commun.* **2012**, *48*, 6821.
[145] O. Kim, S. Y. Kim, J. Lee, M. J. Park, *Chem. Mater.* **2016**, *28*, 318.
[146] S. Cheng, D. M. Smith, Q. Pan, S. Wang, C. Y. Li, *RSC Adv.* **2015**, *5*, 48793.
[147] K. H. Shen, J. R. Brown, L. M. Hall, *ACS Macro Lett.* **2018**, *7*, 1092.
[148] M. J. Folkes, A. Keller, *Polymer* **1971**, *12*, 222.
[149] P. W. Majewski, M. Gopinadhan, W. S. Jang, J. L. Lutkenhaus, C. O. Osuji, *J. Am. Chem. Soc.* **2010**, *132*, 17516.
[150] I. W. Hamley, *Prog. Polym. Sci.* **2009**, *34*, 1161.
[151] H. S. Wang, K. H. Kim, J. Bang, *Macromol. Rapid Commun.* **2019**, *40*, 1800728.
[152] S. M. Hur, V. Thapar, A. Ramírez-Hernández, G. Khaira, T. Segal-Peretz, P. A. Rincon-Delgadillo, W. Li, M. Müller, P. F. Nealey, J. J. De Pablo, *Proc. Natl. Acad. Sci. USA* **2015**, *112*, 14144.
[153] R. A. Lawson, A. J. Peters, P. J. Ludovice, C. L. Henderson, *Proc. SPIE* **2013**, *8680*, 86801Y.
[154] U. Nagpal, M. Müller, P. F. Nealey, J. J. De Pablo, *ACS Macro Lett.* **2012**, *1*, 418.
[155] W. Li, P. F. Nealey, J. J. De Pablo, M. Müller, *Phys. Rev. Lett.* **2014**, *113*, 168301.
[156] E. W. Edwards, M. P. Stoykovich, M. Müller, H. H. Solak, J. J. de Pablo, P. F. Nealey, *J. Polym. Sci., Part B: Polym. Phys.* **2005**, *43*, 3444.
[157] X. Wan, T. Gao, L. Zhang, J. Lin, *Phys. Chem. Chem. Phys.* **2017**, *19*, 6707.
[158] L. Zhang, L. Wang, J. Lin, *Soft Matter* **2014**, *10*, 6713.
[159] S. J. Jeong, J. Y. Kim, B. H. Kim, H. S. Moon, S. O. Kim, *Mater. Today* **2013**, *16*, 468.
[160] S. Ji, L. Wan, C. C. Liu, P. F. Nealey, *Prog. Polym. Sci.* **2016**, *54-55*, 76.
[161] Y.-C. Tseng, S. B. Darling, *Polymers* **2010**, *2*, 470.
[162] C. Pinto-Gómez, F. Pérez-Murano, J. Bausells, L. G. Villanueva, M. Fernández-Regúlez, *Polymers* **2020**, *12*, 2432.
[163] W. Li, M. Müller, *Prog. Polym. Sci.* **2016**, *54-55*, 47.
[164] S. Y. Park, C. Choi, K. S. Lee, E. Kim, S. Ahn, J. Lee, J. K. Kim, *Macromolecules* **2020**, *53*, 3611.
[165] N. Koneripalli, N. Singh, R. Levicky, F. S. Bates, P. D. Gallagher, S. K. Satija, *Macromolecules* **1995**, *28*, 2897.
[166] D. T. Gentekos, J. Jia, E. S. Tirado, K. P. Barteau, D. M. Smilgies, R. A. Distasio, B. P. Fors, *J. Am. Chem. Soc.* **2018**, *140*, 4639.
[167] C. Jin, B. C. Olsen, E. J. Luber, J. M. Buriak, *Chem. Mater.* **2017**, *29*, 176.
[168] H. S. Wang, A. Khan, Y. Choe, J. Huh, J. Bang, *Macromolecules* **2017**, *50*, 5025.
[169] S. Kim, M. Yoo, J. Baettig, E. H. Kang, J. Koo, Y. Choe, T. L. Choi, A. Khan, J. G. Son, J. Bang, *ACS Macro Lett.* **2015**, *4*, 133.
[170] T. Y. Lo, A. Dehghan, P. Georgopanos, A. Avgeropoulos, A. C. Shi, R. M. Ho, *Macromolecules* **2016**, *49*, 624.
[171] C. W. Pester, C. Liedel, M. Ruppel, A. Böker, *Prog. Polym. Sci.* **2017**, *64*, 182.
[172] T. Xu, J. Wang, T. P. Russel, in, *Nanostructured Soft Matter. NanoScience and Technology* (Ed: A. V. Zvelindovsky), Springer, Dordrecht pp. 171–198.
[173] M. Ruppel, C. W. Pester, K. M. Langner, G. J. A. Sevink, H. G. Schoberth, K. Schmidt, V. S. Urban, J. W. Mays, A. Böker, *ACS Nano* **2013**, *7*, 3854.
[174] H. G. Schoberth, K. Schmidt, K. A. Schindler, A. Boker, *Macromolecules* **2009**, *42*, 3433.
[175] K. Schmidt, C. W. Pester, H. G. Schoberth, H. Zettl, K. A. Schindler, A. Böker, *Macromolecules* **2010**, *43*, 4268.
[176] K. Schmidt, H. G. Schoberth, M. Ruppel, H. Zettl, H. Hänsel, T. M. Weiss, V. Urban, G. Krausch, A. Böker, *Nat. Mater.* **2008**, *7*, 142.
[177] C. W. Pester, K. Schmidt, M. Ruppel, H. G. Schoberth, A. Böker, *Macromolecules* **2015**, *48*, 6206.
[178] C. - Y. Chao, X. Li, C. K. Ober, C. Osuji, E. L. Thomas, *Adv. Funct. Mater.* **2004**, *14*, 364.
[179] V. Olszowka, M. Hund, V. Kuntermann, S. Scherdel, L. Tsarkova, A. Böker, *ACS Nano* **2009**, *3*, 1091.
[180] K. Amundson, E. Helfand, D. D. Davis, X. Quan, S. S. Patel, S. D. Smith, *Macromolecules* **1991**, *24*, 6546.
[181] A. Böker, K. Schmidt, A. Knoll, H. Zettl, H. Hänsel, V. Urban, V. Abetz, G. Krausch, *Polymer* **2006**, *47*, 849.
[182] H. U. Jeon, H. M. Jin, J. S. Y. Kim, S. K. Cha, J. H. Mun, K. E. Lee, J. J. Oh, T. Yun, J. S. Y. Kim, S. O. Kim, *Mol. Syst. Des. Eng.* **2017**, *2*, 560.
[183] T. Xu, A. V. Zvelindovsky, G. J. A. Sevink, K. S. Lyakhova, H. Jinnai, T. P. Russell, *Macromolecules* **2005**, *38*, 10788.
[184] T. Xu, Y. Zhu, S. P. Gido, T. P. Russell, *Macromolecules* **2004**, *37*, 2625.
[185] K. Schmidt, A. Böker, H. Zettl, F. Schubert, H. Hänsel, F. Fischer, T. M. Weiss, V. Abetz, A. V. Zvelindovsky, G. J. A. Sevink, G. Krausch, *Langmuir* **2005**, *21*, 11974.
[186] A. V. Zvelindovsky, G. J. A. Sevink, A. Böker, V. Abetz, G. Krausch, *Phys. Rev. Lett.* **2003**, *90*, 496011.
[187] A. Böker, K. Schmidt, in, *Polymers, Liquids, and Colloids in Electric Fields: Interfacial Instabilities, Orientation and Phase Transitions* (Eds: Yoav Tsori, Steiner Ullrich) World Scientific Publishing Co, Singapore pp. 215–244.
[188] J. DeRouchey, T. Thurn-Albrecht, T. P. Russell, R. Kolb, *Macromolecules* **2004**, *37*, 2538.
[189] Y. Tsori, F. Tournilhac, L. Leibler, *Macromolecules* **2003**, *36*, 5873.
[190] T. Xu, J. T. Goldbach, J. Leiston-Belanger, T. P. Russell, *Colloid Polym. Sci.* **2004**, *282*, 927.
[191] J. Y. Wang, T. Xu, J. M. Leiston-Belanger, S. Gupta, T. P. Russell, *Phys. Rev. Lett.* **2006**, *96*, 128301.

[192] K. Amundson, E. Helfand, X. Quan, S. D. Smith, *Macromolecules* **1993**, *26*, 2698.
[193] V. Olszowka, M. Hund, V. Kuntermann, S. Scherdel, L. Tsarkova, A. Böker, G. Krausch, *Soft Matter* **2006**, *2*, 1089.
[194] T. Thurn-Albrecht, J. DeRouchey, T. P. Russell, R. Kolb, *Macromolecules* **2002**, *35*, 8106.
[195] T. L. Morkved, M. Lu, A. M. Urbas, E. E. Ehrichs, H. M. Jaeger, P. Mansky, T. P. Russell, *Science* **1996**, *273*, 931.
[196] T. Thurn-Albrecht, J. Schotter, G. A. Kastle, N. Emley, T. Shibauchi, L. Krusin-Elbaum, K. Guarini, C. T. Black, M. T. Tuominen, T. P. Russell, *Science* **2000**, *290*, 2126.
[197] T. Xu, Y. Zhu, S. P. Gido, T. P. Russell, *Macromolecules* **2004**, *37*, 2625.
[198] P. Mansky, J. DeRouchey, T. P. Russell, J. Mays, M. Pitsikalis, T. Morkved, H. Jaeger, *Macromolecules* **1998**, *31*, 4399.
[199] V. Olszowka, V. Kuntermann, A. Böker, *Macromolecules* **2008**, *41*, 5515.
[200] T. Xu, C. J. Hawker, T. P. Russell, *Macromolecules* **2003**, *36*, 6178.
[201] C. C. Kathrein, C. Pester, M. Ruppel, M. Jung, M. Zimmermann, A. Böker, *Soft Matter* **2016**, *12*, 8417.
[202] H. Xiang, Y. Lin, T. P. Russell, *Macromolecules* **2004**, *37*, 5358.
[203] E. J. W. Crossland, S. Ludwigs, M. A. Hillmyer, U. Steiner, *Soft Matter* **2007**, *3*, 94.
[204] E. J. W. Crossland, S. Ludwigs, M. A. Hillmyer, U. Steiner, *Soft Matter* **2010**, *6*, 670.
[205] V. Olszowka, L. Tsarkova, A. Böker, *Soft Matter* **2009**, *5*, 812.
[206] J. Bae, S. J. Park, O. S. Kwon, J. Jang, *J. Mater. Sci.* **2014**, *49*, 4323.
[207] C. Liedel, K. A. Schindler, M. J. Pavan, C. Lewin, C. W. Pester, M. Ruppel, V. S. Urban, R. Shenhar, A. Böker, *Small* **2013**, *9*, 32376.
[208] C. Liedel, C. W. Pester, M. Ruppel, C. Lewin, M. J. Pavan, V. S. Urban, R. Shenhar, P. Bösecke, A. Böker, *ACS Macro Lett.* **2013**, *2*, 53.
[209] T. Ohta, N. Yamazaki, M. Motoyama, K. Yamada, M. Nonomura, *J. Phys.: Condens. Matter* **2005**, *17*, S2833.
[210] N. Yamazaki, M. Motoyama, M. Nonomura, T. Ohta, *J. Chem. Phys.* **2004**, *120*, 3949.
[211] K. H. Han, H. Kang, G. Y. Lee, H. J. Lee, H. M. Jin, S. K. Cha, T. Yun, J. H. Kim, G. G. Yang, H. J. Choi, Y. K. Ko, H. T. Jung, S. O. Kim, *ACS Appl. Mater. Interfaces* **2020**, *12*, 58113.
[212] S. Jo, S. Jeon, H. Kim, C. Y. Ryu, S. Lee, D. Y. Ryu, *Chem. Mater.* **2020**, *32*, 9633.
[213] Y. Rokhlenko, M. Gopinadhan, C. O. Osuji, K. Zhang, C. S. O'Hern, S. R. Larson, P. Gopalan, P. W. Majewski, K. G. Yager, *Phys. Rev. Lett.* **2015**, *115*, 258302.
[214] M. Gopinadhan, Y. Choo, K. Kawabata, G. Kaufman, X. Feng, X. Di, Y. Rokhlenko, L. H. Mahajan, D. Ndaya, R. M. Kasi, C. O. Osuji, *Proc. Natl. Acad. Sci. USA* **2017**, *114*, E9437.
[215] P. W. Majewski, M. Gopinadhan, C. O. Osuji, *J. Polym. Sci., Part B: Polym. Phys.* **2012**, *50*, 2.
[216] P. Deshmukh, M. Gopinadhan, Y. Choo, S. K. Ahn, P. W. Majewski, S. Y. Yoon, O. Bakajin, M. Elimelech, C. O. Osuji, R. M. Kasi, *ACS Macro Lett.* **2014**, *3*, 462.
[217] C. Osuji, P. J. Ferreira, G. Mao, C. K. Ober, J. B. V. Sande, E. L. Thomas, *Macromolecules* **2004**, *37*, 9903.
[218] M. Gopinadhan, P. W. Majewski, C. O. Osuji, *Macromolecules* **2010**, *43*, 3286.
[219] S. Y. Park, T. Kavitha, T. Kamal, W. Khan, T. Shin, B. Seong, *Macromolecules* **2012**, *45*, 6168.
[220] I. W. Hamley, V. Castelletto, Z. B. Lu, C. T. Imrie, T. Itoh, M. Al-Hussein, *Macromolecules* **2004**, *37*, 4798.
[221] M. Gopinadhan, Y. Choo, C. O. Osuji, *ACS Macro Lett.* **2016**, *5*, 292.
[222] M. Gopinadhan, P. Deshmukh, Y. Choo, P. W. Majewski, O. Bakajin, M. Elimelech, R. M. Kasi, C. O. Osuji, *Adv. Mater.* **2014**, *26*, 5148.
[223] Y. Tao, H. Zohar, B. D. Olsen, R. A. Segalman, *Nano Lett.* **2007**, *7*, 2742.
[224] B. McCulloch, G. Portale, W. Bras, R. A. Segalman, *Macromolecules* **2011**, *44*, 7503.
[225] T. Grigorova, S. Pispas, N. Hadjichristidis, T. Thurn-Albrecht, *Macromolecules* **2005**, *38*, 7430.
[226] Y. Rokhlenko, P. W. Majewski, S. R. Larson, P. Gopalan, K. G. Yager, C. O. Osuji, *ACS Macro Lett.* **2017**, *6*, 404.
[227] T. Kimura, *Polym. J.* **2003**, *35*, 823.
[228] M. Gopinadhan, P. W. Majewski, E. S. Beach, C. O. Osuji, *ACS Macro Lett.* **2012**, *1*, 184.
[229] H. Tran, M. Gopinadhan, P. W. Majewski, R. Shade, V. Steffes, C. O. Osuji, L. M. Campos, *ACS Nano* **2013**, *7*, 5514.
[230] M. Gopinadhan, Y. Choo, L. H. Mahajan, D. Ndaya, G. Kaufman, Y. Rokhlenko, R. M. Kasi, C. O. Osuji, *Mol. Syst. Des. Eng.* **2017**, *2*, 549.
[231] V. Raman, A. Bose, B. D. Olsen, T. A. Hatton, *Macromolecules* **2012**, *45*, 9373.
[232] B. McCulloch, G. Portale, W. Bras, J. A. Pople, A. Hexemer, R. A. Segalman, *Macromolecules* **2013**, *46*, 4462.
[233] X. Liu, Y. Li, J. Xue, W. Zhu, J. Zhang, Y. Yin, Y. Qin, K. Jiao, Q. Du, B. Cheng, X. Zhuang, J. Li, M. D. Guiver, *Nat. Commun.* **2019**, *10*, 842.
[234] J. S. Da Silva, S. G. M. Carvalho, R. P. Da Silva, A. C. Tavares, U. Schade, L. Puskar, F. C. Fonseca, B. R. Matos, *Phys. Chem. Chem. Phys.* **2020**, *22*, 13764.
[235] T. Tu, T. Sakurai, S. Seki, Y. Ishida, Y. Chan, *Angew. Chem.* **2021**, *133*, 1951.
[236] X. Feng, K. Kawabata, M. G. Cowan, G. E. Dwulet, K. Toth, L. Sixdenier, A. Haji-Akbari, R. D. Noble, M. Elimelech, D. L. Gin, C. O. Osuji, *Nat. Mater.* **2019**, *18*, 1235.
[237] A. Keller, E. Pedemonte, F. M. Willmouth, *Kolloid-Z. Z. Polym.* **1970**, *238*, 385.
[238] G. H. Fredrickson, *J. Rheol.* **1994**, *38*, 1045.
[239] S. S. Patel, R. G. Larson, K. I. Winey, H. Watanabe, *Macromolecules* **1995**, *28*, 4313.
[240] V. K. Gupta, R. Krishnamoorti, J. A. Kornfield, S. D. Smith, *Macromolecules* **1995**, *28*, 4464.
[241] H. Wang, M. C. Newstein, A. Krishnan, N. P. Balsara, B. A. Garetz, B. Hammouda, R. Krishnamoorti, *Macromolecules.* **1999**, *32*, 3695.
[242] S. Pujari, M. A. Keaton, P. M. Chaikin, R. A. Register, *Soft Matter* **2012**, *8*, 5358.
[243] O. O. Mykhaylyk, A. J. Parnell, A. Pryke, J. P. A. Fairclough, *Macromolecules* **2012**, *45*, 5260.
[244] A. Chremos, P. M. Chaikin, R. A. Register, A. Z. Panagiotopoulos, *Soft Matter* **2012**, *8*, 7803.
[245] C. Osuji, Y. Zhang, G. Mao, C. K. Ober, E. L. Thomas, *Macromolecules* **1999**, *32*, 7703.
[246] D. E. Angelescu, J. H. Waller, D. H. Adamson, P. Deshpande, S. Y. Chou, R. A. Register, P. M. Chaikin, *Adv. Mater.* **2004**, *16*, 1736.
[247] A. Nikoubashman, R. L. Davis, B. T. Michal, P. M. Chaikin, R. A. Register, A. Z. Panagiotopoulos, *ACS Nano* **2014**, *8*, 8015.
[248] S. Y. Kim, J. Gwyther, I. Manners, P. M. Chaikin, R. A. Register, *Adv. Mater.* **2014**, *26*, 791.
[249] R. L. Davis, P. M. Chaikin, R. A. Register, *Macromolecules* **2014**, *47*, 5277.
[250] R. L. Davis, B. T. Michal, P. M. Chaikin, R. A. Register, *Macromolecules* **2015**, *48*, 5339.
[251] A. P. Marencic, P. M. Chaikin, R. A. Register, *Phys. Rev. E* **2012**, *86*, 021507.
[252] G. Arya, J. Rottler, A. Z. Panagiotopoulos, D. J. Srolovitz, P. M. Chaikin, *Langmuir* **2005**, *21*, 11518.
[253] M. Pinna, A. V. M. Zvelindovsky, X. Guo, C. L. Stokes, *Soft Matter* **2011**, *7*, 6991.
[254] D. E. Angelescu, J. H. Waller, R. A. Register, P. M. Chaikin, *Adv. Mater.* **2005**, *17*, 1878.
[255] A. P. Marencic, M. W. Wu, R. A. Register, P. M. Chaikin, *Macromolecules* **2007**, *40*, 7299.

[256] M. W. Wu, R. A. Register, P. M. Chaikin, *Phys. Rev. E* **2006**, *74*, 040801.
[257] B. M. Yavitt, H. Fei, G. Kopanati, R. Li, M. Fukuto, H. H. Winter, J. J. Watkins, *Macromolecules* **2020**, *53*, 2834.
[258] A. P. Marencic, D. H. Adamson, P. M. Chaikin, R. A. Register, *Phys. Rev. E* **2010**, *81*, 011503.
[259] S. Y. Kim, A. Nunns, J. Gwyther, R. L. Davis, I. Manners, P. M. Chaikin, R. A. Register, *Nano Lett.* **2014**, *14*, 5698.
[260] A. Nikoubashman, R. A. Register, A. Z. Panagiotopoulos, *Soft Matter* **2013**, *9*, 9960.
[261] A. Chremos, P. M. Chaikin, R. A. Register, A. Z. Panagiotopoulos, *Macromolecules* **2012**, *45*, 4406.
[262] L. Wu, T. P. Lodge, F. S. Bates, *Macromolecules* **2004**, *37*, 8184.
[263] P. Xu, J. Lin, L. Wang, L. Zhang, *J. Chem. Phys.* **2017**, *146*, 184903.
[264] R. J. Albalak, E. L. Thomas, *J. Polym. Sci., Part B: Polym. Phys.* **1994**, *32*, 341.
[265] M. E. Vigild, C. Chu, M. Sugiyama, K. A. Chaffin, F. S. Bates, *Macromolecules* **2001**, *34*, 951.
[266] Y. Chen, Q. Xu, Y. Jin, X. Qian, R. Ma, J. Liu, D. Yang, *Soft Matter* **2018**, *14*, 6635.
[267] Y. C. Kim, D. H. Kim, S. H. Joo, N. K. Kwon, T. J. Shin, R. A. Register, S. K. Kwak, S. Y. Kim, *Macromolecules* **2017**, *50*, 3607.
[268] V. Pelletier, D. H. Adamson, R. A. Register, P. M. Chaikin, *Appl. Phys. Lett.* **2007**, *90*, 163105.
[269] C. Zhang, K. A. Cavicchi, R. Li, K. G. Yager, M. Fukuto, B. D. Vogt, *Macromolecules* **2018**, *51*, 4213.
[270] G. Singh, K. G. Yager, B. Berry, H. C. Kim, A. Karim, *ACS Nano* **2012**, *6*, 10335.
[271] R. Zhang, G. Singh, A. Dang, L. Dai, M. R. Bockstaller, B. Akgun, S. Satija, A. Karim, *Macromol. Rapid Commun.* **2013**, *34*, 1642.
[272] Z. Qiang, L. Zhang, G. E. Stein, K. A. Cavicchi, B. D. Vogt, *Macromolecules* **2014**, *47*, 1109.
[273] Z. Qiang, Y. Zhang, J. A. Groff, K. A. Cavicchi, B. D. Vogt, *Soft Matter* **2014**, *10*, 6068.
[274] Z. Qiang, Y. Zhang, Y. Wang, S. M. Bhaway, K. A. Cavicchi, B. D. Vogt, *Carbon* **2015**, *82*, 51.
[275] M. Luo, D. M. Scott, T. H. Epps, *ACS Macro Lett.* **2015**, *4*, 516.
[276] J. Bolton, T. S. Bailey, J. Rzayev, *Nano Lett.* **2011**, *11*, 998.
[277] J. Oh, M. Shin, I. Soo Kim, H. Seon Suh, Y. Kim, J. Kyeong Kim, J. Bang, B. Yeom, J. Gon Son, *ACS Nano* **2021**, *15*, 8549.
[278] H. Yu, T. Iyoda, T. Ikeda, *J. Am. Chem. Soc.* **2006**, *128*, 11010.
[279] L. Cui, Y. Zhao, A. Yavrian, T. Galstian, *Macromolecules* **2003**, *36*, 8246.
[280] Y. Morikawa, T. Kondo, S. Nagano, T. Seki, *Chem. Mater.* **2007**, *19*, 1540.
[281] S. Nagano, *Langmuir* **2019**, *35*, 5673.
[282] T. Seki, *Polym. J.* **2004**, *36*, 435.
[283] T. Seki, S. Nagano, M. Hara, *Polymer* **2013**, *54*, 6053.
[284] T. Seki, *Polym. J.* **2014**, *46*, 751.
[285] M. Sano, S. Nakamura, M. Hara, S. Nagano, Y. Shinohara, Y. Amemiya, T. Seki, *Macromolecules* **2014**, *47*, 7178.
[286] Y. Morikawa, S. Nagano, K. Watanabe, K. Kamata, T. Iyoda, T. Seki, *Adv. Mater.* **2006**, *18*, 883.
[287] T. Wang, X. Li, Z. Dong, S. Huang, H. Yu, *ACS Appl. Mater. Interfaces* **2017**, *9*, 24864.
[288] Y. Chen, S. Huang, T. Wang, H. Yu, *Macromolecules* **2020**, *53*, 1486.
[289] H. Sakaino, B. A. G. Lamers, S. C. J. Meskers, E. W. Meijer, G. Vantomme, *J. Polym. Sci.* **2021**, 59, 1131.
[290] K. T. Lin, Y. J. Chen, M. R. Huang, V. K. Karapala, J. H. Ho, J. T. Chen, *Nano Lett.* **2020**, *20*, 5853.
[291] J. Y. Kim, P. Liu, M. J. Maher, D. H. Callan, C. M. Bates, M. C. Carlson, Y. Asano, G. Blachut, C. T. Rettner, J. Y. Cheng, D. F. Sunday, R. J. Kline, D. P. Sanders, N. A. Lynd, C. J. Ellison, C. G. Willson, C. R. Baiz, *ACS Appl. Mater. Interfaces* **2020**, *12*, 23399.
[292] L.-Y. Shi, S. Lee, Q. Du, B. Zhou, L. Weng, R. Liu, C. A. Ross, *ACS Appl. Mater. Interfaces* **2021**, *13*, 10437.
[293] H. S. Yun, H. W. Do, K. K. Berggren, C. A. Ross, H. K. Choi, *ACS Appl. Mater. Interfaces* **2020**, *12*, 10852.
[294] C. Zhou, N. Tambo, E. M. Ashley, Y. Liao, J. Shiomi, K. Takahashi, G. S. W. Craig, P. F. Nealey, *ACS Nano* **2020**, *14*, 6980.
[295] D. H. Kim, A. Suh, G. Park, D. K. Yoon, S. Y. Kim, *ACS Appl. Mater. Interfaces* **2021**, *13*, 5781.
[296] M. P. Stoykovich, H. Kang, K. C. Daoulas, G. Liu, C. C. Liu, J. J. De Pablo, M. Müller, P. F. Nealey, *ACS Nano* **2007**, *1*, 168.
[297] S. Böhme, J. Arias-Zapata, J. Garnier, C. Girardot, A. Legrain, M. Zelsmann, *Micro Nano Eng.* **2018**, *1*, 56.
[298] H. Tsai, J. W. Pitera, H. Miyazoe, S. Bangsaruntip, S. U. Engelmann, C. C. Liu, J. Y. Cheng, J. J. Bucchignano, D. P. Klaus, E. A. Joseph, D. P. Sanders, M. E. Colburn, M. A. Guillorn, *ACS Nano* **2014**, *8*, 5227.
[299] I. Bita, J. K. W. Yang, S. J. Yeon, C. A. Ross, E. L. Thomas, K. K. Berggren, *Science* **2008**, *321*, 939.
[300] K. Fu, P. W. Bohn, *ACS Appl. Mater. Interfaces* **2017**, *9*, 24908.
[301] S. Park, H. L. Dong, J. Xu, B. Kim, W. H. Sung, U. Jeong, T. Xu, T. P. Russell, *Science* **2009**, *323*, 1030.
[302] M. Kim, E. Han, D. P. Sweat, P. Gopalan, *Soft Matter* **2013**, *9*, 6135.
[303] J. Choi, J. Huh, K. R. Carter, T. P. Russell, *ACS Nano* **2016**, *10*, 7915.
[304] E. Han, H. Kang, C. C. Liu, P. F. Nealey, P. Gopalan, *Adv. Mater.* **2010**, *22*, 4325.
[305] J. Choi, Y. Li, P. Y. Kim, F. Liu, H. Kim, D. M. Yu, J. Huh, K. R. Carter, T. P. Russell, *ACS Appl. Mater. Interfaces* **2018**, *10*, 8324.
[306] S. Xiao, X. Yang, E. W. Edwards, Y. H. La, P. F. Nealey, *Nanotechnology* **2005**, *16*, 324.
[307] M. J. Maher, C. T. Rettner, C. M. Bates, G. Blachut, M. C. Carlson, W. J. Durand, C. J. Ellison, D. P. Sanders, J. Y. Cheng, C. G. Willson, *ACS Appl. Mater. Interfaces* **2015**, *7*, 3323.
[308] G. S. Khaira, J. Qin, G. P. Garner, S. Xiong, L. Wan, R. Ruiz, H. M. Jaeger, P. F. Nealey, J. J. De Pablo, *ACS Macro Lett.* **2014**, *3*, 747.
[309] C. C. Liu, A. Ramírez-Hernández, E. Han, G. S. W. Craig, Y. Tada, H. Yoshida, H. Kang, S. Ji, P. Gopalan, J. J. De Pablo, P. F. Nealey, *Macromolecules* **2013**, *46*, 1415.
[310] S. O. Kim, H. H. Solak, M. P. Stoykovich, N. J. Ferrier, J. J. De Pablo, P. F. Nealey, *Nature* **2003**, *424*, 411.
[311] L. Rockford, Y. Liu, P. Mansky, T. P. Russell, M. Yoon, S. G. J. Mochrie, *Phys. Rev. Lett.* **1999**, *82*, 2602.
[312] F. A. Detcheverry, P. F. Nealey, J. J. De Pablo, *Macromolecules* **2010**, *43*, 6495.
[313] L. Rockford, S. G. J. Mochrie, T. P. Russell, *Macromolecules* **2001**, *34*, 1487.
[314] E. W. Edwards, M. F. Montague, H. H. Solak, C. J. Hawker, P. F. Nealey, *Adv. Mater.* **2004**, *16*, 1315.
[315] E. W. Edwards, M. Müller, M. P. Stoykovich, H. H. Solak, J. J. De Pablo, P. F. Nealey, *Macromolecules* **2007**, *40*, 90.
[316] G. Pandav, W. J. Durand, C. J. Ellison, C. G. Willson, V. Ganesan, *Soft Matter* **2015**, *11*, 9107.
[317] M. P. Stoykovich, M. Müller, S. O. Kim, H. H. Solak, E. W. Edwards, J. J. De Pablo, P. F. Nealey, *Science* **2005**, *308*, 1442.
[318] J. Y. Cheng, C. T. Rettner, D. P. Sanders, H. - C. Kim, W. D. Hinsberg, *Adv. Mater.* **2008**, *20*, 3155.
[319] R. Ruiz, H. Kang, F. A. Detcheverry, E. Dobisz, D. S. Kercher, T. R. Albrecht, J. J. De Pablo, P. F. Nealey, *Science* **2008**, *321*, 936.
[320] M. A. Morris, *Microelectron. Eng.* **2015**, *132*, 207.
[321] R. A. Griffiths, A. Williams, C. Oakland, J. Roberts, A. Vijayaraghavan, T. Thomson, *J. Phys. D: Appl. Phys.* **2013**, *46*, 503001.
[322] X. Gu, I. Gunkelk, T. P. Russell, *Philos. Trans. R. Soc., A* **2013**, *371*, 20120306.
[323] J. Y. Kim, B. H. Kim, J. O. Hwang, S. J. Jeong, D. O. Shin, J. H. Mun, Y. J. Choi, H. M. Jin, S. O. Kim, *Adv. Mater.* **2013**, *25*, 1331.

[324] B. H. Kim, J. Y. Kim, S. J. Jeong, J. O. Hwang, D. H. Lee, D. O. Shin, S. Y. Choi, S. O. Kim, *ACS Nano* **2010**, *4*, 5464.
[325] M. J. Maher, C. M. Bates, G. Blachut, S. Sirard, J. L. Self, M. C. Carlson, L. M. Dean, J. D. Cushen, W. J. Durand, C. O. Hayes, C. J. Ellison, C. G. Willson, *Chem. Mater.* **2014**, *26*, 1471.
[326] E. Kim, W. Kim, K. H. Lee, C. A. Ross, J. G. Son, *Adv. Funct. Mater.* **2014**, *24*, 6981.
[327] T. Seshimo, Y. Utsumi, T. Dazai, T. Maehashi, T. Matsumiya, Y. Suzuki, C. Hirano, R. Maeda, K. Ohmori, T. Hayakawa, *Polym. J.* **2016**, *48*, 407.
[328] E. Yoon, E. Kim, D. Kim, J. G. Son, *Adv. Funct. Mater.* **2015**, *25*, 913.
[329] I. H. Ryu, Y. J. Kim, Y. S. Jung, J. S. Lim, C. A. Ross, J. G. Son, *ACS Appl. Mater. Interfaces* **2017**, *9*, 17427.
[330] E. Han, I. In, S. M. Park, Y. H. La, Y. Wang, P. F. Nealey, P. Gopalan, *Adv. Mater.* **2007**, *19*, 4448.
[331] E. Han, K. O. Stuen, M. Leolukman, C. C. Liu, P. F. Nealey, P. Gopalan, *Macromolecules* **2009**, *42*, 4896.
[332] D. Y. Ryu, K. Shin, E. Drockenmuller, C. J. Hawker, T. P. Russell, *Science* **2005**, *308*, 236.
[333] S. Ji, C. C. Liu, J. G. Son, K. Gotrik, G. S. W. Craig, P. Gopalan, F. J. Himpsel, K. Char, P. F. Nealey, *Macromolecules* **2008**, *41*, 9098.
[334] I. In, Y. - H. La, S. - M. Park, P. F. Nealey, P. Gopalan, *Langmuir* **2006**, *22*, 7855.
[335] I. Keen, A. Yu, H. H. Cheng, K. S. Jack, T. M. Nicholson, A. K. Whittaker, I. Blakey, *Langmuir* **2012**, *28*, 15876.
[336] Y. Morimitsu, D. Salatto, N. Jiang, M. Sen, S. Nishitsuji, B. M. Yavitt, M. K. Endoh, A. Subramanian, C. Y. Nam, R. Li, M. Fukuto, Y. Zhang, L. Wiegart, A. Fluerasu, K. Tanaka, T. Koga, *Macromolecules* **2019**, *52*, 5157.
[337] R. Guo, E. Kim, J. Gong, S. Choi, S. Ham, D. Y. Ryu, *Soft Matter* **2011**, *7*, 6920.
[338] W. Lee, S. Park, Y. Kim, V. Sethuraman, N. Rebello, V. Ganesan, D. Y. Ryu, *Macromolecules* **2017**, *50*, 5858.
[339] Y. Kim, W. Lee, S. Jo, H. Ahn, K. Kim, J. U. Kim, D. Y. Ryu, *Macromolecules* **2020**, *53*, 6213.
[340] W. Lee, Y. Kim, S. Jo, S. Park, H. Ahn, D. Y. Ryu, *ACS Macro Lett.* **2019**, *13*, 519.
[341] J. Y. Kim, J. Lim, H. M. Jin, B. H. Kim, S. - J. Jeong, D. S. Choi, D. J. Li, S. O. Kim, *Adv. Mater.* **2016**, *28*, 1591.
[342] T. Deng, Y. H. Ha, J. Y. Cheng, C. A. Ross, E. L. Thomas, *Langmuir* **2002**, *18*, 6719.
[343] B. H. Kim, D. H. Lee, J. Y. Kim, D. O. Shin, H. Y. Jeong, S. Hong, J. M. Yun, C. M. Koo, H. Lee, S. O. Kim, *Adv. Mater.* **2011**, *23*, 5618.
[344] S. Park, J. M. Yun, U. N. Maiti, H. S. Moon, H. M. Jin, S. O. Kim, *Nanotechnology* **2014**, *25*, 014008.
[345] P. Mansky, T. P. Russell, C. J. Hawker, J. Mays, D. C. Cook, S. K. Satija, *Phys. Rev. Lett.* **1997**, *79*, 237.
[346] S. Ham, C. Shin, E. Kim, D. Y. Ryu, U. Jeong, T. P. Russell, C. J. Hawker, *Macromolecules.* **2008**, *41*, 6431.
[347] A. V. Berezkin, C. M. Papadakis, I. I. Potemkin, *Macromolecules* **2016**, *49*, 415.
[348] S. Lee, L. C. Cheng, K. G. Yager, M. Mumtaz, K. Aissou, C. A. Ross, *Macromolecules* **2019**, *52*, 1853.
[349] Y. Chen, H. Huang, Z. Hu, T. He, *Langmuir* **2004**, *20*, 3805.
[350] J. Peng, D. H. Kim, W. Knoll, Y. Xuan, B. Li, Y. Han, *J. Chem. Phys.* **2006**, *125*, 064702.
[351] F. Ferrarese Lupi, T. J. Giammaria, M. Ceresoli, G. Seguini, K. Sparnacci, D. Antonioli, V. Gianotti, M. Laus, M. Perego, *Nanotechnology* **2013**, *24*, 31560.
[352] A. Ramírez-Hernández, H. S. Suh, P. F. Nealey, J. J. De Pablo, *Macromolecules* **2014**, *47*, 3520.
[353] H. Yoshida, H. S. Suh, A. Ramirez-Herunandez, J. I. Lee, K. Aida, L. Wan, Y. Ishida, Y. Tada, R. Ruiz, J. de Pablo, P. F. Nealey, *J. Photopolym. Sci. Technol.* **2013**, *26*, 55.
[354] C. M. Bates, T. Seshimo, M. J. Maher, W. J. Durand, J. D. Cushen, L. M. Dean, G. Blachut, C. J. Ellison, C. G. Willson, *Science* **2012**, *338*, 775.
[355] W. J. Durand, M. C. Carlson, M. J. Maher, G. Blachut, L. J. Santos, S. Tein, V. Ganesan, C. J. Ellison, C. G. Willson, *Macromolecules* **2016**, *49*, 308.
[356] C. M. Bates, J. R. Strahan, L. J. Santos, B. K. Mueller, B. O. Bamgbade, J. A. Lee, J. M. Katzenstein, C. J. Ellison, C. G. Willson, *Langmuir* **2011**, *27*, 2000.
[357] J. Jeong, J. S. Ha, S.-S. Lee, J. G. Son, *Macromol. Rapid Commun.* **2015**, *36*, 1261.
[358] H. S. Suh, D. H. Kim, P. Moni, S. Xiong, L. E. Ocola, N. J. Zaluzec, K. K. Gleason, P. F. Nealey, *Nat. Nanotechnol.* **2017**, *12*, 575.
[359] A. Vora, K. Schmidt, G. Alva, N. Arellano, T. Magbitang, A. Chunder, L. E. Thompson, E. Lofano, J. W. Pitera, J. Y. Cheng, D. P. Sanders, *ACS Appl. Mater. Interfaces* **2016**, *8*, 29808.
[360] J. Zhang, M. B. Clark, C. Wu, M. Li, P. Trefonas, P. D. Hustad, *Nano Lett.* **2016**, *16*, 728.
[361] A. Tracz, J. K. Jeszka, M. D. Watson, W. Pisula, K. Müllen, T. Pakula, *J. Am. Chem. Soc.* **2003**, *125*, 1682.
[362] D. W. Breiby, O. Bunk, W. Pisula, T. I. Sølling, A. Tracz, T. Pakula, K. Müllen, M. M. Nielsen, *J. Am. Chem. Soc.* **2005**, *127*, 11288.
[363] C. Tang, A. Tracz, M. Kruk, R. Zhang, D. M. Smilgies, K. Matyjaszewski, T. Kowalewski, *J. Am. Chem. Soc.* **2005**, *127*, 6918.
[364] C. Tang, W. Wu, D. M. Smilgies, K. Matyjaszewski, T. Kowalewski, *J. Am. Chem. Soc.* **2011**, *133*, 11802.
[365] K. G. Yager, N. J. Fredin, X. Zhang, B. C. Berry, A. Karim, R. L. Jones, *Soft Matter* **2009**, *6*, 92.
[366] K. Mita, H. Tanaka, K. Saijo, M. Takenaka, T. Hashimoto, *Macromolecules* **2007**, *40*, 5923.
[367] Z. Cong, L. Zhang, L. Wang, J. Lin, *J. Chem. Phys.* **2016**, *144*, 114901.
[368] L. Zhang, L. Liu, J. Lin, *Phys. Chem. Chem. Phys.* **2017**, *20*, 498.
[369] G. Singh, K. G. Yager, D. M. Smilgies, M. M. Kulkarni, D. G. Bucknall, A. Karim, *Macromolecules* **2012**, *45*, 7107.
[370] J. Xue, G. Singh, Z. Qiang, A. Karim, B. D. Vogt, *Nanoscale* **2013**, *5*, 7928.
[371] J. Xue, G. Singh, Z. Qiang, K. G. Yager, A. Karim, B. D. Vogt, *Nanoscale* **2013**, *5*, 12440.
[372] H. Hu, J. P. Singer, C. O. Osuji, *Macromolecules* **2014**, *47*, 5703.
[373] H. Hu, S. Rangou, M. Kim, P. Gopalan, V. Filiz, A. Avgeropoulos, C. O. Osuji, *ACS Nano* **2013**, *7*, 2960.
[374] Y. Choo, H. Hu, K. Toth, C. O. Osuji, *J. Polym. Sci., Part B: Polym. Phys.* **2016**, *54*, 247.
[375] A. Jaworek, *J. Mater. Sci.* **2007**, *42*, 266.
[376] H. Hu, Y. Choo, X. Feng, C. O. Osuji, *Macromol. Rapid Commun.* **2015**, *36*, 1290.
[377] S. M. Park, M. P. Stoykovich, R. Ruiz, Y. Zhang, C. T. Black, P. F. Nealey, *Adv. Mater.* **2007**, *19*, 607.
[378] D. E. Lee, J. Ryu, D. Hong, S. Park, D. H. Lee, T. P. Russell, *ACS Nano* **2018**, *12*, 1642.
[379] Q. Tong, S. J. Sibener, *J. Phys. Chem. C* **2014**, *118*, 13752.
[380] C. C. Kathrein, W. Bai, J. A. Currivan-Incorvia, G. Liontos, K. Ntetsikas, A. Avgeropoulos, A. Böker, L. Tsarkova, C. A. Ross, *Chem. Mater.* **2015**, *27*, 6890.
[381] S. M. Nicaise, K. R. Gadelrab, K. G. Amir Tavakkoli, C. A. Ross, A. Alexander-Katz, K. K. Berggren, *Nano Futures* **2017**, *1*, 035006.
[382] K. A. Cavicchi, T. P. Lodge, *Macromolecules* **2004**, *37*, 6004.
[383] M. S. Alshammasi, F. A. Escobedo, *Soft Matter* **2019**, *15*, 851.
[384] M. C. Dalvi, T. P. Lodge, *Macromolecules* **1993**, *26*, 859.
[385] M. C. Dalvi, C. E. Eastman, T. P. Lodge, *Phys. Rev. Lett.* **1993**, *71*, 2591.
[386] T. P. Lodge, M. C. Dalvi, *Phys. Rev. Lett.* **1995**, *75*, 657.
[387] M. W. Hamersky, M. Tirrell, T. P. Lodge, *Langmuir* **1998**, *14*, 6974.

[388] F. Rittig, J. Kärger, C. M. Papadakis, G. Fleischer, P. Štěpánek, K. Almdal, *Phys. Chem. Chem. Phys.* **1999**, *1*, 3923.
[389] F. Rittig, G. Fleischer, J. Kärger, C. M. Papadakis, K. Almdal, P. Stěpânek, *Macromolecules* **1999**, *32*, 5872.
[390] M. W. Hamersky, M. A. Hillmyer, M. Tirrell, F. S. Bates, T. P. Lodge, E. D. Von Meerwall, *Macromolecules* **1998**, *31*, 5363.
[391] P. Shewmon, *Diffusion in Solids*, 2nd ed., The Minerals, Metals & Materials Society, Warrendale, PA **1989**.
[392] A. A. Deschamps, M. B. Claase, W. J. Sleijster, J. D. De Bruijn, D. W. Grijpma, J. Feijen, *J. Controlled Release* **2002**, *78*, 175.
[393] A. Patel, A. K. Gaharwar, G. Iviglia, H. Zhang, S. Mukundan, S. M. Mihaila, D. Demarchi, A. Khademhosseini, *Biomaterials* **2013**, *34*, 3970.
[394] D. Cohn, H. Younes, *J. Biomed. Mater. Res.* **1988**, *22*, 993.
[395] Z. Zhao, J. Wang, S. Li, S. Zhang, *J. Power Sources* **2011**, *196*, 4445.
[396] S. Maity, T. Jana, *ACS Appl. Mater. Interfaces* **2014**, *6*, 6851.
[397] B. Bae, K. Miyatake, M. Watanabe, *ACS Appl. Mater. Interfaces* **2009**, *1*, 1279.
[398] W. A. Phillip, B. O'neill, M. Rodwogin, M. A. Hillmyer, E. L. Cussler, *ACS Appl. Mater. Interfaces* **2010**, *2*, 847.
[399] R. M. Dorin, W. A. Phillip, H. Sai, J. Werner, M. Elimelech, U. Wiesner, *Polymer* **2014**, *55*, 347.
[400] N. Wang, T. Wang, Y. Hu, *ACS Appl. Mater. Interfaces* **2017**, *9*, 31018.
[401] C. Y. Ryu, T. P. Lodge, *Macromolecules* **1999**, *32*, 7190.
[402] K. Luo, Y. Yang, *Macromolecules* **2002**, *35*, 3722.
[403] H. Hahn, J. H. Lee, N. P. Balsara, B. A. Garetz, H. Watanabe, *Macromolecules* **2001**, *34*, 8701.
[404] Y. Takahashi, M. Noda, S. Kitade, K. Matsuoka, Y. Matsushita, I. Noda, *Polym. J.* **2005**, *37*, 894.
[405] Y. Takahashi, M. Noda, N. Ochiai, I. Noda, *Polymer* **1996**, *37*, 5943.
[406] T. Meins, K. Hyun, N. Dingenouts, M. Fotouhi Ardakani, B. Struth, M. Wilhelm, *Macromolecules* **2012**, *45*, 455.
[407] M. Steube, T. Johann, E. Galanos, M. Appold, C. Rüttiger, M. Mezger, M. Gallei, A. H. E. Müller, G. Floudas, H. Frey, *Macromolecules* **2018**, *51*, 10246.
[408] C. de Ruijter, E. Mendes, H. Boerstoel, S. J. Picken, *Polymer* **2006**, *47*, 8517.
[409] W. Wang, X. Wang, F. Jiang, Z. Wang, *Polym. Chem.* **2018**, *9*, 3067.
[410] C. Ye, T. Takigawa, O. Burtovvy, L. Langsdorf, D. Jablonski, A. Bell, B. D. Vogt, *ACS Appl. Mater. Interfaces* **2015**, *7*, 11765.
[411] B. J. Dair, C. C. Honeker, D. B. Alward, A. Avgeropoulos, N. Hadjichristidis, L. J. Fetters, M. Capel, E. L. Thomas, *Macromolecules* **1999**, *32*, 8145.
[412] B. J. Dair, A. Avgeropoulos, N. Hadjichristidis, E. L. Thomas, *J. Mater. Sci.* **2000**, *35*, 5207.
[413] S. Saikrasun, S. Bualek-Limcharoen, S. Kohjiya, K. Urayama, *J. Polym. Sci., Part B: Polym. Phys.* **2005**, *43*, 135.
[414] K. Domansky, J. D. Sliz, N. Wen, C. Hinojosa, G. Thompson, J. P. Fraser, T. Hamkins-Indik, G. A. Hamilton, D. Levner, D. E. Ingber, *Microfluid. Nanofluid.* **2017**, *21*, 107.
[415] Y. Li, Y. Iwakura, K. Nakayama, H. Shimizu, *Compos. Sci. Technol.* **2007**, *67*, 2886.
[416] R. G. C. Arridge, M. J. Folkes, *J. Phys. D: Appl. Phys.* **1972**, *5*, 344.
[417] C. Ye, G. Singh, M. L. Wadley, A. Karim, K. A. Cavicchi, B. D. Vogt, *Macromolecules* **2013**, *46*, 8608.
[418] J. Y. Chung, J. H. Lee, K. L. Beers, C. M. Stafford, *Nano Lett.* **2011**, *11*, 3361.
[419] E. P. Chan, K. A. Page, S. H. Im, D. L. Patton, R. Huang, C. M. Stafford, *Soft Matter* **2009**, *5*, 4638.
[420] C. M. Stafford, B. D. Vogt, C. Harrison, D. Julthongpiput, R. Huang, *Macromolecules* **2006**, *39*, 5095.
[421] J. Y. Chung, A. J. Nolte, C. M. Stafford, *Adv. Mater.* **2011**, *23*, 349.
[422] G. Raumann, D. W. Saunders, *Proc. Phys. Soc.* **1961**, *77*, 1028.
[423] C. Ye, C. Wang, J. Wang, C. G. Wiener, X. Xia, S. Z. D. Cheng, R. Li, K. G. Yager, M. Fukuto, B. D. Vogt, *Soft Matter* **2017**, *13*, 7074.
[424] P. Allan, R. G. C. Arridge, F. Ehtaiatkar, M. J. Folkes, *J. Phys. D: Appl. Phys.* **1991**, *24*, 1381.
[425] C. C. Honeker, E. L. Thomas, *Chem. Mater.* **1996**, *8*, 1702.
[426] N. Mahmood, A. M. Anton, G. Gupta, T. Babur, K. Knoll, T. Thurn-Albrecht, F. Kremer, M. Beiner, R. Weidisch, *Polymer* **2014**, *55*, 3782.
[427] J. S. Montana, S. Roland, E. Richaud, G. Miquelard-Garnier, *Polymer* **2018**, *149*, 124.
[428] J. J. Hernandez, H. Zhang, Y. Chen, M. Rosenthal, M. D. Lingwood, M. Goswami, X. Zhu, M. Moeller, L. A. Madsen, D. A. Ivanov, *Macromolecules* **2017**, *50*, 5392.
[429] S. A. Chopade, J. G. Au, Z. Li, P. W. Schmidt, M. A. Hillmyer, T. P. Lodge, *ACS Appl. Mater. Interfaces* **2017**, *9*, 14561.
[430] B. A. Fultz, T. Terlier, B. Dunoyer De Segonzac, R. Verduzco, J. G. Kennemur, *Macromolecules* **2020**, *53*, 5638.
[431] K. Timachova, I. Villaluenga, L. Cirrincione, M. Gobet, R. Bhattacharya, X. Jiang, J. Newman, L. A. Madsen, S. G. Greenbaum, N. P. Balsara, *J. Phys. Chem. B* **2018**, *122*, 1537.
[432] H. D. Nguyen, G. T. Kim, J. Shi, E. Paillard, P. Judeinstein, S. Lyonnard, D. Bresser, C. Iojoiu, *Energy Environ. Sci.* **2018**, *11*, 3298.
[433] M. D. Galluzzo, W. S. Loo, A. A. Wang, A. Walton, J. A. Maslyn, N. P. Balsara, *J. Phys. Chem. B* **2020**, *124*, 921.
[434] M. S. Alshammasi, F. A. Escobedo, *Macromolecules* **2018**, *51*, 9213.
[435] J. P. Coote, T. Kinsey, D. P. Street, S. M. Kilbey, J. R. Sangoro, G. E. Stein, *ACS Macro Lett.* **2020**, *9*, 565.
[436] G. K. Sethi, X. Jiang, R. Chakraborty, W. S. Loo, I. Villaluenga, N. P. Balsara, *ACS Macro Lett.* **2018**, *7*, 1056.
[437] K. W. Gao, X. Jiang, Z. J. Hoffman, G. K. Sethi, S. Chakraborty, I. Villaluenga, N. P. Balsara, *J. Polym. Sci.* **2020**, *58*, 363.
[438] J. H. Choi, Y. Ye, Y. A. Elabd, K. I. Winey, *Macromolecules* **2013**, *46*, 5290.
[439] J. Li, K. Kamata, M. Komura, T. Yamada, H. Yoshida, T. Iyoda, *Macromolecules* **2007**, *40*, 8125.
[440] S. N. Patel, A. E. Javier, G. M. Stone, S. A. Mullin, N. P. Balsara, *ACS Nano* **2012**, *6*, 1589.
[441] C. G. Arges, K. Li, L. Zhang, Y. Kambe, G. P. Wu, B. Lwoya, J. N. L. Albert, P. F. Nealey, R. Kumar, *Mol. Syst. Des. Eng.* **2019**, *4*, 365.
[442] M. Park, C. Harrison, P. M. Chaikin, R. A. Register, D. H. Adamson, *Science* **1997**, *276*, 1401.
[443] P. Mansky, P. haikin, E. L. Thomas, *J. Mater. Sci.* **1995**, *30*, 1987.
[444] C. M. Bates, M. J. Maher, D. W. Janes, C. J. Ellison, C. G. Willson, *Macromolecules* **2014**, *47*, 2.
[445] C. J. Hawker, T. P. Russell, *MRS Bull.* **2005**, *30*, 952.
[446] M. P. Stoykovich, P. F. Nealey, *Mater. Today* **2006**, *9*, 20.
[447] Z. T. Belete, E. Baer, A. Erdmann, *Proc. SPIE* **2018**, 10589, 105890U.
[448] W. J. Durand, G. Blachut, M. J. Maher, S. Sirard, S. Tein, M. C. Carlson, Y. Asano, S. X. Zhou, A. P. Lane, C. M. Bates, C. J. Ellison, C. G. Willson, *J. Polym. Sci., Part A: Polym. Chem.* **2015**, *53*, 344.
[449] K. G. A. Tavakkoli, S. M. Nicaise, K. R. Gadelrab, A. Alexander-Katz, C. A. Ross, K. K. Berggren, *Nat. Commun.* **2016**, *7*, 10518.
[450] T. Yun, H. M. Jin, D. Kim, K. H. Han, G. G. Yang, G. Y. Lee, G. S. Lee, J. Y. Choi, I. Kim, S. O. Kim, *Adv. Funct. Mater.* **2018**, *28*, 1804508.
[451] M. Park, P. M. Chaikin, R. A. Register, D. H. Adamson, *Appl. Phys. Lett.* **2001**, *79*, 257.
[452] K. Brassat, D. Kool, J. Bürger, J. K. N. Lindner, *Nanoscale* **2018**, *10*, 10005.
[453] C. Cummins, A. Bell, M. Morris, *Nanomaterials* **2017**, *7*, 304.
[454] H.-S. Moon, J. Y. Kim, H. M. Jin, W. J. Lee, H. J. Choi, J. H. Mun, Y. J. Choi, S. K. Cha, S. H. Kwon, S. O. Kim, *Adv. Funct. Mater.* **2014**, *24*, 4343.
[455] J. Arias-Zapata, D. Ferrah, J. Garnier, S. Böhme, O. Mouray, H. Okuno, G. Cunge, M. Zelsmann, *Mater. Today: Proc.* **2017**, *4*, 6827.

[456] E. Cara, I. Murataj, G. Milano, N. De Leo, L. Boarino, F. F. Lupi, *Nanomaterials* **2021**, *11*, 994.
[457] Y. C. Tseng, Q. Peng, L. E. Ocola, J. W. Elam, S. B. Darling, *J. Phys. Chem. C* **2011**, *115*, 17725.
[458] C. T. Black, K. W. Guarini, Y. Zhang, H. Kim, J. Benedict, E. Sikorski, I. V. Babich, K. R. Milkove, *IEEE Electron Device Lett.* **2004**, *25*, 622.
[459] Y. Chang, C. Ku, Y. Zhang, H. Wang, J. Chen, *Adv. Funct. Mater.* **2020**, *30*, 2000764.
[460] Y.-C. Chiu, I. Otsuka, S. Halila, R. Borsali, W.-C. Chen, *Adv. Funct. Mater.* **2014**, *24*, 4240.
[461] C. T. Black, K. W. Guarini, K. R. Milkove, S. M. Baker, T. P. Russell, M. T. Tuominen, *Appl. Phys. Lett.* **2001**, *79*, 409.
[462] C. T. Black, *Appl. Phys. Lett.* **2005**, *87*, 163116.
[463] S. Rasappa, D. Borah, C. C. Faulkner, T. Lutz, M. T. Shaw, J. D. Holmes, M. A. Morris, *Nanotechnology* **2013**, *24*, 065503.
[464] D. Zschech, D. H. Kim, A. P. Milenin, R. Scholz, R. Hillebrand, C. J. Hawker, T. P. Russell, M. Steinhart, U. Gösele, *Nano Lett.* **2007**, *7*, 1516.
[465] Y. S. Jung, J. H. Lee, J. Y. Lee, C. A. Ross, *Nano Lett.* **2010**, *10*, 3722.
[466] C. Sinturel, F. S. Bates, M. A. Hillmyer, *ACS Macro Lett.* **2015**, *4*, 1044.
[467] J. K. Kim, S. Y. Yang, Y. Lee, Y. Kim, *Prog. Polym. Sci.* **2010**, *35*, 1325.
[468] H. Cao, L. Dai, Y. Liu, X. Li, Z. Yang, H. Deng, *Macromolecules* **2020**, *53*, 8757.
[469] J. G. Son, M. Son, K. J. Moon, B. H. Lee, J. M. Myoung, M. S. Strano, M. H. Ham, C. A. Ross, *Adv. Mater.* **2013**, *25*, 4723.
[470] H. Huang, R. Liu, C. A. Ross, A. Alexander-Katz, *ACS Nano* **2020**, *14*, 15182.
[471] A. Subramanian, G. Doerk, K. Kisslinger, D. H. Yi, R. B. Grubbs, C. Y. Nam, *Nanoscale* **2019**, *11*, 9533.
[472] S. Greil, A. Rahman, M. Liu, C. T. Black, *Chem. Mater.* **2017**, *29*, 9572.
[473] H. Y. Hsueh, H. Y. Chen, M. S. She, C. K. Chen, R. M. Ho, S. Gwo, H. Hasegawa, E. L. Thomas, *Nano Lett.* **2010**, *10*, 4994.
[474] P. W. Majewski, A. Rahman, C. T. Black, K. G. Yager, *Nat. Commun.* **2015**, *6*, 7448.
[475] Z. Qiang, M. L. Wadley, B. D. Vogt, K. A. Cavicchi, *J. Polym. Sci., Part B: Polym. Phys.* **2015**, *53*, 1058.
[476] Y. Ren, Y. Zou, Y. Liu, X. Zhou, J. Ma, D. Zhao, G. Wei, Y. Ai, S. Xi, Y. Deng, *Nat. Mater.* **2020**, *19*, 203.
[477] H. Jung, W. H. Shin, T. W. Park, Y. J. Choi, Y. J. Yoon, S. H. Park, J. H. Lim, J. D. Kwon, J. W. Lee, S. H. Kwon, G. H. Seong, K. H. Kim, W. I. Park, *Nanoscale* **2019**, *11*, 8433.
[478] D. S. Jung, J. Bang, T. W. Park, S. H. Lee, Y. K. Jung, M. Byun, Y. R. Cho, K. H. Kim, G. H. Seong, W. I. Park, *Nanoscale* **2019**, *11*, 18559.
[479] S. K. Cha, G. Y. Lee, J. H. Mun, H. M. Jin, C. Y. Moon, J. S. Kim, K. H. Kim, S. J. Jeong, S. O. Kim, *ACS Appl. Mater. Interfaces* **2017**, *9*, 15727.
[480] J. H. Mun, S. K. Cha, Y. C. Kim, T. Yun, Y. J. Choi, H. M. Jin, J. E. Lee, H. U. Jeon, S. Y. Kim, S. O. Kim, *Small* **2017**, *13*, 1603939.
[481] C. Vix-Guterl, E. Frackowiak, K. Jurewicz, M. Friebe, J. Parmentier, F. Béguin, *Carbon* **2005**, *43*, 1293.
[482] J. Niu, R. Shao, M. Liu, J. Liang, Z. Zhang, M. Dou, Y. Huang, F. Wang, *Energy Storage Mater.* **2018**, *12*, 145.
[483] T. Liu, J. Serrano, J. Elliott, X. Yang, W. Cathcart, Z. Wang, Z. He, G. Liu, *Sci. Adv.* **2020**, *6*, eaaz0906.
[484] S. M. Bhaway, Z. Qiang, Y. Xia, X. Xia, B. Lee, K. G. Yager, L. Zhang, K. Kisslinger, Y. M. Chen, K. Liu, Y. Zhu, B. D. Vogt, *ACS Nano* **2017**, *11*, 1443.
[485] Y. Sun, J. Xue, S. Dong, Y. Zhang, Y. An, B. Ding, T. Zhang, H. Dou, X. Zhang, *J. Mater. Sci.* **2020**, *55*, 5166.
[486] J. Wang, P. Zhang, L. Liu, Y. Zhang, J. Yang, Z. Zeng, S. Deng, *Chem. Eng. J.* **2018**, *348*, 57.
[487] T. Liu, G. Liu, *J. Mater. Chem. A* **2019**, *7*, 23476.
[488] F. W. Richey, B. Dyatkin, Y. Gogotsi, Y. A. Elabd, *J. Am. Chem. Soc.* **2013**, *135*, 12818.
[489] S. M. Mahurin, J. S. Lee, X. Wang, S. Dai, *J. Membr. Sci.* **2011**, *368*, 41.
[490] X. Q. Zhang, W. C. Li, A. H. Lu, *New Carbon Mater.* **2015**, *30*, 481.
[491] L. Liu, W. Zeng, S. (Johnathan) Tan, M. Liu, D. D. Do, *Carbon* **2021**, *179*, 477.
[492] D. Wang, J. Jiang, Z. Pan, Q. Li, J. Zhu, L. Tian, P. K. Shen, *Front. Mater.* **2019**, *6*, 245.
[493] Z. Qiang, B. Gurkan, J. Ma, X. Liu, Y. Guo, M. Cakmak, K. A. Cavicchi, B. D. Vogt, *Microporous Mesoporous Mater.* **2016**, *227*, 57.
[494] M. R. Benzigar, S. N. Talapaneni, S. Joseph, K. Ramadass, G. Singh, J. Scaranto, U. Ravon, K. Al-Bahily, A. Vinu, *Chem. Soc. Rev.* **2018**, *47*, 2680.
[495] S. L. Suib, *Chem. Rec.* **2017**, *17*, 1169.
[496] L. Chuenchom, R. Kraehnert, B. M. Smarsly, *Soft Matter* **2012**, *8*, 10801.
[497] H. Yan, *Chem. Commun.* **2012**, *48*, 3430.
[498] K. Kailasam, Y. S. Jun, P. Katekomol, J. D. Epping, W. H. Hong, A. Thomas, *Chem. Mater.* **2010**, *22*, 428.
[499] S. Tanaka, N. Nakatani, A. Doi, Y. Miyake, *Carbon* **2011**, *49*, 3184.
[500] Z. Qiang, J. Xue, K. A. Cavicchi, B. D. Vogt, *Langmuir* **2013**, *29*, 3428.
[501] G. Deng, Z. Qiang, W. Lecorchick, K. A. Cavicchi, B. D. Vogt, *Langmuir* **2014**, *30*, 2530.
[502] C. Liang, Z. Li, S. Dai, *Angew. Chem., Int. Ed.* **2008**, *47*, 3696.
[503] C. Liang, K. Hong, G. A. Guiochon, J. W. Mays, S. Dai, *Angew. Chem., Int. Ed.* **2004**, *43*, 5785.
[504] S. Tomita, H. Urakawa, I. Wataoka, S. Sasaki, S. Sakurai, *Polym. J.* **2016**, *48*, 1123.
[505] Y. Wu, X. Lu, Q. Lu, *Microporous Mesoporous Mater.* **2015**, *211*, 152.
[506] P. Yang, D. Zhao, D. I. Margolese, B. F. Chmelka, G. D. Stucky, *Chem. Mater.* **1999**, *11*, 2813.
[507] J.-L. Blin, A. Léonard, Z.-Y. Yuan, L. Gigot, A. Vantomme, A. K. Cheetham, B.-L. Su, *Angew. Chem.* **2003**, *115*, 2978.
[508] J. Lee, M. Christopher Orilall, S. C. Warren, M. Kamperman, F. J. Disalvo, U. Wiesner, *Nat. Mater.* **2008**, *7*, 222.
[509] P. Yang, D. Zhao, D. I. Margolese, B. F. Chmelka, G. D. Stucky, *Nature* **1998**, *396*, 152.
[510] P. Yang, T. Deng, D. Zhao, P. Feng, D. Pine, B. F. Chmelka, G. M. Whitesides, G. D. Stucky, *Science* **1998**, *282*, 2244.
[511] H. N. Lokupitiya, A. Jones, B. Reid, S. Guldin, M. Stefik, *Chem. Mater.* **2016**, *28*, 1653.
[512] Y. Xia, Z. Qiang, B. Lee, M. L. Becker, B. D. Vogt, *CrystEngComm* **2017**, *19*, 4294.
[513] B. Eckhardt, E. Ortel, D. Bernsmeier, J. Polte, P. Strasser, U. Vainio, F. Emmerling, R. Kraehnert, *Chem. Mater.* **2013**, *25*, 2749.
[514] A. Sarkar, M. Stefik, *J. Mater. Chem. A* **2017**, *5*, 11840.
[515] S. Wang, P. Tangvijitsakul, Z. Qiang, S. M. Bhaway, K. Lin, K. A. Cavicchi, M. D. Soucek, B. D. Vogt, *Langmuir* **2016**, *32*, 4077.
[516] Z. Yi, P. B. Zhang, C. J. Liu, L. P. Zhu, *Macromolecules* **2016**, *49*, 3343.
[517] H. Yu, X. Qiu, S. P. Nunes, K. V. Peinemann, *Angew. Chem., Int. Ed.* **2014**, *53*, 10072.
[518] M. Radjabian, V. Abetz, *Prog. Polym. Sci.* **2020**, *102*, 101219.
[519] G. M. Geise, H.-S. Lee, D. J. Miller, B. D. Freeman, J. E. McGrath, D. R. Paul, *J. Polym. Sci., Part B: Polym. Phys.* **2010**, *48*, 1685.
[520] M. E. Arnold, K. Nagai, R. J. Spontak, B. D. Freeman, D. Leroux, D. E. Betts, J. M. DeSimone, F. A. DiGiano, C. K. Stebbins, R. W. Linton, *Macromolecules* **2002**, *35*, 3697.
[521] D. Ma, J. Zhou, Z. Wang, Y. Wang, *J. Membr. Sci.* **2020**, *598*, 117656.
[522] Y. Gu, U. Wiesner, *Macromolecules* **2015**, *48*, 6153.
[523] H. Ahn, S. Park, S. W. Kim, P. J. Yoo, D. Y. Ryu, T. P. Russell, *ACS Nano* **2014**, *8*, 11745.
[524] R. Shevate, M. Kumar, M. Karunakaran, C. Canlas, K. V. Peinemann, *J. Mater. Chem. A* **2018**, *6*, 4337.

[525] Y. Luo, X. Wang, R. Zhang, M. Singh, A. Ammar, D. Cousins, M. K. Hassan, D. Ponnamma, S. Adham, M. A. A. Al-Maadeed, A. Karim, *Soft Matter* **2020**, *16*, 9648.
[526] D. W. Weller, L. Galuska, W. Wang, D. Ehlenburg, K. Hong, X. Gu, *Macromolecules* **2019**, *52*, 5026.
[527] X. Qiu, H. Yu, M. Karunakaran, N. Pradeep, S. P. Nunes, K. V. Peinemann, *ACS Nano* **2013**, *7*, 768.
[528] S. Y. Yang, I. Ryu, H. Y. Kim, J. K. Kim, S. K. Jang, T. P. Russell, *Adv. Mater.* **2006**, *18*, 709.
[529] Y. Zhang, N. E. Almodovar-Arbelo, J. L. Weidman, D. S. Corti, B. W. Boudouris, W. A. Phillip, *npj Clean Water* **2018**, *1*, 2.
[530] J. Wang, M. M. Rahman, C. Abetz, V. Abetz, *J. Membr. Sci.* **2020**, *614*, 118535.
[531] D. Keskin, J. I. Clodt, J. Hahn, V. Abetz, V. Filiz, *Langmuir* **2014**, *30*, 8907.
[532] J. I. Clodt, V. Filiz, S. Rangou, K. Buhr, C. Abetz, D. Höche, J. Hahn, A. Jung, V. Abetz, *Adv. Funct. Mater.* **2013**, *23*, 731.
[533] D. G. Kim, T. Takigawa, T. Kashino, O. Burtovyy, A. Bell, R. A. Register, *Chem. Mater.* **2015**, *27*, 6791.
[534] C. Shin, X. Chelsea Chen, J. M. Prausnitz, N. P. Balsara, *J. Membr. Sci.* **2017**, *523*, 588.
[535] Z. Zhang, M. M. Rahman, C. Abetz, A. Höhme, E. Sperling, V. Abetz, *Adv. Mater.* **2020**, *32*, 1907014.
[536] S. Saleem, S. Rangou, C. Abetz, V. Filiz, V. Abetz, *Polymers* **2019**, *12*, 41.
[537] G. Singh, S. Batra, R. Zhang, H. Yuan, K. G. Yager, M. Cakmak, B. Berry, A. Karim, *ACS Nano* **2013**, *7*, 5291.
[538] A. A. Leniart, P. Pula, E. H. R. Tsai, P. W. Majewski, *Macromolecules* **2020**, *53*, 11178.
[539] J. E. Seppala, R. L. Lewis, T. H. Epps, *ACS Nano* **2012**, *6*, 9855.
[540] P. W. Majewski, K. G. Yager, *Macromolecules* **2015**, *48*, 4591.
[541] P. W. Majewski, K. G. Yager, *ACS Nano* **2015**, *9*, 3896.
[542] P. W. Majewski, K. G. Yager, *Nano Lett.* **2015**, *15*, 5221.
[543] D. E. Angelescu, J. H. Waller, D. H. Adamson, R. A. Register, P. M. Chaikin, *Adv. Mater.* **2007**, *19*, 2687.
[544] Y. C. Kim, T. J. Shin, S. M. Hur, S. J. Kwon, S. Y. Kim, *Sci. Adv.* **2019**, *5*, eaaw3974.
[545] J. Li, P. A. Rincon-Delgadillo, H. S. Suh, G. Mannaert, P. F. Nealey, *J. Micro/Nanolithogr., MEMS, MOEMS* **2019**, *18*, 043502.
[546] J. B. Chang, H. K. Choi, A. F. Hannon, A. Alexander-Katz, C. A. Ross, K. K. Berggren, *Nat. Commun.* **2014**, *5*, 3305.
[547] J. K. W. Yang, Y. S. Jung, J. B. Chang, R. A. Mickiewicz, A. Alexander-Katz, C. A. Ross, K. K. Berggren, *Nat. Nanotechnol.* **2010**, *5*, 256.
[548] G. Liu, C. S. Thomas, G. S. W. Craig, P. F. Nealey, *Adv. Funct. Mater.* **2010**, *20*, 1251.
[549] Z. Qiang, S. A. Akolawala, M. Wang, *ACS Macro Lett.* **2018**, *7*, 566.
[550] R. Zhang, Z. Qiang, M. Wang, *Adv. Funct. Mater.* **2021**, *31*, 2005819.
[551] S. H. Park, D. O. Shin, B. H. Kim, D. K. Yoon, K. Kim, S. Y. Lee, S. H. Oh, S. W. Choi, S. C. Jeon, S. O. Kim, *Soft Matter* **2009**, *6*, 120.
[552] S. H. Kim, K. Char, S. I.l Yoo, B. Sohn, *Adv. Funct. Mater.* **2017**, *27*, 1606715.
[553] M. S. Onses, C. Song, L. Williamson, E. Sutanto, P. M. Ferreira, A. G. Alleyne, P. F. Nealey, H. Ahn, J. A. Rogers, *Nat. Nanotechnol.* **2013**, *8*, 667.
[554] H. Tran, H. M. Bergman, K. R. Parenti, A. M. Van Der Zande, C. R. Dean, L. M. Campos, *Polym. Chem.* **2019**, *10*, 3194.
[555] B. B. Patel, D. J. Walsh, D. H. Kim, J. Kwok, B. Lee, D. Guironnet, Y. Diao, *Sci. Adv.* **2020**, *6*, 7202.
[556] K. W. Tan, U. Wiesner, *Macromolecules* **2019**, *52*, 395.
[557] F. Ferrarese Lupi, T. J. Giammaria, A. Miti, G. Zuccheri, S. Carignano, K. Sparnacci, G. Seguini, N. De Leo, L. Boarino, M. Perego, M. Laus, *ACS Nano* **2018**, *12*, 7076.
[558] S. Samant, J. Strzalka, K. G. Yager, K. Kisslinger, D. Grolman, M. Basutkar, N. Salunke, G. Singh, B. Berry, A. Karim, *Macromolecules* **2016**, *49*, 8633.
[559] V. Körstgens, J. Wiedersich, R. Meier, J. Perlich, S. V. Roth, R. Gehrke, P. Müller-Buschbaum, *Anal. Bioanal. Chem.* **2010**, *396*, 139.
[560] J. M. Virgili, Y. Tao, J. B. Kortright, N. P. Balsara, R. A. Segalman, *Macromolecules* **2007**, *40*, 2092.
[561] M. M. Abul Kashem, G. Kaune, A. Diethert, W. Wang, K. Schlage, S. Couet, R. Röhlsberger, S. V. Roth, P. Müller-Buschbaum, *Macromolecules* **2011**, *44*, 1621.
[562] N. Mahadevapuram, I. Mitra, A. Bozhchenko, J. Strzalka, G. E. Stein, *J. Polym. Sci., Part B: Polym. Phys.* **2016**, *54*, 339.
[563] S. A. Vaselabadi, D. Shakarisaz, P. Ruchhoeft, J. Strzalka, G. E. Stein, *J. Polym. Sci., Part B: Polym. Phys.* **2016**, *54*, 1074.
[564] G. E. Stein, J. A. Liddle, A. L. Aquila, E. M. Gullikson, *Macromolecules* **2010**, *43*, 433.
[565] E. M. McCready, W. R. Burghardt, *Macromolecules* **2015**, *48*, 264.
[566] D. F. Sunday, X. Chen, T. R. Albrecht, D. Nowak, P. Rincon Delgadillo, T. Dazai, K. Miyagi, T. Maehashi, A. Yamazaki, P. F. Nealey, R. J. Kline, *Chem. Mater.* **2020**, *32*, 2399.
[567] D. F. Sunday, F. Delachat, A. Gharbi, G. Freychet, C. D. Liman, R. Tiron, R. J. Kline, *J. Appl. Crystallogr.* **2019**, *52*, 106.
[568] D. F. Sunday, S. List, J. S. Chawla, R. J. Kline, *J. Appl. Crystallogr.* **2015**, *48*, 1355.
[569] N. P. Balsara, B. Hammouda, P. K. Kesani, S. V. Jonnalagadda, G. C. Straty, *Macromolecules* **1994**, *27*, 2566.
[570] E. Huang, T. P. Russell, C. Harrison, P. M. Chaikin, R. A. Register, C. J. Hawker, J. Mays, *Macromolecules* **1998**, *31*, 7641.
[571] E. Huang, P. Mansky, T. P. Russell, C. Harrison, P. M. Chaikin, R. A. Register, C. J. Hawker, J. Mays, *Macromolecules* **2000**, *33*, 80.
[572] R. W. Richards, J. L. Thomason, *Macromolecules* **1983**, *16*, 982.
[573] N. Torikai, N. L. Yamada, A. Noro, M. Harada, D. Kawaguchi, A. Takano, Y. Matsushita, *Polym. J.* **2007**, *39*, 1238.
[574] C. K. Shelton, R. L. Jones, J. A. Dura, T. H. Epps, *Macromolecules* **2016**, *49*, 7525.
[575] J. G. Raybin, S. J. Sibener, *Macromolecules* **2019**, *52*, 5985.
[576] U. Mansfeld, S. Hoeppener, U. S. Schubert, *Adv. Mater.* **2013**, *25*, 761.
[577] L. R. Parent, E. Bakalis, A. Ramírez-Hernández, J. K. Kammeyer, C. Park, J. De Pablo, F. Zerbetto, J. P. Patterson, N. C. Gianneschi, *J. Am. Chem. Soc.* **2017**, *139*, 17140.
[578] L. R. Parent, K. Gnanasekaran, J. Korpanty, N. C. Gianneschi, *ACS Macro Lett.* **2021**, *10*, 14.
[579] G. M. Scheutz, M. A. Touve, A. S. Carlini, J. B. Garrison, K. Gnanasekaran, B. S. Sumerlin, N. C. Gianneschi, *Matter* **2021**, *4*, 722.
[580] J. Raybin, J. Ren, X. Chen, R. Gronheid, P. F. Nealey, S. J. Sibener, *Nano Lett.* **2017**, *17*, 7717.
[581] I. W. Hamley, S. D. Connell, S. Collins, *Macromolecules* **2004**, *37*, 5337.
[582] T. Segal-Peretz, J. Winterstein, M. Doxastakis, A. Ramírez-Hernández, M. Biswas, J. Ren, H. S. Suh, S. B. Darling, J. A. Liddle, J. W. Elam, J. J. De Pablo, N. J. Zaluzec, P. F. Nealey, *ACS Nano* **2015**, *9*, 5333.
[583] T. Segal-Peretz, J. Ren, S. Xiong, G. Khaira, A. Bowen, L. E. Ocola, R. Divan, M. Doxastakis, N. J. Ferrier, J. De Pablo, P. F. Nealey, *ACS Nano* **2017**, *11*, 1307.
[584] B. Kuei, E. D. Gomez, *Nat. Commun.* **2021**, *12*, 153.
[585] B. Kuei, M. P. Aplan, J. H. Litofsky, E. D. Gomez, *Mater. Sci. Eng., R* **2020**, *139*, 100516.
[586] B. Kuei, C. Bator, E. D. Gomez, *Macromolecules* **2020**, *53*, 8296.

[587] C. E. Boott, R. F. Laine, P. Mahou, J. R. Finnegan, E. M. Leitao, S. E. D. Webb, C. F. Kaminski, I. Manners, *Chem. - Eur. J.* **2015**, *21*, 18539.
[588] W. L. Gong, J. Yan, L. X. Zhao, C. Li, Z. L. Huang, B. Z. Tang, M. Q. Zhu, *Photochem. Photobiol. Sci.* **2016**, *15*, 1433.
[589] J. A. Hinckley, D. V. Chapman, K. R. Hedderick, K. W. Oleske, L. A. Estroff, U. B. Wiesner, *ACS Macro Lett.* **2019**, *8*, 1378.
[590] Z. Qiang, K. M. Shebek, M. Irie, M. Wang, *ACS Macro Lett.* **2018**, *7*, 1432.
[591] C. Li, H. Yan, L. X. Zhao, G. F. Zhang, Z. Hu, Z. L. Huang, M. Q. Zhu, *Nat. Commun.* **2014**, *5*, 5709.
[592] L. Albertazzi, D. Van Der Zwaag, C. M. A. Leenders, R. Fitzner, R. W. Van Der Hofstad, E. W. Meijer, *Science* **2014**, *344*, 491.
[593] S. Pujals, N. Feiner-Gracia, P. Delcanale, I. Voets, L. Albertazzi, *Nat. Rev. Chem.* **2019**, *3*, 68.
[594] D. Wöll, C. Flors, *Small Methods* **2017**, *1*, 1700191.
[595] Z. Qiang, M. Wang, *ACS Macro Lett.* **2020**, *9*, 1342.
[596] D. J. Mai, C. M. Schroeder, *ACS Macro Lett.* **2020**, *9*, 1332.
[597] D. Yong, H. M. Jin, S. O. Kim, J. U. Kim, *Macromolecules* **2018**, *51*, 1418.
[598] A. Ianiro, S. P. Armes, R. Tuinier, *Soft Matter* **2020**, *16*, 2342.
[599] Y. Ding, K. R. Gadelrab, K. Mizrahi Rodriguez, H. Huang, C. A. Ross, A. Alexander-Katz, *Nat. Commun.* **2019**, *10*, 2974.
[600] A. F. Hannon, D. F. Sunday, A. Bowen, G. Khaira, J. Ren, P. F. Nealey, J. J. De Pablo, R. J. Kline, *Mol. Syst. Des. Eng.* **2018**, *3*, 376.
[601] G. L. Shebert, Y. L. Joo, *Soft Matter* **2018**, *14*, 1389.
[602] J. Qin, G. S. Khaira, Y. Su, G. P. Garner, M. Miskin, H. M. Jaeger, J. J. De Pablo, *Soft Matter* **2013**, *9*, 11467.
[603] T. E. Gartner, A. Jayaraman, *Macromolecules* **2019**, *52*, 755.
[604] J. D. Hill, P. C. Millett, *Sci. Rep.* **2017**, *7*, 5250.
[605] C. T. Bezik, J. J. De Pablo, *Macromolecules* **2020**, *53*, 10446.

Mark Robertson completed his B.S. in chemical engineering at the University of Mississippi in 2019. He joined the Polymer Science and Engineering program at the University of Southern Mississippi in 2019 and is currently a Ph.D. student in the Qiang research group. His research focuses on block copolymer self-assembly, and a breadth of block copolymer derived functional materials.

Qingya Zhou earned his Master's degree from the College of Chemistry and Materials Science at Shanghai Normal University in 2019, and then worked as a research assistant in the Engineering College at West Lake University. He is currently a Ph.D. student in the College of Materials Science and Engineering at Donghua University starting from 2020. His research interests focus on design and fabrication of conductive hydrogels in electronic skins, sensors, and energy storage.

Changhuai Ye obtained his Ph.D. in polymer engineering from the University of Akron and is currently a professor in the College of Materials Science and Engineering at Donghua University. His research interests focus on processing–structure–property relationships in self-assembled block copolymers, conductive composite materials, and porous polymer materials, as well as the applications of these materials in EMI shielding, thermal insulation, and sensing applications.

Zhe Qiang is an assistant professor of polymer science and engineering at the University of Southern Mississippi. He received his M.S. and Ph.D. degrees in polymer engineering from the University of Akron, and was a postdoc fellow at Northwestern University. His current research interests include self-assembly and interfacial phenomenon in soft matter and composites, including in situ characterization of polymer chain conformations and nanostructures and manufacturing of functional porous materials for energy and environmental applications.